

Volume 3, Issue 1, 2025

**Print ISSN: 2960-0251
Online ISSN: 2960-026X**

FRONTIERS IN ENVIRONMENTAL RESEARCH



Copyright© Upubscience Publisher

Frontiers in Environmental Research

Volume 3, Issue 1, 2025



Published by Upubscience Publisher

Copyright© The Authors

Upubscience Publisher adheres to the principles of Creative Commons, meaning that we do not claim copyright of the work we publish. We only ask people using one of our publications to respect the integrity of the work and to refer to the original location, title and author(s).

Copyright on any article is retained by the author(s) under the Creative Commons Attribution license, which permits unrestricted use, distribution, and reproduction in any medium, provided the original work is properly cited.

Authors grant us a license to publish the article and identify us as the original publisher.

Authors also grant any third party the right to use, distribute and reproduce the article in any medium, provided the original work is properly cited.

Frontiers in Environmental Research

Print ISSN: 2960-0251 Online ISSN: 2960-026X

Email: info@upubscience.com

Website: <http://www.upubscience.com/>

Table of Content

ADVANCING ENVIRONMENTAL RESEARCH IN AFRICA: TOWARDS A SUSTAINABLE AND RESILIENT FUTURE Okechukwu Chidoluo Vitus	1-7
OPTIMIZATION AND MODELLING FOR WET BENEFICIATION OF KAOLIN BY SEDIMENTATION Tayyaba Jamil	8-25
LOW-CARBON TRANSFORMATION OF CHINA ' S COAL-FIRED POWER INDUSTRY: CURRENT SITUATION INSIGHTS AND TREND PROSPECTS Rui Yang	26-31
SUPPLY AND DEMAND EVALUATION OF URBAN RECREATIONAL GREEN SPACES IN ZHAOQING CITY FROM THE PERSPECTIVE OF SUPPLY AND DEMAND BALANCE HongJun Xie, SiRu Ye*	32-41
NEW DEVELOPMENT OF BIOLOGICAL NITROGEN AND PHOSPHORUS REMOVAL PROCESSES FOR MUNICIPAL WASTEWATER ZouTing Sun	42-47
CURRENT STATUS AND PROSPECTS OF ADVANCED COMPRESSED AIR ENERGY STORAGE IN CHINA YanPeng Li, HaoRan Zhou*, RiPeng Cong, TianChen Rao	48-55
PREPARATION OF HIGH-TOUGHNESS THERMOPLASTIC STARCH FILMS VIA ENZYMATIC HYDROLYSIS AND CROSS-LINKING MODIFICATION Hao Wang, ChuanWei Zhang*	56-68
THE DEVELOPMENT OF THE INCLUSION OF THE SHIPPING INDUSTRY IN EMISSION TRADING SYSTEMS AND ITS IMPACT ON THE SHIPPING SECTOR Cong Xu	69-73
ASSESSING LANDSCAPE SUSTAINABILITY BY COUPLING ECOSYSTEM SERVICE SUPPLY-DEMAND AND ES-SDG LINKAGES: A CASE STUDY OF YIXING CITY IN THE TAIHU LAKE BASIN HengHui Xi	74-83
SUITABILITY EVALUATION OF WATER INDEX UNDER EXTRACTION OF COMPLEX ENVIRONMENTAL WATER BODIES ZhiHua Liu	84-88

ADVANCING ENVIRONMENTAL RESEARCH IN AFRICA: TOWARDS A SUSTAINABLE AND RESILIENT FUTURE

Okechukwu Chidoluo Vitus

Omnibus Institute of Professional Learning and Development, Lagos 42100, Nigeria.

Corresponding Email: jlcmedias@gmail.com

Abstract: This research article examines the critical role of environmental research in Africa, emphasizing its significance in addressing the continent's unique ecological challenges. The study highlights the multifaceted environmental issues faced by African nations, including deforestation, desertification, biodiversity loss, and the impacts of climate change. These problems not only threaten the continent's natural resources but also jeopardize the livelihoods of millions of people who depend on these ecosystems. Key findings from this research indicate that while there has been a growing body of environmental studies in Africa, there remains a substantial gap in data and resources. The research underscores the need for enhanced collaboration among governments, local communities, and international organizations to develop comprehensive strategies aimed at mitigating environmental degradation. The study also identifies successful case studies where integrated approaches have led to improved conservation outcomes and community resilience. The implications of this research extend to policy and practice, suggesting that targeted investment in environmental research can lead to more informed decision-making. Policymakers are encouraged to prioritize funding for research initiatives that address local environmental issues while fostering sustainable development. Furthermore, the article advocates for the involvement of indigenous knowledge and local expertise in environmental management strategies to ensure that solutions are culturally relevant and effective. Ultimately, this research serves as a call to action for stakeholders across Africa and beyond to recognize the urgency of environmental issues and to commit to collaborative efforts that promote ecological sustainability and enhance the quality of life for all citizens. Through a concerted focus on environmental research, Africa can pave the way toward a more sustainable and resilient future.

Keywords: Environments; Environmental research; Africa; Eco system; Citizens; Sustainable and resilient future

1 INTRODUCTION

Environmental research in Africa plays a pivotal role in understanding and addressing the continent's diverse ecosystems, which are among the richest in the world. With over 1,500 distinct species of mammals, birds, and reptiles, Africa's biodiversity is invaluable not only for ecological balance but also for the cultural and economic benefits it provides to its inhabitants. However, this rich tapestry of life faces significant threats from various environmental challenges, including climate change, deforestation, habitat loss, and pollution. The implications of these issues extend beyond the environment, affecting food security, health, and socio-economic stability for millions of people across the continent. Climate change, in particular, poses a formidable challenge to Africa, with rising temperatures and shifting precipitation patterns impacting agriculture and water resources essential for survival. Deforestation, driven by agricultural expansion and urbanization, further exacerbates these challenges by diminishing the natural habitats that sustain wildlife and regulate climatic conditions. The loss of biodiversity and degradation of ecosystems not only threaten wildlife but also disrupt the livelihoods of communities that depend on these natural resources for their daily needs [1].

This article aims to shed light on the significance of environmental research in Africa by outlining its scope and research objectives. It seeks to explore the current state of environmental research initiatives across the continent, with a focus on understanding the interplay between human activities and environmental sustainability. The objectives include identifying key environmental research areas, assessing gaps in data and resources, and highlighting successful case studies that demonstrate effective conservation strategies. By illuminating these aspects, the article endeavors to foster a deeper understanding of the urgent need for comprehensive environmental research in Africa and its potential to inform policy-making and promote sustainable practices [2].

1.1 Historical Context of Environmental Research in Africa

The journey of environmental research in Africa has evolved significantly over the past few decades, reflecting a growing awareness of ecological issues and the need for sustainable practices. In the early years, most environmental studies were largely descriptive, focusing on cataloging biodiversity and natural resources. The 1970s marked a pivotal moment as the United Nations Conference on the Human Environment in Stockholm (1972) brought global attention to environmental issues, prompting African nations to recognize the importance of integrating environmental considerations into development planning [3].

Key milestones in African environmental research include the establishment of the African Centre for Technology Studies in 1980 and the African Environmental Outlook reports initiated by the United Nations Environment Programme (UNEP) in the late 1990s. These reports highlighted regional environmental challenges, such as land degradation and water scarcity, and emphasized the need for collaborative solutions. The early 2000s witnessed a surge in research initiatives, notably the New Partnership for Africa's Development (NEPAD), which aimed to promote sustainable development through scientific innovation and environmental stewardship.

Influential studies, such as the Millennium Ecosystem Assessment [1], provided a comprehensive understanding of ecosystem services in Africa and their role in human well-being. This assessment laid the groundwork for further research into the impacts of climate change on ecosystems and livelihoods. Furthermore, international collaborations have played a crucial role in advancing environmental research. Initiatives like the African Climate and Development Initiative (ACDI) and partnerships with institutions in Europe and North America have facilitated knowledge transfer and capacity building, enabling local researchers to engage in impactful studies.

Understanding the historical context of environmental research in Africa is essential for grasping its current landscape. The evolution from basic cataloging of resources to comprehensive studies addressing complex environmental challenges has underscored the necessity of interdisciplinary approaches and the integration of local knowledge systems. As the continent continues to grapple with pressing ecological issues, the legacy of past research efforts serves as a foundation for future endeavors aimed at fostering sustainable development.

1.2 Current Challenges in Environmental Research

Despite the critical need for robust environmental research in Africa, researchers face a myriad of challenges that impede their efforts. One significant hurdle is funding limitations. Many research projects are underfunded or lack financial backing entirely, which restricts the scope and depth of studies. International grants and aid can be competitive and often prioritize different regions or issues, leaving African researchers struggling to secure necessary resources for local projects. This funding gap can result in incomplete studies and a lack of long-term research continuity, undermining the overall quality of environmental science on the continent.

Additionally, inadequate infrastructure poses a significant barrier to effective research. Many regions in Africa lack the essential facilities, technology, and transportation systems necessary for conducting environmental studies. This deficiency not only hampers data collection but also limits researchers' ability to collaborate and share findings with the broader scientific community. As a result, research efforts can become fragmented, and important data may remain inaccessible or underutilized, further complicating efforts to address environmental issues.

Political instability in various African nations also complicates the research landscape. Frequent changes in government, civil unrest, and policy shifts can disrupt research initiatives, making it difficult for scientists to maintain focus on long-term goals. In some cases, researchers may face restrictions on their work or difficulty in obtaining necessary permits, which can delay or halt projects entirely. This instability can lead to a brain drain, where talented researchers leave their home countries in search of more stable environments, further diminishing local expertise [4].

Lastly, data shortages are a pervasive issue in environmental research in Africa. The lack of reliable and comprehensive datasets makes it challenging to draw meaningful conclusions and develop effective interventions. Many existing datasets are outdated or limited in scope, which can skew research outcomes and affect policy decisions. This scarcity of data highlights the need for improved monitoring systems and collaborative data-sharing initiatives among African nations.

These challenges collectively impact the quality and quantity of environmental research conducted across the continent. To foster a more sustainable and resilient future, it is imperative to address these barriers through increased funding, infrastructure development, political support, and enhanced data collection efforts.

2 KEY AREAS OF ENVIRONMENTAL RESEARCH

Environmental research in Africa encompasses a myriad of critical areas, each vital to understanding and addressing the continent's unique ecological challenges. Four key fields stand out: biodiversity conservation, climate change impacts, sustainable agriculture, and pollution management.

2.1 Biodiversity Conservation

Biodiversity conservation is essential for maintaining the ecological balance and ensuring the survival of numerous species. In Africa, significant studies have highlighted the importance of protected areas in safeguarding biodiversity. For instance, research on the Serengeti ecosystem demonstrates how protected areas can support large mammal populations and contribute to ecosystem services. Furthermore, studies have shown that community-based conservation initiatives, such as those in Namibia, have effectively empowered local communities to manage wildlife sustainably, leading to increased biodiversity and improved livelihoods.

2.2 Climate Change Impacts

The effects of climate change are profound in Africa, with rising temperatures and erratic rainfall patterns threatening food security and water resources. A notable study conducted in the Sahel region examined the impacts of climate variability on crop yields and highlighted the need for adaptive strategies. Researchers found that integrating traditional knowledge with modern agricultural practices could enhance resilience among farming communities. Additionally, the Intergovernmental Panel on Climate Change (IPCC) reports underscore the urgency of addressing climate change, particularly in vulnerable regions like sub-Saharan Africa.

2.3 Sustainable Agriculture

Sustainable agriculture is crucial for food security and environmental preservation. Research in this area has focused on agroecological practices that promote biodiversity and soil health. For instance, studies in Ethiopia have shown that intercropping and organic farming methods improve crop resilience and increase yields while minimizing the use of chemical fertilizers. Implementing sustainable agricultural techniques not only enhances food production but also contributes to ecosystem restoration and climate mitigation efforts.

2.4 Pollution Management

Pollution management is an increasingly pressing issue in Africa, where urbanization and industrialization have led to significant environmental degradation. Research on air and water pollution in cities like Lagos and Nairobi has revealed alarming levels of contaminants affecting public health and ecosystems. Effective management strategies, such as the introduction of waste recycling programs and stricter regulations on emissions, have been shown to mitigate pollution's adverse effects. Studies advocating for community engagement in pollution management efforts highlight the importance of local participation in creating sustainable solutions.

These key areas of environmental research are interconnected, reflecting the complex challenges Africa faces. Addressing these issues through targeted research can lead to innovative solutions that support both ecological health and human well-being.

3 GOVERNMENT POLICIES AND INITIATIVES

African governments have increasingly recognized the need for robust policies and initiatives aimed at promoting environmental research. These policies are crucial for addressing the continent's pressing ecological challenges and fostering sustainable development. Various nations have implemented strategies that encourage collaboration among researchers, governmental bodies, and local communities, ultimately enhancing the scope and impact of environmental research.

One notable example is Kenya's National Climate Change Action Plan (NCCAP), which emphasizes the importance of research in developing climate adaptation and mitigation strategies. The NCCAP encourages partnerships between governmental agencies, academic institutions, and non-governmental organizations (NGOs) to facilitate knowledge exchange and bolster research capacity. This collaborative approach has led to successful initiatives, such as the Kenya Wetlands Toolkit, which provides guidelines for sustainable wetland management, underscoring the effectiveness of government-supported research initiatives.

In South Africa, the Department of Science and Innovation (DSI) has launched the South African Research Chairs Initiative (SARChI), which aims to attract and retain top researchers in various fields, including environmental science. By providing funding and infrastructure support, SARChI fosters collaboration between universities and research institutions, leading to impactful studies on biodiversity conservation and climate resilience. A successful outcome of this initiative is the establishment of research chairs focused on critical areas like water security and ecosystem services, which have generated valuable insights for policymakers [5].

Moreover, the African Union's Agenda 2063 promotes science, technology, and innovation as key drivers for sustainable development. The Agenda emphasizes the establishment of regional research networks that facilitate collaboration among African countries. The African Climate and Development Initiative (ACDI) exemplifies this approach by supporting joint research efforts across multiple nations to address climate change impacts on vulnerable populations. This initiative has led to the development of actionable policies and frameworks that enhance regional capacity to respond to environmental challenges.

While these policies and initiatives demonstrate notable progress, their effectiveness largely depends on sustained funding, political commitment, and active participation from local communities. By continuing to prioritize environmental research through collaborative frameworks, African nations can make substantial strides toward achieving ecological sustainability and improving the quality of life for their citizens.

3.1 Role of Non-Governmental Organizations (NGOs)

Non-Governmental Organizations (NGOs) play a pivotal role in facilitating environmental research in Africa, significantly contributing to funding, capacity building, and advocacy efforts. These organizations often fill the gaps left by governmental and institutional bodies, providing essential resources and support for various environmental initiatives across the continent.

One of the primary contributions of NGOs is financial support for environmental research projects. Many African researchers struggle to secure funding from traditional sources, such as government grants or international funding bodies. NGOs, such as the World Wildlife Fund (WWF) and Conservation International, provide critical financial backing for research efforts focused on biodiversity conservation, climate change, and sustainable resource management. By channeling funds into local research initiatives, NGOs enable scientists to undertake meaningful studies that address pressing environmental issues.

In addition to funding, NGOs also focus on capacity building. They often conduct training programs and workshops to enhance the skills and knowledge of local researchers and community members. Organizations like the African Wildlife Foundation (AWF) and the International Union for Conservation of Nature (IUCN) emphasize the importance of empowering local communities through education and skill development. This approach not only builds a strong foundation for environmental research but also fosters a sense of ownership among local stakeholders, ensuring that research outcomes are culturally relevant and sustainable.

Advocacy is another critical area where NGOs make a significant impact. Through campaigns and partnerships, they raise awareness about environmental issues and influence policy decisions at national and international levels. For instance, organizations such as Greenpeace and the Global Forest Coalition advocate for policies that protect forests and promote sustainable land use practices. Their efforts help to create a supportive environment for environmental research and encourage governments to prioritize ecological sustainability.

Notable NGOs like the African Centre for Technology Studies and the Centre for Environmental Policy and Advocacy have also made significant strides in promoting research initiatives that address climate change and biodiversity loss. Their collaborative efforts with local communities and researchers exemplify the vital role that NGOs play in advancing environmental research and fostering a culture of sustainability across Africa.

3.2 International Collaboration and Partnerships

International collaboration is crucial in addressing environmental issues in Africa, where the confluence of local challenges and global influences necessitates a multifaceted approach. Partnerships between African institutions and global organizations have emerged as effective strategies for tackling ecological problems, fostering innovation, and building research capacity. These collaborations not only enhance scientific understanding but also facilitate the sharing of resources, expertise, and best practices.

One prominent case is the collaboration between the African Union and the United Nations Environment Programme (UNEP) on the African Regional Seas Programme. This initiative aims to protect marine and coastal environments across Africa through a coordinated approach that involves multiple stakeholders, including governments, NGOs, and local communities. By leveraging international expertise, the program has successfully established marine protected areas and implemented sustainable fishing practices, showcasing how global partnerships can lead to tangible conservation outcomes.

Another significant example is the partnership between the International Institute for Environment and Development (IIED) and various African governments on climate resilience projects. These collaborations focus on developing adaptive strategies for vulnerable communities affected by climate change. For instance, in Ethiopia, IIED's work with local farmers has resulted in the implementation of agroecological practices that enhance food security while preserving biodiversity. This partnership highlights the importance of integrating local knowledge with global expertise to produce effective solutions.

Furthermore, the Global Environment Facility (GEF) has funded numerous projects across Africa that address biodiversity loss and land degradation. The GEF's approach often involves collaboration with local NGOs and research institutions to ensure that initiatives are context-specific and sustainable. For example, projects aimed at combating desertification in the Sahel have successfully engaged local communities in land restoration efforts, leading to improved livelihoods and ecosystem health.

These case studies illustrate that international collaboration and partnerships are vital for addressing environmental challenges in Africa. By bringing together diverse stakeholders and leveraging a wide range of resources, these initiatives not only foster scientific advancements but also contribute to sustainable development and resilience against ecological threats.

3.3 Technological Advances in Environmental Research

Recent technological innovations have significantly enhanced environmental research capabilities in Africa, enabling more efficient data collection and analysis. Two prominent technologies that have revolutionized this field are remote sensing and

Geographic Information Systems (GIS). These advancements are instrumental in addressing the continent's pressing environmental challenges, such as deforestation, climate change, and biodiversity loss.

Remote sensing technology utilizes satellite imagery and aerial photography to monitor and analyze environmental changes over large areas. This approach permits researchers to track deforestation rates in real-time, assess land use changes, and evaluate the health of ecosystems without the need for extensive fieldwork. For instance, initiatives like the Global Forest Watch utilize satellite data to provide up-to-date information on forest cover loss, empowering stakeholders to take action against illegal logging and land conversion. This capacity for continuous monitoring allows for timely interventions and more informed decision-making regarding conservation efforts.

On the other hand, Geographic Information Systems (GIS) provide a powerful tool for spatial analysis and visualization of environmental data. GIS allows researchers to integrate various data sources, such as climate data, topography, and land use patterns, to create comprehensive maps that depict environmental vulnerabilities and trends. For example, GIS has been instrumental in analyzing the impacts of climate change on water resources in sub-Saharan Africa, helping to identify areas most at risk of drought or flooding. This information is crucial for developing targeted adaptation strategies that enhance community resilience.

Moreover, the combination of remote sensing and GIS facilitates participatory approaches in environmental research. Local communities can be engaged in data collection through mobile applications that feed into larger GIS databases, allowing for community-driven monitoring of environmental changes. This not only democratizes data collection but also enhances local ownership of conservation initiatives.

In summary, the integration of advanced technologies like remote sensing and GIS into environmental research is transforming the way data is collected, analyzed, and applied in Africa. These innovations are crucial for understanding complex environmental dynamics and devising effective strategies for sustainable management of natural resources.

3.4 Community Involvement and Indigenous Knowledge

Local communities and indigenous knowledge are paramount in shaping environmental research agendas, particularly in Africa, where diverse ecological landscapes are intertwined with rich cultural heritage. Engaging local populations not only enhances the relevance of research but also fosters a sense of stewardship over natural resources. Indigenous knowledge, which encompasses traditional practices, ecological wisdom, and cultural values, offers invaluable insights into sustainable resource management and biodiversity conservation.

A prominent case study illustrating the significance of community involvement is the collaborative approach adopted in the management of the Makuleke Contractual Park in South Africa. After the end of apartheid, the Makuleke community, who were forcibly removed from their ancestral lands, regained control over a portion of the Kruger National Park. Through participatory management practices, the community integrated traditional ecological knowledge with modern conservation strategies. This collaboration led to improved wildlife monitoring, sustainable tourism initiatives, and enhanced biodiversity protection, demonstrating that local input can yield effective environmental management practices.

Another notable example is the work of the Kalahari Peoples Fund in Botswana, which emphasizes the integration of indigenous knowledge in climate adaptation strategies. The organization collaborates with local communities to document their understanding of climate patterns, land use, and animal behavior. By utilizing this knowledge, the fund has developed community-led adaptation strategies that are culturally appropriate and highly effective. This initiative not only empowers local populations but also enhances resilience to climate change impacts.

Furthermore, the case of the Indigenous Peoples of the Amazon showcases how indigenous knowledge can guide environmental research and policy-making. In Brazil, indigenous groups have successfully advocated for the recognition of their land rights, arguing that their traditional practices are vital for preserving the rainforest. Their holistic understanding of ecosystems has informed conservation efforts that prioritize biodiversity and ecosystem services, leading to more effective environmental policies.

In conclusion, the integration of community involvement and indigenous knowledge into environmental research agendas is essential for achieving sustainable management of natural resources. By valuing and incorporating local perspectives, researchers and policymakers can develop more effective strategies that address both ecological and social challenges, ultimately promoting the resilience and well-being of communities across Africa.

3.5 Impact of Climate Change on Environmental Research

Climate change is profoundly reshaping the landscape of environmental research in Africa, driving a shift in focus towards understanding the intricate interactions between climate systems and ecological dynamics. As the continent grapples with rising temperatures, altered rainfall patterns, and increased frequency of extreme weather events, researchers are compelled to reevaluate existing paradigms and adopt innovative approaches to study these phenomena. The urgency of addressing climate impacts has catalyzed collaborative research initiatives aimed at both mitigation and adaptation strategies.

One striking case study is the work conducted in the Sahel region, where researchers have investigated the impacts of climate change on food security and agricultural practices. The International Crops Research Institute for the Semi-Arid

Tropics (ICRISAT) has partnered with local farmers to implement climate-resilient agricultural practices, such as drought-resistant crop varieties and improved soil management techniques. These initiatives not only aim to enhance food production but also to empower local communities to adapt to changing climatic conditions. The findings from these studies underscore the necessity of integrating scientific knowledge with local farming practices to develop sustainable solutions.

In East Africa, the impact of climate change on biodiversity and ecosystem services has spurred significant research efforts. The East African regional climate models have been utilized to predict changes in habitat suitability for various species, particularly in protected areas like the Serengeti National Park. Research findings indicate that shifting climatic conditions could lead to altered migration patterns and habitat loss for key species, prompting the need for adaptive management strategies. Such studies illustrate the critical role of climate projections in informing conservation policies and enhancing ecosystem resilience.

Moreover, community-based research initiatives have emerged as essential avenues for addressing climate change. In Namibia, the Integrated Rural Development and Nature Conservation (IRDNC) program involves local communities in wildlife management and climate adaptation efforts. By leveraging indigenous knowledge and local insights, researchers have been able to develop strategies that not only protect biodiversity but also enhance community livelihoods in the face of climate challenges [6].

These case studies exemplify the evolving relationship between climate change and environmental research in Africa. As researchers increasingly recognize the interplay between ecological systems and climatic shifts, the focus has shifted towards collaborative, adaptive management approaches that prioritize both scientific rigor and local engagement. Through these efforts, Africa can build a more resilient future in the face of an uncertain climate.

3.6 Future Directions for Environmental Research in Africa

As Africa faces an array of pressing environmental challenges, it is critical to identify future research directions that address existing gaps and leverage interdisciplinary approaches. One significant direction involves enhancing the integration of social sciences with environmental research. Understanding the socio-economic dynamics that drive environmental degradation is essential for developing effective conservation strategies. Research that examines the relationships between communities, land use practices, and resource management can yield insights that inform policy and facilitate sustainable practices [7].

Additionally, there is an urgent need for increased investment in research capacity across the continent. This includes funding for local researchers and institutions, as well as the establishment of training programs that enhance skills in data collection, analysis, and interpretation. Strengthening research infrastructure, such as laboratories and field stations, will also empower African scientists to conduct high-quality research that is relevant to local contexts. Collaborative funding models involving governments, NGOs, and international donors can help bridge the financial gap that often hinders environmental research initiatives (International Crops Research Institute for the Semi-Arid Tropics ICRISAT) [8].

Moreover, future research should embrace technology and innovation. The adoption of advanced methodologies such as artificial intelligence and machine learning can enhance data analysis and predictive modeling, enabling researchers to better understand complex environmental issues. For instance, these technologies can be applied to monitor biodiversity changes or assess the impacts of climate change on various ecosystems.

Interdisciplinary collaborations should also extend beyond the realm of academia to include policymakers, local communities, and the private sector. Engaging stakeholders from diverse backgrounds ensures that research is not only scientifically sound but also socially acceptable and practically applicable. Such partnerships can help translate research findings into actionable policies and community-driven initiatives, fostering a holistic approach to environmental management.

Finally, emphasizing the importance of indigenous knowledge systems in environmental research is paramount. Future studies should prioritize collaboration with local communities to integrate traditional ecological practices with contemporary scientific approaches. This synthesis can lead to more culturally relevant and effective solutions for environmental conservation and sustainable development across Africa.

4 CONCLUSION

In summary, this article has explored the vital role of environmental research in Africa, highlighting the continent's unique ecological challenges and the urgent need for sustainable solutions. Key points discussed include the multifaceted environmental issues such as deforestation, desertification, biodiversity loss, and the impacts of climate change that threaten both ecosystems and the livelihoods of millions. The necessity for increased funding, improved infrastructure, and enhanced collaboration among various stakeholders has been emphasized as a means to bridge the existing gaps in research and data. The historical context of environmental research in Africa has shown a significant evolution from mere cataloging of resources to comprehensive studies that address intricate environmental dynamics. This shift underscores the importance of interdisciplinary approaches and the need to incorporate local knowledge systems in research and policy-making.

Community involvement is integral, as demonstrated through successful case studies, which illustrate how local expertise can lead to effective conservation practices and bolster resilience against climate change.

Furthermore, the implications of this research extend to sustainable development and policy-making. By prioritizing investment in environmental research, African nations can develop informed strategies that align with local contexts and cultural values. This not only enhances ecological sustainability but also improves the quality of life for communities across the continent.

Ultimately, the call to action for stakeholders is clear: recognizing the urgency of environmental issues and committing to collaborative efforts is essential for ensuring a sustainable and resilient future in Africa. The integration of advanced technologies, social sciences, and indigenous knowledge into research agendas will be pivotal in addressing the continent's pressing environmental challenges.

COMPETING INTERESTS

The authors have no relevant financial or non-financial interests to disclose.

REFERENCES

- [1] Millennium Ecosystem Assessment. *Ecosystems and human well-being: Synthesis*. Washington, DC: Island Press, 2005.
- [2] New Partnership for Africa's Development (NEPAD). *NEPAD and the environment: A strategy for sustainable development*. African Union, 2001.
- [3] United Nations Environment Programme (UNEP). *African Environmental Outlook: Past, present and future*. Nairobi, Kenya: UNEP, 1999.
- [4] United Nations Environment Programme (UNEP). *Global Environment Outlook: Summary for Policymakers*. Nairobi, Kenya: UNEP, 2018.
- [5] Zhou Y, Wang J. The role of indigenous knowledge in climate change adaptation: A case study of the Kalahari Peoples Fund. *International Journal of Climate Change Strategies and Management*, 2018, 10(2): 244-259. DOI: <https://doi.org/10.1108/IJCCSM-03-2018-0041>.
- [6] African Centre for Technology Studies. *Annual Report*. Nairobi, Kenya: African Centre for Technology Studies, 1980.
- [7] Adger W N, Hughes T P, Folke C, et al. Social-ecological resilience to coastal disasters. *Science*, 2005, 309(5737): 1036-1039. DOI: <https://doi.org/10.1126/science.1115129>.
- [8] International Crops Research Institute for the Semi-Arid Tropics (ICRISAT). *Climate-resilient agriculture: A case study in the Sahel*, 2020. Retrieved from <https://www.icrisat.org>.

OPTIMIZATION AND MODELLING FOR WET BENEFICIATION OF KAOLIN BY SEDIMENTATION

Tayyaba Jamil

Department of Chemical Engineering, University of Engineering and Technology Lahore, Punjab 39161, Pakistan.

Corresponding Email: Tayyaba.uetian786@gmail.com

Abstract: Kaolinite is widely used in the paper, rubber, and paint industry. Global processing of kaolin is carried out by dry and wet processing. The dry processing provides lower yield and average product quality, than wet processing limiting their industrial applications. This study increases the kaolinite grade by developing a cheaper, simpler, and more efficient technique for utilization in the paper industry. The mineralogy of kaolin was analyzed by XRD, SEM, Size distribution, and XRF analysis. From these analyses, we found kaolin having kaolinite 59.6%, quartz 12% at 4.5% moisture content, was then beneficiated by dispersion and sedimentation. Kaolin was crushed, grounded, and screened through 325 mesh (44 μm) then performed dispersion at different solid percentages and dispersant dosages using sodium tri-polyphosphate as dispersants. The dispersed solution was agitated at 800 rpm for 15 minutes and settled for 30 minutes in a measuring cylinder. The Central composite design was used to optimize parameters varying solid percentage (5-30) % and dispersant dosage percentage (0.1-0.3) % for kaolin recovery. Results showed that the maximum grade and recovery of kaolinite was 88.8% and 76.03% at a dispersant dosage of 0.3% and a solid percentage of 17.5%. Overall, the grade of kaolin was successfully increased from 59.6% to 88.8%. It is also recommended to use ball mill with rubber coated steel balls instead of pin mill for efficient grinding.

Keywords: Kaolin; Wet processing; Dispersion; Sedimentation; Grade; Recovery

1 INTRODUCTION

Mineral processing is the art of separating valuable minerals from gangue by treatment of metallic and non-metallic ores [1]. Among the non-metallic ores, clays are the most important and widely processed ores. Kaolin is one of the clay minerals that is abundantly present in the earth [2]. Kaolin has been widely used in various industries such as cement production, papermaking, sanitary ware, plastic, cosmetics, fertilizers, pharmaceuticals, and adsorbents [3] due to its chemical reactivity and surface properties [4]. It is a hydrous aluminum silicate having an approximate composition of $2\text{H}_2\text{O}\cdot\text{Al}_2\text{O}_3\cdot 2\text{SiO}_2$ and it contains 46.54% SiO_2 , 39.5% Al_2O_3 , and 13.96% H_2O . Kaolin is usually associated with various auxiliary mineral impurities such as quartz, sulfides, titania, ferrous minerals, various iron oxides, mica, feldspar, and organic matter etc. The use of kaolin in the paper industry as a filler and coating agent is limited by the presence of these quartz, iron, and titaniferous impurities, etc. [5]. These impurities impart the color and brightness of kaolin which results in low-quality products. For any value-added application, impurities present in kaolin are needed to be reduced or removed by beneficiation or processing. In Pakistan, due to the lack of kaolin processing, its utilization is restricted to limited low-cost sanitary and crockery products [6].

Globally, the removal of impurities from kaolin is being carried out by two methods such as dry and wet processing. Wet processing consists of both chemical and physical processes. Mostly wet physical processing consists of electromagnetic separation [7] and sedimentation [8]. Some important wet chemical processes include selective flocculation [9], flotation [10], and microbial purification [11]. Wet processing techniques are preferred due to their better product quality and yield than the dry method. Furthermore, the processing kaolin product is exclusively used in the paper industry as filler pigments only, but wet-processed kaolin is used as coating pigments as well [12]. low-grade phosphate underwent optimization via wet beneficiation and a grade of 28.61% with 71.5% recovery was achieved [13]. Wet beneficiation of kaolin can achieve the brightness grade of 80% to 90% required by the paper industry, 80% to 85% for the filler industry, 85% to 90% for the coating industry, and 94% for the high-specification kaolin products. [14]. Flotation has the highest potential to achieve a 90% brightness grade [15]. High gradient techniques such as magnetic separation may produce kaolin grade from more than 90% [16]. Bioleaching for iron from pristine kaolin may produce quality products of 85% brightness grade and 70% whiteness grade [17]. However, these methods are expensive and not green. Very limited work has been done on dispersion and sedimentation which is a green and efficient method for kaolin beneficiation. The dry processing uses an air-classifier, or a technique called air flotation to separate impurities from kaolin. Several studies have been carried out for the purification of kaolin by flotation or dispersion. They revealed that alkyl hydroxamate is more effective for Titania removal than organic acids Sodium tripolyphosphate (STPP, $\text{Na}_5\text{P}_3\text{O}_{10}$) acts as a dispersing agent of solid particles, modifying the rheological behavior and properties of kaolin suspensions [18].

A study [19] worked to evaluate the effectiveness of some commercial dispersing agents employed for maximizing the solid loading of kaolin suspensions. They found sodium polyphosphate to be more effective as a dispersant for kaolin suspensions. The amount of dispersant used hugely affects the dispersion characteristics of clays. Keeping the dosage of STPP between 0.1-0.3 is found to be optimum. Increasing the dosage rendered the impurities to the products lowering the quality, while a decrease in the dosage lowered the yield. [20] However, these techniques are expensive, energy-

intensive, and not environment friendly or green. Contrarily, sedimentation is easy, inexpensive, green and effective in separation of heavy impurities due to differences in their densities or sizes. The heavier particles tend to settle quickly while finer stay suspended for longer. Based on this phenomenon, kaolinite is separated from quartz, mica, titanium-oxide (anatase) etc [21]. In Pakistan, due to the lack of kaolin processing, its utilization is restricted to limited low-cost sanitary and crockery products [22]. Kaolin processing can be done by dispersion and sedimentation to remove heavy impurities. Dispersion is described as the behavior of clay particles separating from one another when dissolved in water. This behavior is promoted by the addition of chemicals known as dispersants. Some of the dispersants commonly used for kaolin dispersion are Sodium Tripolyphosphate (STPP), Sodium Hexametaphosphate, and Sodium Polyacrylate. Sodium Tripolyphosphate is used as a dispersing agent to enhance the dispersion of kaolin in seawater [23]. However, the research didn't encounter the removal of heavy impurities. Kaolin, particles are usually heterogeneous consisting of positive charges at the edges and negative charges on the basal face, and the interaction of these charges with the surrounding environment promotes the aggregation of particles.

The statistical design of experiments (DOE) is a widely used method to explore the beneficiation of different minerals. It has several benefits to compare the conventional method of (OFAT) considering one parameter at a time. The DOE provides data about how various factors interact and how the system works. The DOE is a very simple and cheap technique for lowering effort, time, and process costs [24, 25]. Different DOE methods have been used for mineral processing optimization and modeling. The most practiced methods are the Box–Behnken experimental design (BBD), central composite design (CCD), and the full factorial design (FFD). Response surface methodology (RSM) is performed to model the parameters on the settling of heavy impurities from kaolin and explore the optimum dispersant dosage and solid percentages.

This study is concerned with the processing of Nagar Parkar, Sindh, Pakistan kaolin by dispersion and sedimentation to remove heavy impurities. Based on the density differences between kaolinite and gangue minerals, it was assumed that sedimentation will result in kaolinite in supernatant with impurities like quartz and titanium oxide settle in the bottom of the sedimentation tank.

This study aims to increase the grade of kaolin from Nagar Parkar, Sindh, Pakistan up to 97% by developing a cheaper, simpler, and more efficient processing technique for its application in the paper industry. Center composite design (CCD) was applied for optimization of the dispersant dosage and solid percentages on settling of heavy impurities to improve the kaolin quality for utilization in the paper industry. The interactions of these variables and the model developed were evaluated by Analysis of variance (ANOVA). RSM provides the optimum conditions for the removal of heavy impurities. It will encourage research and development of new methods and techniques for beneficiation of kaolin processing in Pakistan for application in a wide range of industries. The surface area roughness, size and porosity distribution of kaolin is also investigated using SEM images. As per authors knowledge, no previous studies have been made on image analysis of Nagar parker kaolin to investigate the adsorption mechanism. This study will also provide useful information for sustainable development goals for kaolin processing, especially in countries facing water scarcity and exporting kaolin on bulk scale such as Germany, China, and the USA.

2 MATERIALS AND METHODS

2.1 Materials

Kaolin samples, weighing 22 kilograms (kg), were provided by Ahmad Saeed and Co. (Private) Limited. These were obtained from various locations of Nagar Parker, Sindh, Pakistan in Figure 1. The samples were mixed properly to homogenize and then crushed at the set size of 1 mm using a Denver Roll crusher having a capacity of 2 tons/hr. The product of the roll crusher was subjected to grinding in (DERBY MRL-16) pin mill. Pin mill product was screened to get a -325-mesh size fraction and this process was followed in a closed loop. The -325-mesh kaolin was used for dispersion as shown in Figure 2.



Figure 1 Google Image Showing Areas Having Kaolin Reserves in Pakistan. Black Pin Represents Nagar Parkar, Sindh, Yellow Pin represents Swat and Green pin Represents Shah Dheri, KPK

2.2 Beneficiation of Pristine Kaolin

PROLABO an Electric Water Distillation unit was used to produce distilled water which was used in the dispersion of kaolin. The pH of the distilled water was measured using a pHep (HI-98107) pocket-size pH meter. The kaolin was weighed using a digital weight balance. Then, it was added to water to prepare 100 ml slurry. Again, the pH of the slurry was measured. The pH moderators, Sodium carbonate (Na_2CO_3) and Hydrochloric acid (HCl) [26] were added and mixed until a required pH value of 8.5 was achieved [27]. The -325-mesh kaolin was dispersed in distilled water at different combinations of solid percentages (5-30%) and dispersant dosages (0.1-0.3%) [28]. The required amount of dispersant, sodium tri-polyphosphate (STPP), was added to the slurry, which was then agitated at 800 rpm for 15 minutes using a lab agitator (ESJ-500, Shanghai, China) having a maximum speed of 3600 rpm. The slurry was then poured into a 28 mm internal diameter measuring cylinder and was allowed to settle for 30 minutes under the action of gravity [29]. After 30 minutes, the supernatant was siphoned off using a medical drip line of 3 mm. diameter and 150 cm. length. The supernatant and settled impurities were poured into separate beakers and dried in a Fisher Laboratory oven (Thermo fisher scientific, US) for 1 hour at 110°C .

The flowsheet of the experimental setup is shown in Figure 2

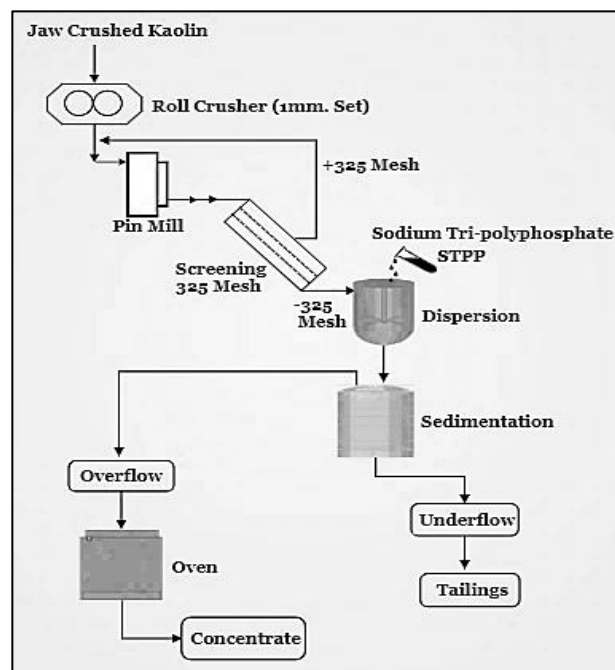


Figure 2 Flowsheet for the Removal of Heavy Impurities From Kaolin, Drawn Using Smart-Draw Software

2.3 Design of Experiments (DOE)

The effect of two independent variables solid percentage and dispersant dosage on the settling of heavy impurities present in the kaolin were analyzed. Experiments were designed using the Central-Composite design (CCD) for the optimization of these variables. In this study, statistical and mathematical analysis was performed using Minitab software (21.4.2, USA). The variables were solid percentage (5-30) %, and Dispersant dosage (0.1-0.3) % as shown in Table 1.

Table 1 Range of Coded Variable for Kaolin Sedimentation Parameters

Variables for Optimization	Coded variable Level		
	Low	Centre	High
Solid percentage (%)	5	17.5	30
Dispersant Dosage (%)	0.1	0.2	0.3

Fourteen sets of experiments were designed. All experiment sets were performed according to the combinations given in Table 2.

Table 2 Different Experiment Combinations Using Central Composite Design

Run Order	Pt Type	Blocks	Solid percentage	Dispersant Dosages percentage
1	1	1	26.34	0.27
2	1	1	8.66	0.27
3	0	1	17.50	0.20
4	0	1	17.50	0.20
5	1	1	8.66	0.13
6	0	1	17.50	0.20
7	1	1	26.34	0.13
8	0	2	17.50	0.20
9	0	2	17.50	0.20
10	-1	2	17.50	0.10
11	-1	2	17.50	0.30
12	-1	2	30.00	0.20
13	-1	2	5.00	0.20
14	0	2	17.50	0.20

2.4 Characterization

XRD was performed using Philips PANalytical X'Pert Powder diffractometer utilizing Cu-K α radiation from COMSATS University Islamabad, Lahore Campus. XRD technique was employed to find out the mineral content of the different kaolin samples. All samples were examined between 4° and 70° 2 θ . The step size and time per setup were 0.02 and 30s respectively to find relative percentages of various crystals. Scan Electron Microscopy (SEM, P TESCAN, and Vega LMU) with an accelerating voltage of 10 V was used to find the surface morphology of the samples. X-ray fluorescence (XRF, Thermos fisher scientist NitoN XL2 Handheld) was performed by Geoscience Advanced Research Laboratory, Islamabad, Pakistan for the analysis of the major and minor traces of elements present in the pristine kaolin.

3 RESULTS AND DISCUSSIONS

3.1 XRD Analysis of Kaolin

The XRD pattern of as received kaolin samples is shown in Figure 3. It shows the presence of 59.6% kaolinite along with the impurities of vaterite 11.7%, hematite 6.4%, dorokite 6.1%, magnesite 5.7%, mica 5%, quartz 4.7% and titanium 1.2%.

The kaolin after passing pin mill was screened through a 325-mesh sieve and subjected to XRD and the result is shown in Figure 4. The analysis shows that the grade of kaolinite increases from 59.6% to 63.4% after screening. While other impurities such as vaterite, magnesite, quartz, and titanium decreased from 11.7% to 5.7%, 5.7% to 2.9%, 4.7% to 3%, and 1.2% to 0.9% respectively.

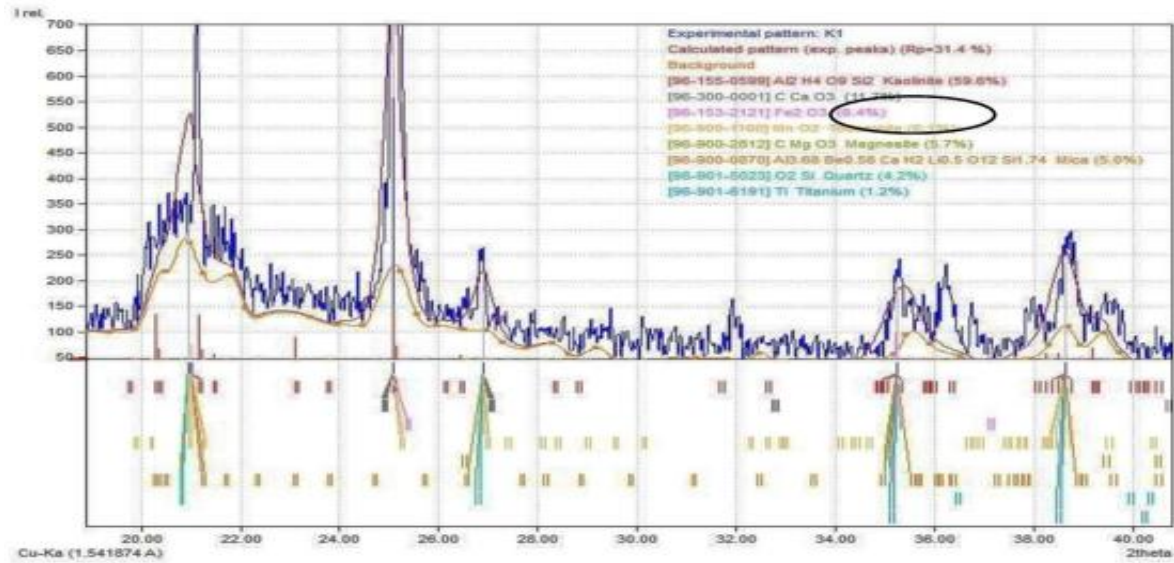


Figure 3 XRD Pattern of as Received Kaolin Sample Shows 59.6% Kaolinite and 4.2% Quartz

This shows that in finer particle size, the percentage of kaolinite increases, and impurities decrease in the -325-mesh sample. It is because of the selective grinding of kaolinite particles in pin mills. Quartz, titanium dioxide, and other impurities are harder. So, the impurities did not reduce as much as kaolinite.

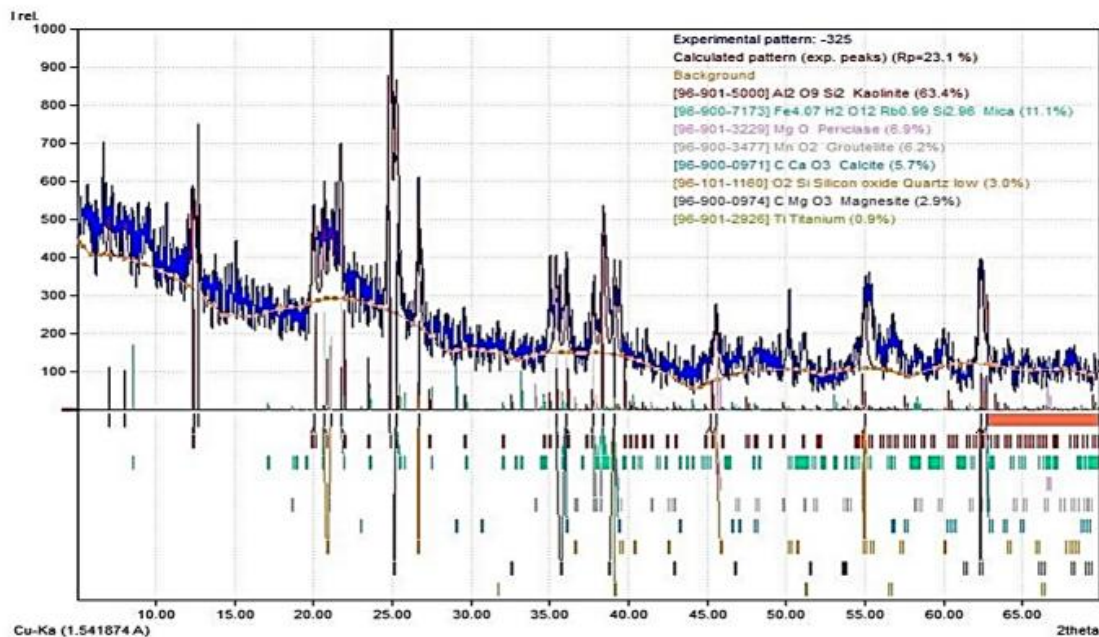


Figure 4 XRD Pattern of Screened Kaolin from 325 Mesh Sieve Showing 63.4% Kaolinite and 3.0% Quartz

3.2 X-ray Fluorescence

Raw kaolin samples from Viravah, Pardhro, Karkhi, Moti jo Vandio, Dhedvero, and Ramji jo Vandio deposits of Nagar Parkar were analyzed using the XRF technique [21]. The results are given in Table 3.

The SiO_2 content of raw kaolin ranges from 48.7 to 59.2%. The raw Nagar Parkar kaolin has higher SiO_2 content than the ideal kaolin (46.6%), due to the presence of quartz [30]. The Al_2O_3 content of Nagar Parkar kaolin is lower (21.3-26.8%) than in the ideal kaolinite (39.5%) due to the presence of quartz and clay mineral impurities. The Al_2O_3 content of clays depends upon the intensity of kaolinization. Incomplete kaolinization indicates a lesser amount of kaolin minerals and thus lowers Al_2O_3 content. The loss on ignition (LOI) of kaolinitic clays allows estimation of the kaolinite

content. The LOI at 1000°C of the raw Nagar Parkar kaolin ranges from 11.1 to 13.7%. The Fe₂O₃ content of the Nagar Parkar kaolin ranges from 0.29 to 1.62%, which is close to the maximum allowed limit of 1% Fe₂O₃. The presence of iron oxide in these kaolin deposits can be attributed to the breakdown of biotite and other ferromagnesian minerals of the source rock.

Table 3 The Composition of Nagar Parkar Kaolin with Kaolin Deposits (Wt. %)

Oxides	Nagar Parkar kaolin deposits						Washed kaolin
	Viravah (Raw)	Pardhro (Raw)	Karkhi (Raw)	Moti jo & Vandio (Raw)	Ramji jo Vandio	Dhedvero (Raw)	
SiO ₂	52.9	59.2	58.2			58.8	45.1
TiO ₂	1.3	0.4	0.7	0.4	0.6	0.4	0.7
Al ₂ O ₃	24.7	24.4	23.8	21.3	26.8	24.1	35.1
Fe ₂ O ₃	0.7	0.6	0.9	0.9	1.0	0.7	0.7
MnO	-	-	-	-	-	-	-
MgO	0.2	0.2	0.2	0.4	0.6	0.3	0.6
CaO	4.8	2.0	3.1	9.8	5.4	2.4	1.8
Na ₂ O	1.4	1.7	1.1	0.8	1.7	1.1	1.2
K ₂ O	0.3	0.2	0.3	0.6	0.3	0.1	0.2
P ₂ O ₅	0.0	0.1	0.1	-	0.1	-	-
*LOI	13.7	11.9	11.4	12.1	15.1	11.1	14.8

However, the Fe₂O₃ is not the only factor affecting the color of the ceramic wares. The CaO content in these kaolin samples is relatively high (2-9.8%).

3.3 SEM Analysis

SEM images of different origins of kaolin possess characteristic textures. It can be seen from SEM images that Kaolin of hydrothermal origin is typically very fine-grained, hexagonal booklet, tightly packed, and thus has low porosity. The textural studies show that Nagar Parkar kaolin consists of irregular stacks of books of kaolinite particles (Figure. 5a) with angular edges and porous (Figure 5b) and a lack of hexagonal booklet structure Figure 5c. The luminous part in Figure 5(d) represents the presence of silica in pristine kaolin.

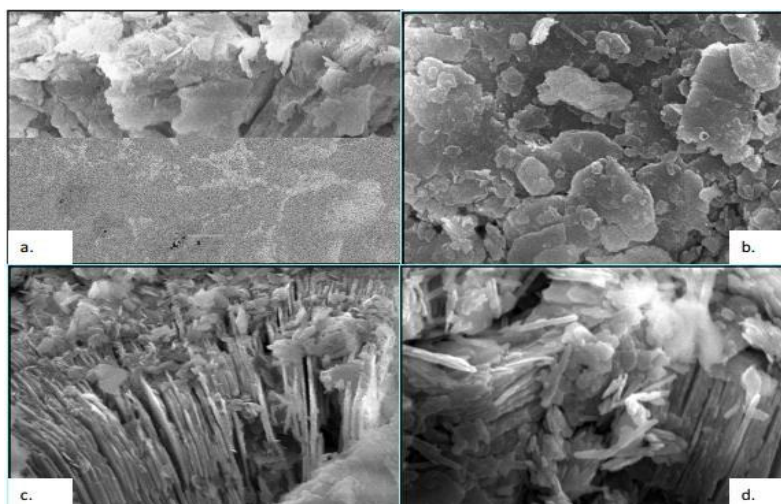


Figure 5 SEM of Nagar-Parkar Kaolin Deposit. (a) Irregular Stack of Kaolinite Particles. (b) Angular Edges of Kaolin Particles. (c) Lack of Hexagonal Booklet Structure. (d) Enlarged View of Image (c)

3.4 Porosity and Surface Area Analysis for Kaolin

3.4.1 The porosity and pore size distribution

The porosity and pore size distribution of raw kaolin can be found for SEM images by image processing technique using open source Image j software (1.51p). The 50 particle was selected from SEM images. The gray scale image thresholding (255) was applied to binerallized the image. The red regions showed the porosity in figure 6(a,b). The pore size distribution curve clearly indicate that the majority of the raw kaolin contains particles pore radius lies in the range of 1.29nm.[31].

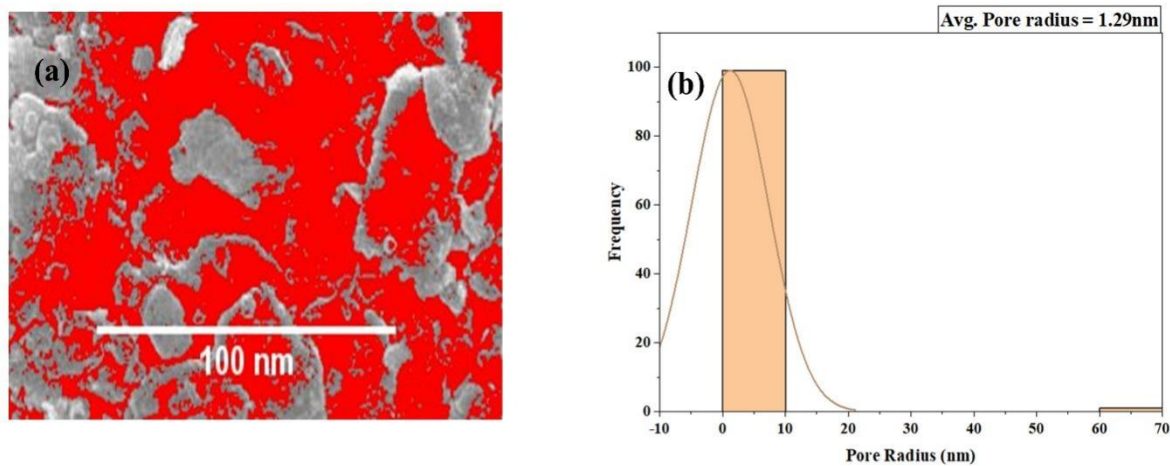


Figure 6 (a) Image Thresholding for Porosity Calculations (b) Pore size Distribution

3.4.2 Surface area and size distribution

The surface area of the raw kaolin obtained from Nagar parker can be found using SEM images by open source image processing tool shown in Figure 7 (a, b). The huge surface area of 122.97nm² clearly indicate the affinity of the pristine kaolin to adsorb dispersant and release impurities such as quartz, mica and Feldspar. It can be clearly estimated from figure 7 (a) that the majority of the particles size has uniform size distributions in the range of 5-25nm and surface area form 50-125 nm². This shows the Kaolin surface has more exposed surface area and size for adsorption of dispersant.

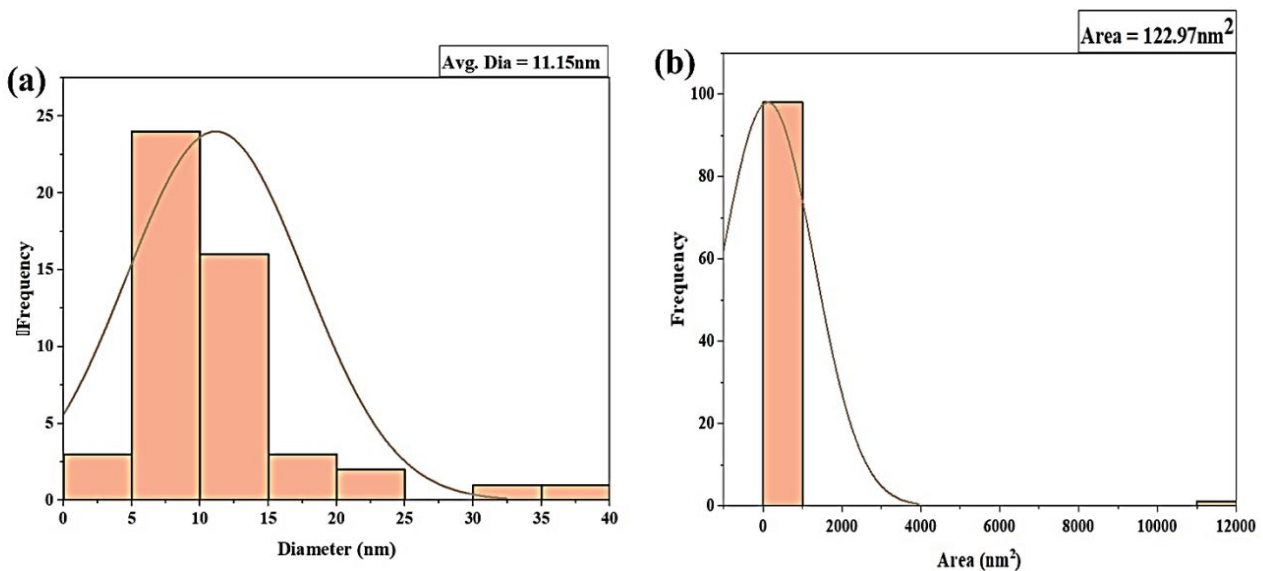


Figure 7 (a) Particle size Distribution Curve of Raw Kaolin. (b) Surface Area of Raw Kaolin

3.4.3 Surface roughness of kaolin

The surface roughness was also calculated from the image processing tools. The 3D surface plot of raw kaolin obtained from nagar paker confirmed by image Figure 8 (a)The average surface roughness Ra was calculated to be 24nm. The root mean square roughness was estimated to be as 20nm shown in Figure 8(b).

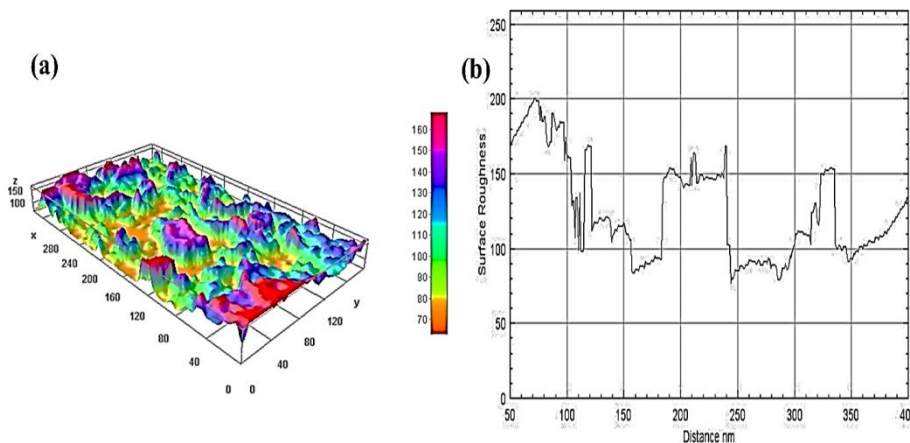


Figure 8 (a) 3D Surface Plot (b) Average Surface Roughness Plot of Raw Kaolin Obtained Form Nagar parker

3.4.4 Particle size distribution analysis

To analyze the particle size distribution in as received (Feed) and crushed kaolin sample, sieve analysis was performed. The data showing the particle size distribution are presented in Figure 9. Figure 9 explains that 50% of particles are less than 25 mesh. Similarly, 80% of as received sample passed through the screen size of 8 mesh. This shows that 80% of particles of kaolin are smaller than 8 mesh. Moreover, P₅₀, and P₉₀ of as received kaolin samples are 25, and 5 mesh respectively.

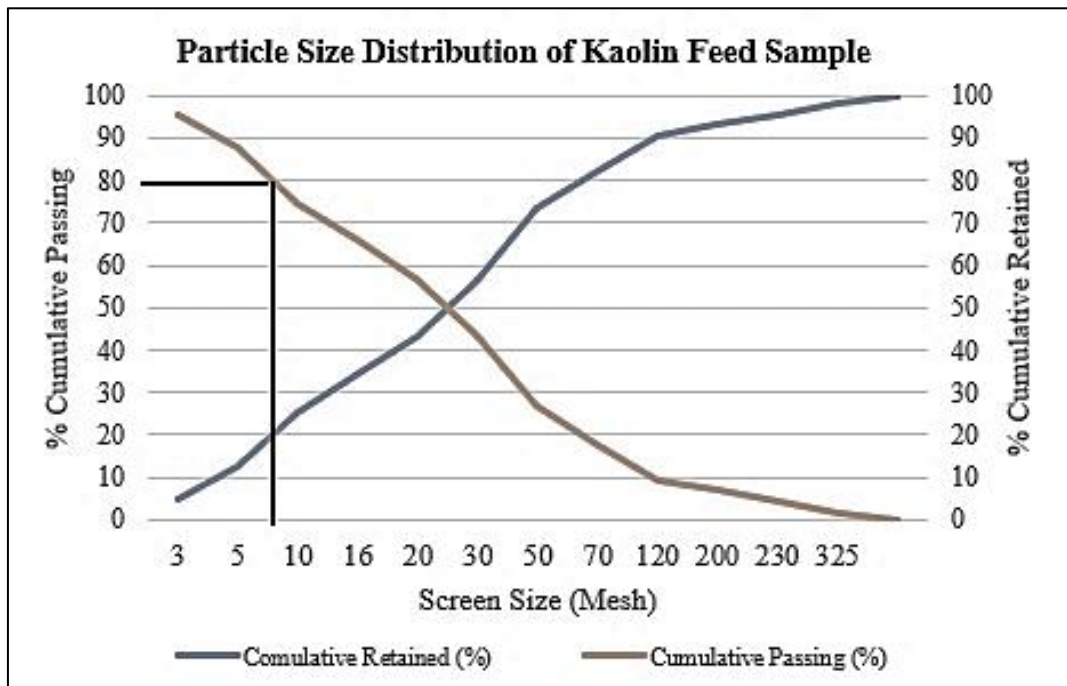


Figure 9 Graphical Representation of Size Distribution of as Received Kaolin

After crushing, size analysis was performed on a sample of roll crusher product. The distribution of particle sizes and their related weights of roll crusher products can be seen in Figure 9. Figure 10 shows the particle size distribution of the roll crusher product. Fifty percent of kaolin particles were retained on 27 mesh sieve size while 90% of particles were passed from 7 mesh sieve. Moreover, P₅₀, and P₉₀ of roll crushed kaolin samples are 25,12, and 7 mesh respectively.

The reduction ratio of the Roll Crusher product can be calculated by following the formula

$$\text{Reduction Ratio}_{80} = \text{Passing Feed Size} / \text{Passing Product Size}$$

$$\text{Reduction Ratio}_{80} = 2838\mu\text{m} / 1699.14\mu\text{m}$$

Reduction ratio = 1.67

The reduction ratio shows that by the ratio of 1.67 particles entered and left the roll crusher.

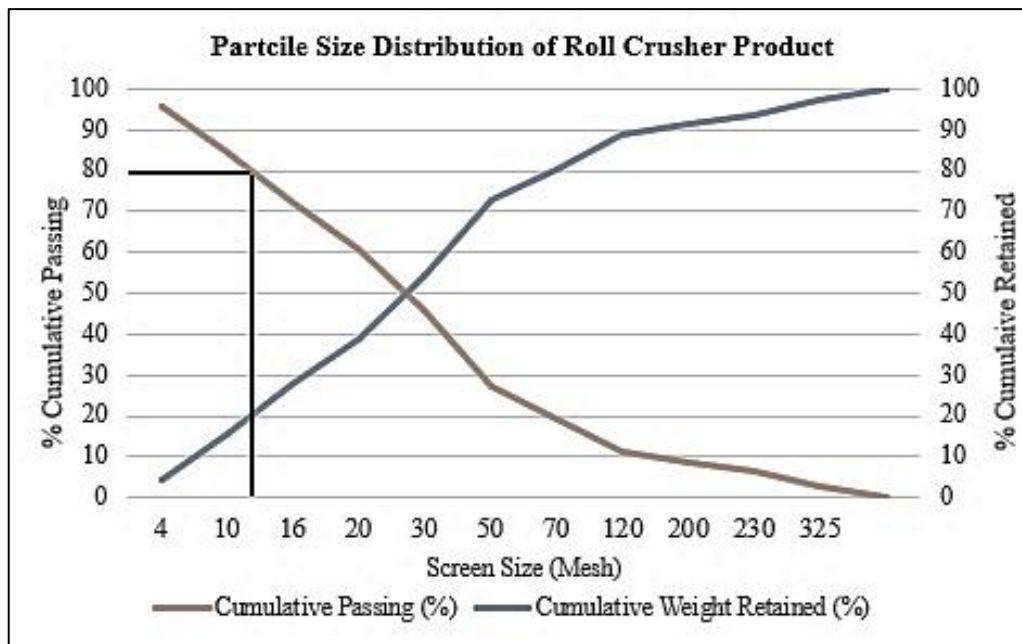


Figure 10 Graphical Representation of Size Distribution of Roll Crushed Kaolin

3.5 Experimental Analysis

The experimental design for the dispersion and sedimentation is shown in Table 4. Furthermore, the masses obtained in concentrate and tailings at different combinations of solid and dispersant dosage are presented in Table 5.

Table 4 Experimental Results Obtained after Experimentation

Run Order	Solid percentage (%)	Dispersant Dosage (%)	Mass in Concentrate (g)	Mass in Tailings (g)	Grade (%)	Recovery (%)
1	26.34	0.27	15.00	10.00	82.00	73.66
2	8.66	0.27	5.50	3.00	70.60	70.71
3	17.50	0.20	13.00	3.50	69.10	80.96
4	17.50	0.20	10.00	7.00	80.30	72.37
5	8.66	0.13	4.00	4.50	62.40	45.45
6	17.50	0.20	8.50	11.00	78.00	59.76
7	26.34	0.13	16.00	10.00	68.20	65.35
8	17.50	0.20	9.50	7.00	72.30	61.91
9	17.50	0.20	11.00	7.50	73.20	72.57
10	17.50	0.10	12.00	5.00	61.80	66.84
11	17.50	0.30	9.50	8.00	88.80	76.03
12	30.00	0.20	25.50	3.00	60.20	80.71
13	5.00	0.20	3.00	2.00	68.10	64.45
14	17.50	0.20	12.50	4.50	66.10	74.47

It can be seen from Table 4 that the maximum grade of kaolinite achieved is 88.80% with 1.7% quartz at run order 11. At this run order, the values for solid percentage and dispersant dosage are 17.5% and 0.3% and 0.2% respectively. The recovery is maximum at this combination at the cost of grade. Using average dispersant dosage, the grade has deteriorated which causes impurities to report in overflow instead of underflow. Moreover, optimum grade and recovery are obtained at run order 11 with solid percentage and dispersant dosage of 17.50% and 0.3% respectively. Using this combination, an 88.8% grade of kaolinite with 76.03% recovery is achieved. Grade and recovery are optimum because of the maximum adsorption of dispersant on kaolinite particles. The electrostatic repulsion on the edges of kaolinite particles resulted in de-agglomeration, which resulted in maximum grade with good recovery.

In experimental analysis we have seen that percentage of kaolinite increases from 59.6% to 88.8%. Figure 11 represents the comparison of increasing kaolinite grade and decreasing quartz percentage at different stages of experimentation. After screening, grade is increased because of selective grinding of kaolinite particles in pin mill. As quartz, titanium and other impurities are harder in nature. So, the impurities did not reduce as much as kaolinite and could not pass through 325 mesh sieve. And after sedimentation further grade is increased from 63.4% to 88.8% due to settlement of heavy impurities in bottom of cylinder and removal of suspended kaolinite.

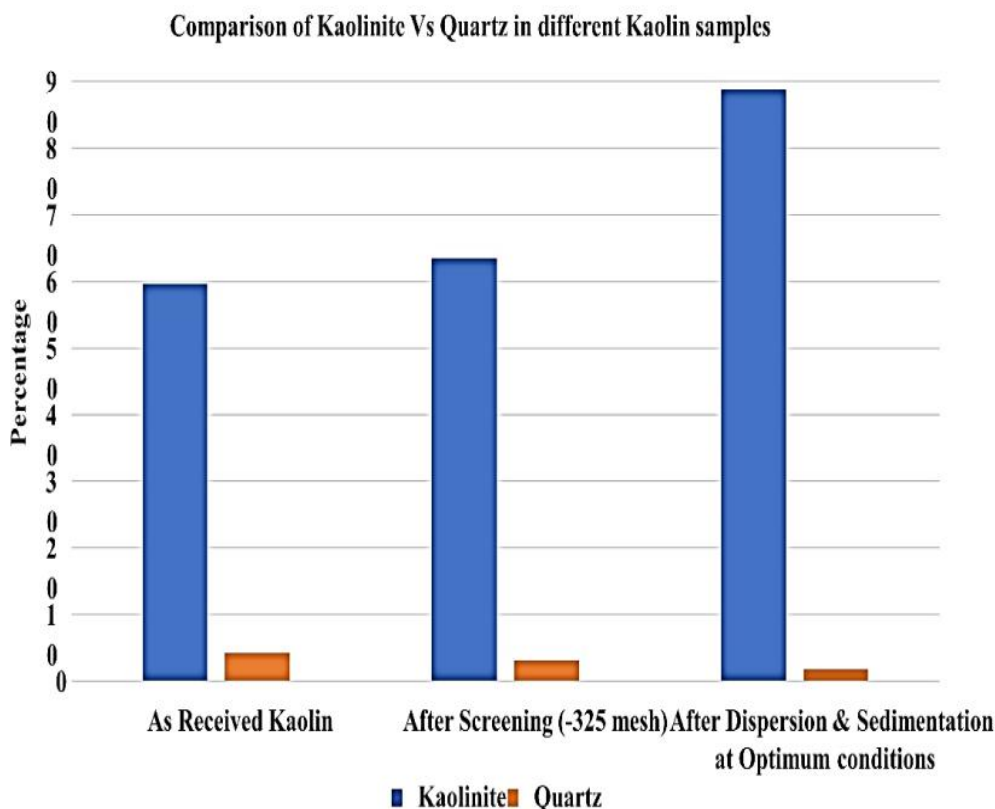


Figure 11 Comparison between Kaolinite and Quartz at Different Stages of Beneficiation

3.5 Statistical Analysis

The data obtained after the analysis of kaolin dispersion and sedimentation results was statistically analyzed using Central Composite Design. This design was used to determine the individual and interaction effects between parameters. The stepwise procedure was used to determine the regression equations for kaolin recovery and grade. In this procedure, the terms having P-values greater than the value of alpha specified were not included to maintain a hierarchical model at each step. The values of alpha used for both recovery and grade were maintained at α to enter = 0.05, and α to remove = 0.05. Based on our experimental results, Grade and recovery for kaolin dispersion and sedimentation experiments can be estimated using regression equations (1) and (2) by changing the solids percentage and dispersant dosage values in it.

$$\text{Kaolinite Grade} = 34.20 + 2.031 A + 106.4 B - 0.0556 A^*A \tag{1}$$

$$\text{Kaolinite Recovery} = 41.14 + 0.648 A + 82.3 B \tag{2}$$

Where A and B are solids percentage and dispersant dosage respectively.

3.5.1 Analysis of variance (ANOVA) for grade and recovery

3.5.1.1 For grade

ANOVA ensures the adequacy of the developed model based on p-value and Fisher test (F-value) in Table 5. The regression equation had a p-value of 0.009 which was less than the value of alpha in stepwise surface regression and thus showed its significance. The p-value of linear effects is less than the value of alpha which showed a linear relationship between the experimental conditions and regression equations. Moreover, the lower p-value of dispersant dosage (P = 0.003) than the p-value of solids percentage (P = 0.705), which indicates that it has a significant effect on the grade than solids percentage. The p-value of solids percentage*solids percentage is 0.05 showing this factor has a significant effect on the grade. For the lack of fit test, the p-value of 0.410, (p>0.005) was greater than the value of alpha. As a result, the model terms are insignificant. Coefficient of Determination (R-sq.) that considers the number of variables in a data set. It showed that 10% of points are insignificant that is overfitting the model. R-sq. (Adj.) removed

that 10% term. It determines that the model will predict 16.62% responses for new responses. The value of standard deviation (S) 5.46 or less for S is better because it indicates that observations are closer to the fitted line.

Table 5 Analysis of Variance in Grade in Response to Surface Regression

Source	DF	Adj. SS	Adj. MS	F-Value	P-Value
Model	3	597.373	199.124	6.68	0.009
Linear	2	457.302	228.651	7.67	0.010
Solids Percentage	1	4.542	4.542	0.15	0.705
Dispersant Dosage	1	452.761	452.761	15.19	0.003
<i>Square</i>	1	140.070	140.070	4.70	0.055
Solids percentage*Solids Percentage	1	140.070	140.070	4.70	0.055
Error	10	298.156	29.816		
Source	DF	Adj. SS	Adj. MS	F-Value	P-Value
Lack-of-Fit	6	198.290	33.048	1.32	0.410
Pure Error	4	99.867	24.967		
Total	13	895.529			

3.5.1.2. For Recovery

The regression equation for recovery was significant with a P-value of 0.031 which is less than the value of alpha in the stepwise procedure. The p-value of linear effects is less than the value of alpha which showed a linear relationship between the experimental conditions and recovery regression equation. For Lack of Fit, the p-value is 0.795, greater than the value of alpha. So, the model is insignificant for this value. The analysis of variance of recovery is shown in Table 6.

Table 6 Analysis of Variance in Recovery in Response Surface Regression

Source	DF	Adj. SS	Adj. MS	F-Value	P-Value
Model	2	533.8	266.89	4.87	0.031
Linear	2	533.8	266.89	4.87	0.031
Solids Percentage	1	262.7	262.72	4.79	0.051
Dispersant Dosage	1	271.1	271.06	4.94	0.048
Error	11	603.4	54.85		
Lack-of-Fit	7	284.3	40.61	0.51	0.795
Pure Error	4	319.1	79.77		
Total	13	1137.1			

By analyzing the trend of recovery, it is seen that recovery and dispersant dosage have a direct relation. The coefficient of determination showed that 46.94% of the points fell within the regression line while 9% of terms were insignificant. Moreover, the model will predict 14.46% responses for the new observations and 7.40 was the standard regression error.

3.6 Optimal Conditions for Grade and Recovery

In Minitab, once surface regression model was developed, optimum conditions for sedimentation were estimated for both grade and recovery using a response optimizer tool. Plots in Figure 9 show different settings of variables for grade. The vertical red lines on the graph represent the current factor settings for the prediction of maximum grade i.e. 84.66% when all the factors are at their highest settings (Solids percentage = 18.26% and dispersant dosage = 0.3% respectively). It is seen that grade has a direct relation with dispersant dosage, i.e., increasing the dispersant dosage beyond 0.3% might result in a higher value for grade. Moreover, the grade at these values of solid percentage and dispersant dosage is maximum because the higher value of the dispersant used prevented the aggregation of kaolin particles by inducing electrostatic repulsion between them via adsorbing on their surface [32], which resulted in a better grade of kaolinite. The desirability factor of 0.85525 indicates the model is showing good solutions.

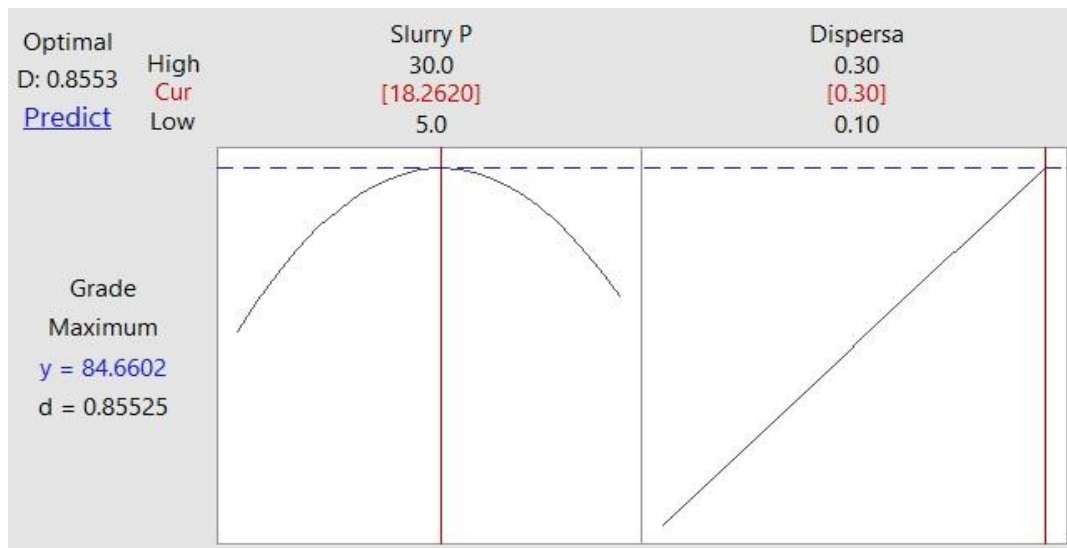


Figure 12 Optimization Plot for Grade Using Minitab

Similarly, the optimization plot for maximum recovery is shown in Figure 12. It predicted that 85.28% kaolinite recovery can be obtained using solids percentage and dispersant dosage of 30% and 0.3% respectively. The recovery is maximum at this dosage as the maximum amount of the dispersant was adsorbed on the surface of particles, resulting in better recovery in the overflow. Furthermore, the recovery model shows an excellent optimal solution as it has a composite desirability of 1.



Figure 13 Optimization Plot for Recovery

In Figure 13, optimization plots of combined grade and recovery are summarized. It is analyzed that the trend of lines is same as mentioned in the above graphs shown in Figure 12 and Figure 13. It is indicated that the model shows the composite desirability of 89% for the maximum predicted grade and recovery. It is predicted that maximum grade and recovery of 83.81% and 80.26% can be obtained using a solids percentage of 22% and dispersant dosage value of 0.3%. Further, the increasing trend lines indicate that by increasing dispersant dosage above 0.3%, both grade and recovery are highly likely to increase. Based on the optimization plots for maximum grade and recovery, an experiment was performed to check the trend of grade and recovery at 0.6% dispersant dosage. The results showed that the kaolinite grade at 0.6% dispersant dosage decreased to 79.8% whereas, the recovery was increased to 86.3% as shown in Figure 14 and Figure 15.

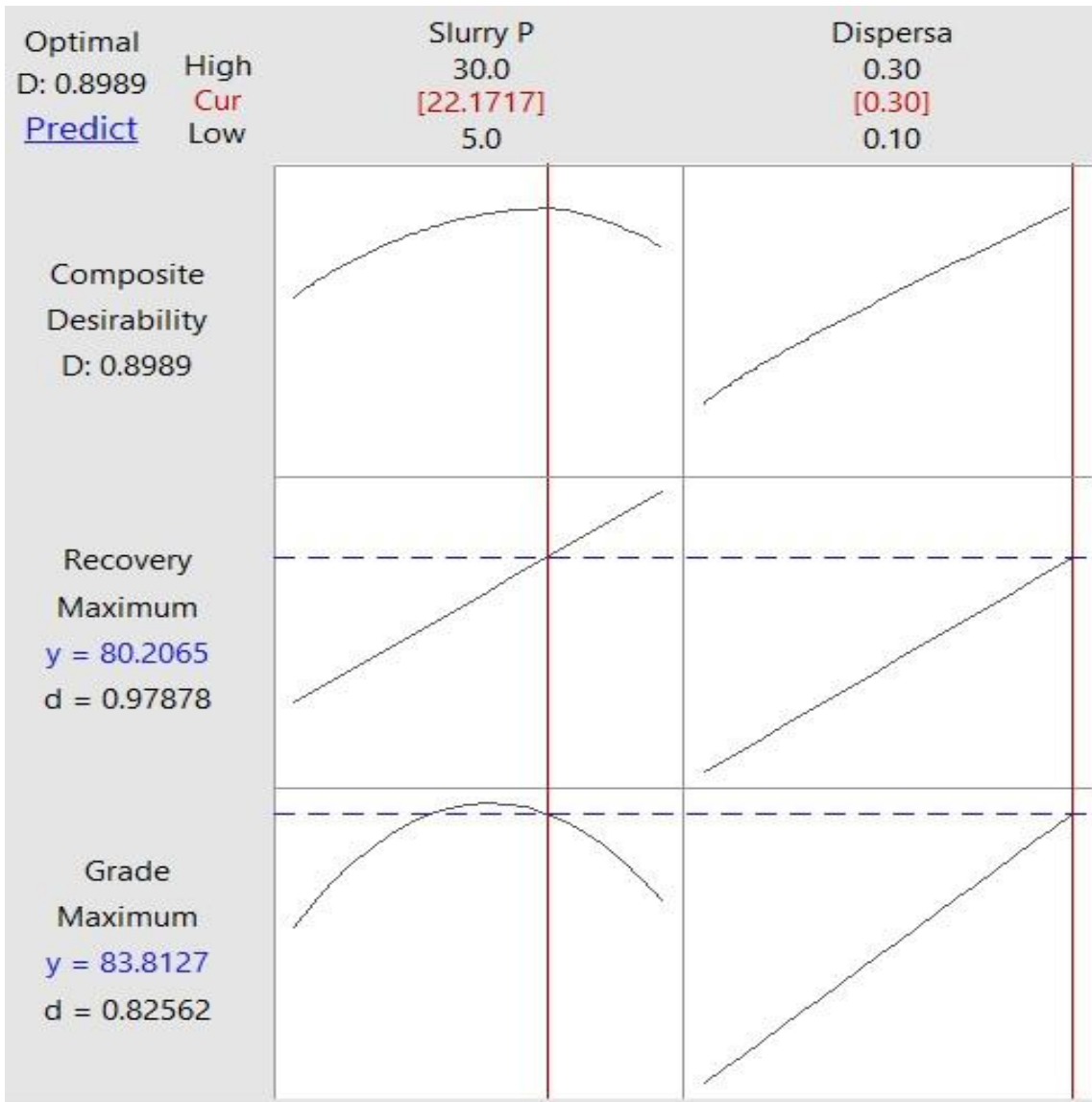


Figure 14 Optimization Plot for Both Maximum Grade and Recovery

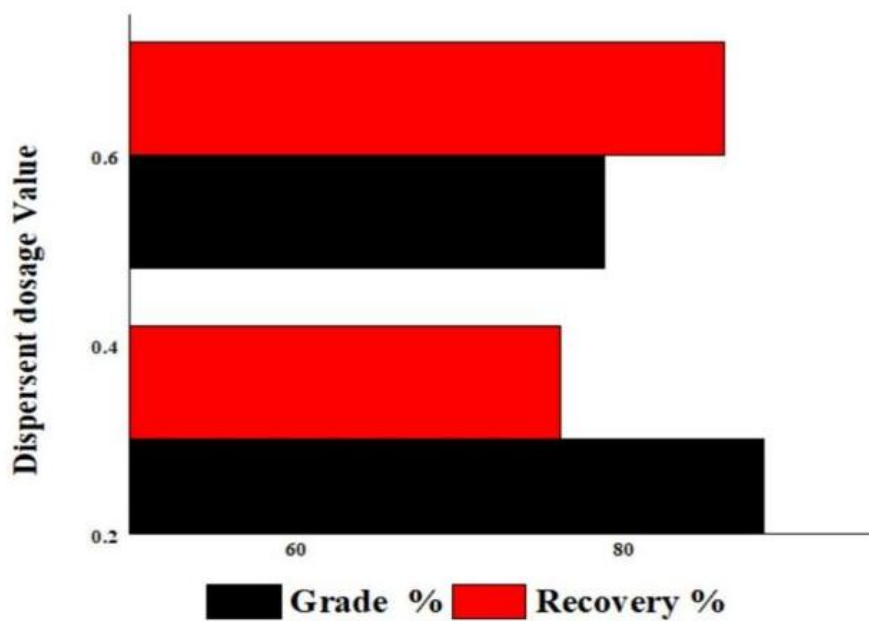


Figure 15 Grade and Recovery Values at 0.3 and 0.6 Percent Dispersant Dosage

3.7 Comparison of Experimental and Statistical Analysis

For the removal of heavy impurities from kaolin by sedimentation, optimum conditions acquired from experimental and statistical analysis are shown in Table 7. It is seen that the optimum value for dispersant dosage is the same in both analyses (i.e. 0.3%). The optimum value for solids percentage from experimental analysis is 17.50% while it is slightly higher in the case of statistical analysis.

Table 7 Comparison of Optimum Conditions Obtained in this Study from Experimental and Statistical Analysis

Factors	Experimental Analysis	Statistical Analysis
Dispersant Dosage (STPP)	0.3%	0.3%
Solid Percentage	17.50%	22%
Max. Grade	88.8%	83.81%
Max. Recovery	76.03%	80.20%

By analyzing the conditions given in Table 8, it is concluded that there is a difference between experimental and statistical results. Statistical results are not suitable due to the lack of fit. The prediction of regression equations obtained from dispersion and sedimentation experiments prediction is very low. It will predict responses for new observation of grade and recovery with an accuracy of 16.62% and 14.46% respectively. Moreover, the model gives less grade as compared to actual results. On the other hand, optimum conditions obtained through experimental analysis give an 82.5% kaolinite grade with a 78.3% recovery value. Hence, the best-selected conditions for the kaolin sedimentation observed in this study are given in Table 8.

Table 8 Optimum Values for Dispersant Dosage and Solid Percentage Selected for Kaolin Sedimentation

Factors	Optimum Conditions
Dispersant Dosage	0.3%
Solid percentage	17.50%

3.8 Contour Plots

Contour plots display a two-dimensional view in which all the points that have the same response are connected to produce contour lines of constant responses. It shows the fitted response i.e. grade and recovery related to two variables. In Figure 16, the response surface generated a graph by calculating grade (z-value) using the x-variable solid percentage and y-variable dispersant dosage. It is seen that grade is maximum by using the highest dispersant dosage value and solid percentage within the range between (16% - 20%). Whereas in Figure 17, a maximum recovery of >80% is predicted when using the highest value of both variables.

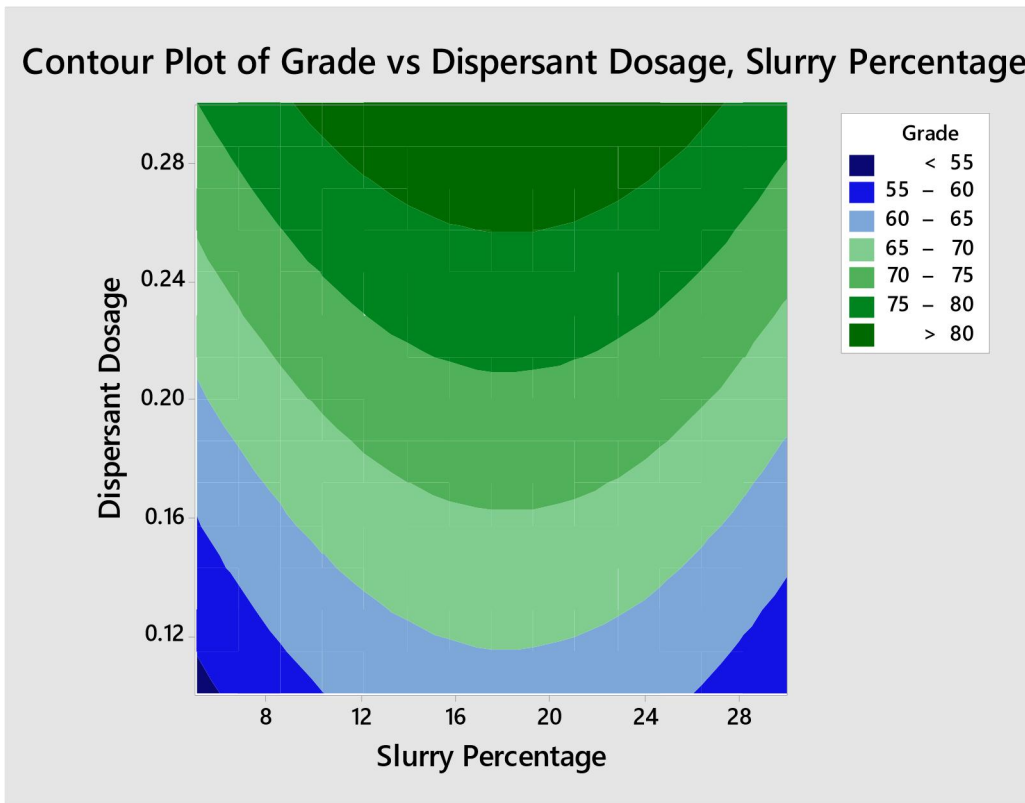


Figure 16 Contour Plot of Grade against the Solids Percentage and Dispersant Dosage

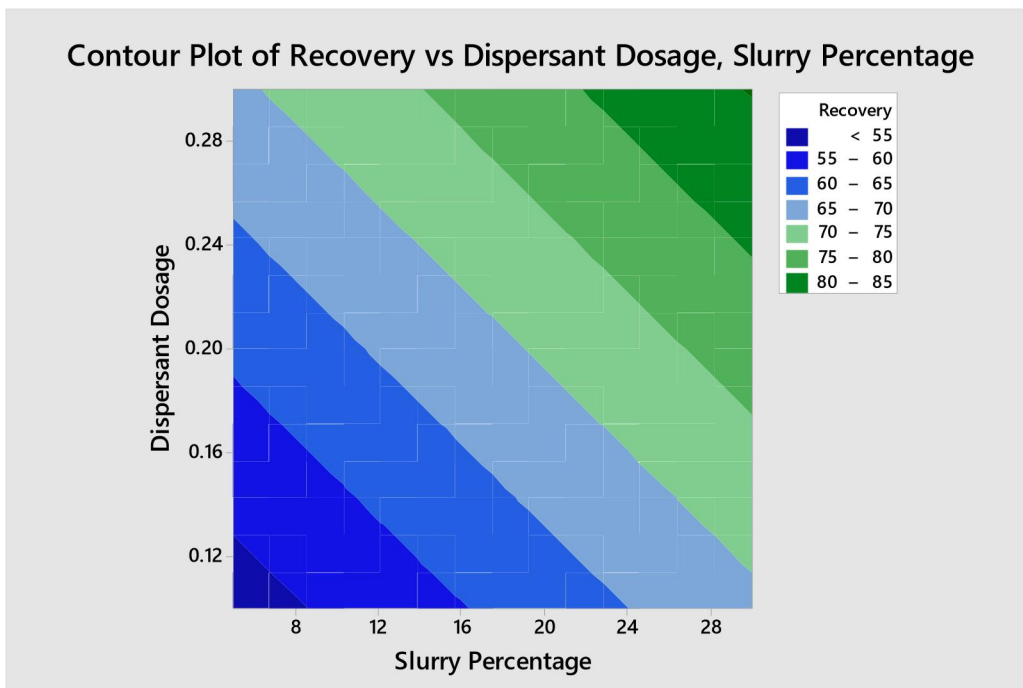


Figure 17 Contour Plot of Recovery against the Solids Percentage and Dispersant Dosage

3.9 Validation

To ensure the accuracy of developed predictions, a set of experiments was carried out according to the optimum operating conditions in Figure 15. The XRD result of the concentrate is shown in Figure 18. The difference in recovery between actual and predicted values was 3.97% and in grade was 4.90%.

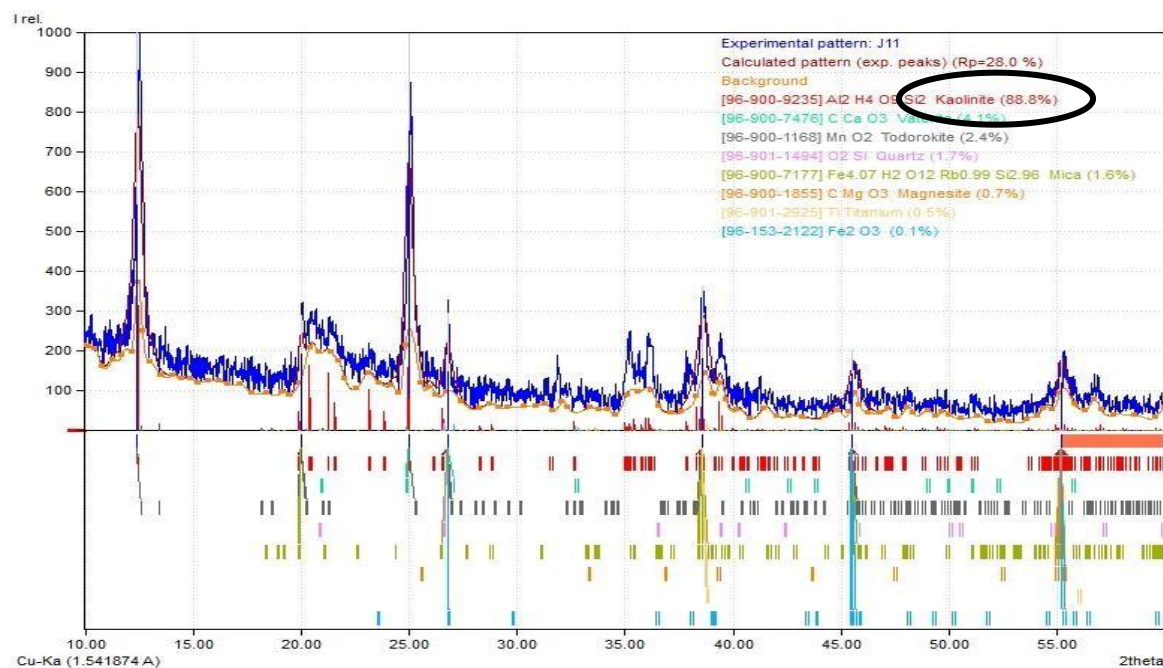


Figure 18 XRD Pattern of Concentrate with Maximum Kaolinite Content and Recovery

3.10 Comparison with Other Methods

The various methods have been developed for purification of kaolin as shown in Table 9. Fluoride has been successfully removed from kaolin by sedimentation 90% recovery was obtained [33]. Quartz, mica and feldspar were removed from Nagar Parkar Sindh, Pakistan by dry beneficiation the 91.2 % grade and recovery = 27.1% was obtained [30]. The present study has provided better grade and recovery compared to previous studies. This confirms the process is scalable.

Table 9 Comparison with Other Methods

Target removal	leachate	Method	Removal	Mechanism	Ref.
Fluoride	Kaolinite of Tabelbala	Dispersion and sedimentation	90	Electrostatic repulsion on the kaolinite surface	[33]
Al & Fe	kaolin	Poly-aluminum-ferric-sulfate coagulant	Al (98.8%), Fe (98.1%)	Sulphuric acid (H ₂ SO ₄) intercalation assisted activation based mechanism	[34]
Quartz, Mica &	Kaolin	Dry-beneficiation	91.2 % grade Recovery = 27.1%	Sulphuric acid (H ₂ SO ₄) intercalation assisted activation based mechanism	[30]
Fe & TiO ₂	kaolin	Selective flocculation	88% grade Recover 60%	Electrostatic repulsion on the kaolinite surface	[35]
Quartz, Mica & kaolin	Weathered Granite	Selective flocculation	Recover 99.51%	Electrostatic repulsion on the kaolinite surface	[27]
Al	Rare earth leachate	Sedimentation and flocculation	97% recovery	Electrostatic repulsion on the kaolinite surface	[2]
Kaolinite, Quartz, titaniferous, mica, feldspar	kaolin	Dispersion and sedimentation	88.8% grade with 76.03% kaolinite recovery	Electrostatic repulsion on the kaolinite surface	Present study

4 CONCLUSIONS

The purpose of this study was to remove heavy impurities from Nagar Parkar, Sindh, Pakistan by using an economical, less energy-intensive, and environment-friendly technique. Dispersion and sedimentation processes were used for the removal of heavy impurities from kaolin. The particle size analysis of as received kaolin from Nagar-Parkar showed that 80% of kaolin particles were smaller than 8 mesh. The XRD pattern of as received kaolin showed the presence of 59.6% kaolinite along with vaterite 11.7%, hematite 6.4%, todorokite 6.1%, magnesite 5.7%, mica 5%, quartz 4.7% and titanium 1.2%. The kaolinite grade in the undersize fraction of 325 mesh sieve was improved from 59.6% to 63.4%, while the percentages of impurities such as vaterite, magnesite, quartz, and titanium also decreased from 11.7% to 5.7%,

5.7% to 2.9%, 4.7% to 3% and 1.2% to 0.9% respectively. The experimental results showed that the maximum possible grade of 88.8% with 76.03% kaolinite recovery was obtained using solid percentage and dispersant dosage of 17.5% and 0.3% respectively. Regression equations predicted that 83.81% grade with 80.20% kaolinite recovery could be obtained using solid percentage and dispersant dosage values of 22% and 0.3% respectively. This means that increasing the dosage after a certain value between 0.3% and 0.6% dispersant dosage will start deteriorating the grade. On the other hand, the kaolinite recovery value increased from 79.8% (0.3% dispersant dosage) to 86.31% (0.6% dispersant dosage). Overall, this study successfully improves the grade of Nagar Parkar kaolin from 59.6% to 88.8% with 79.8% kaolinite recovery. This study confirms the suitability of wet beneficiation the best approach for kaolin purification on large commercial scale. It is also recommended to use ball mill with rubber coated steel balls instead of pin mill for efficient grinding.

COMPETING INTERESTS

The authors have no relevant financial or non-financial interests to disclose.

ACKNOWLEDGMENTS

We are also obliged to UET Lahore Mining engineering department Faculty and staff members (lab assistant, Mineral Processing lab), who assisted us in the performance of dispersion and sedimentation experiments.

REFERENCES

- [1] A J Whitworth, E Forbes, I Verster V, et al. Review on advances in mineral processing technologies suitable for critical metal recovery from mining and processing wastes. *Clean. Eng. Technol*, 2022, 7: 100451.
- [2] X Wu, J Feng, F Zhou, et al. High sedimentation efficiency and enhanced rare earth recovery in the impurity removal process of rare earth leachate by flocculation system. *Environ. Chem. Eng*, 2024, 12(3): 112626.
- [3] T Jamil, et al. Treatment of Textile Wastewater by a Novel Clay/TiO₂/ZnO-Based Catalyst, Applying a Synergic Catalytic Ozonation–Electroflocculation Process. *Catalysts*, 2023, 13: 9.
- [4] M Hernández-Chávez, et al. Thermodynamic analysis of the influence of potassium on the thermal behavior of kaolin raw material. *Physicochem. Probl. Miner. Process*, 2020, 57(1): 39–52.
- [5] X Kang, Z Xia, R Chen, et al. Effects of inorganic ions, organic polymers, and fly ashes on the sedimentation characteristics of kaolinite suspensions. *Appl. Clay Sci.* 2019, 181: 105220.
- [6] F M G Madrid, M P Arancibia-Bravo, F D Sepúlveda, et al. Ultrafine Kaolinite Removal in Recycled Water from the Overflow of Thickener Using Electroflotation: A Novel Application of Saline Water Splitting in Mineral Processing. *Molecules*, 2023, 28: 9.
- [7] V Singh, S Nag, N Gurulaxmi Srikakulapu, et al. Development of a novel magnetic separator for segregation of minerals of dissimilar electromagnetic properties. *Miner. Eng*, 2023, 193: 108009.
- [8] Y M Kwon, S J Kang, G C Cho, et al. Effect of microbial biopolymers on the sedimentation behavior of kaolinite. *Geomech. Eng*, 2023, 33(2): 121–131.
- [9] X Li. Selective flocculation performance of amphiphilic quaternary ammonium salt in kaolin and bentonite suspensions. *Colloids Surfaces A Physicochem. Eng. Asp*, 2022, 636: 128140.
- [10] J Zhao, Y Zhang, X Wei, et al. Chemisorption and physisorption of fine particulate matters on the floating beads during Zhundong coal combustion. *Fuel Process. Technol*, 2020, 200: 106310.
- [11] Y H Jun, Y S Nee, C W Qi, et al. Bioleaching of kaolin with *Bacillus cereus*: Effects of bacteria source and concentration on iron removal. *Sustain. Sci. Manag*, 2020, 15(4): 91–99.
- [12] M S Prasad, K J Reid, H H Murray. Kaolin: processing, properties and applications. *Appl. Clay Sci.* 1991, 6(2): 87–119.
- [13] M F Cheira, M N Rashed, A E Mohamed, et al. Removal of some harmful metal ions from wet-process phosphoric acid using murexide-reinforced activated bentonite. *Mater. Today Chem*. 2019, 14: 100176.
- [14] M Afshar, A Alipour, R Norouzbeigi. Kaolin-based stable colloidal nano-silica: Peptization factors and stability assessments via designed experiments. *Results Eng*, 2024, 21: 101654.
- [15] Y Gao, X Fu, Z Pan, et al. Surface complexation model theory application in NaOL and CTAB collector adsorption differences of diaspore and kaolinite flotation. *Sep. Purif. Technol*, 2022, 295: 121288.
- [16] J Ku, K Wang, Q Wang, et al. Application of Magnetic Separation Technology in Resource Utilization and Environmental Treatment. *Separations*, 2024, 11: 5.
- [17] I Tezyapar Kara, S T Wagland, F Coulon. Techno-economic assessment of bioleaching for metallurgical by-products. *Environ. Manage*, 2024, 358: 120904.
- [18] W Leiva, et al. Sodium acid pyrophosphate as a rheological modifier of clay-based tailings in saline water. *Appl. Clay Sci*, 2024, 253: 107352.
- [19] E Durgut, M Cinar, M Terzi, et al. Evaluation of Different Dispersants on the Dispersion/Sedimentation Behavior of Halloysite, Kaolinite, and Quartz Suspensions in the Enrichment of Halloysite Ore by Mechanical Dispersion. *Minerals*, 2022, 12: 11.
- [20] Q Ma, Y Li, J Liu, et al. Enhanced dispersing properties of kaolin due to high-strength kneading process. *Appl. Clay Sci.* 2024, 247: 107218.

- [21] A K M M Hasan, S C Dey, M Mominur, et al. Kaolinite / TiO₂ / ZnO Based Novel Ternary Composite for Photocatalytic Degradation of Anionic Azo Dyes Department of Applied Chemistry and Chemical Engineering , Faculty of Engineering and Corresponding Author The authors are grateful to the Centre fo.
- [22] S Ismail, V Husain, G Hamid, et al. Physico-chemical characteristics of Nagar Parkar kaolin deposits, Thar Parkar district, Sindh, Pakistan. *Himal. Earth Sci*, 2015, 48: 1.
- [23] 1-9. et al. Scholar (3). *Annals of Tourism Research*, 2015, 3(1): 1–2.
- [24] M Taran, E Aghaie. Designing and optimization of separation process of iron impurities from kaolin by oxalic acid in bench-scale stirred-tank reactor. *Appl. Clay Sci*. 2015, 107: 109–116.
- [25] A Gad, B A Al-Mur, W A Alsiary, et al. Optimization of Carboniferous Egyptian Kaolin Treatment for Pharmaceutical Applications. *Sustainability*, 2022, 14: 4.
- [26] M Rabbani, J Werner, A Fahimi, et al. Innovative pilot-scale process for sustainable rare earth oxide production from coal byproducts: A comprehensive environmental impact assessment. *Rare Earths*, 2024.
- [27] H Huang, S Li, H Gou, et al. Efficient Recovery of Feldspar, Quartz, and Kaolin from Weathered Granite. *Minerals*, 2024, 14: 3.
- [28] A Shete, A Chavan, P Potekar, et al. Modification of physicochemical properties of chitosan to improve its pharmaceutical and agrochemical potential applications. *Int. J. Biol. Macromol*, 2024, 267: 131404.
- [29] M Omotioma, O N Dorothy, G O Mbah. Effects of process factors on the characteristics of water based mud viscosified by kaolin and bentonite, 2024, 192(April): 270–288.
- [30] M B Hayat, M Danishwar, A Hamid, et al. Quadratic mathematical modeling of sustainable dry beneficiation of kaolin. *Minerals*, 2021, 11: 4.
- [31] W Liu, Y Zhang, S Wang, et al. Effect of pore size distribution and amination on adsorption capacities of polymeric adsorbents. *Molecules*, 2021, 26: 17.
- [32] C Wu, et al. Fe(II)-catalyzed phase transformation of Cd(II)-bearing ferrihydrite-kaolinite associations under anoxic conditions: New insights to role of kaolinite and fate of Cd(II). *Hazard. Mater*, 2024, 468: 133798.
- [33] N Nabbou, et al. Removal of fluoride from groundwater using natural clay (kaolinite): Optimization of adsorption conditions. *Comptes Rendus Chim*, 2019, 22(2): 105–112.
- [34] J Chen, et al. High-efficiency extraction of aluminum from low-grade kaolin via a novel low-temperature activation method for the preparation of poly-aluminum-ferric-sulfate coagulant. *Clean. Prod*, 2020, 257: 120399.
- [35] A B Luz, A Middea. Purification of Clay By Selective Flocculation. 43rd Annu. Conf. Metall. CI, 2004, 243–253.

LOW-CARBON TRANSFORMATION OF CHINA'S COAL-FIRED POWER INDUSTRY: CURRENT SITUATION INSIGHTS AND TREND PROSPECTS

Rui Yang

School of Management, China University of Mining and Technology-Beijing, Beijing 100083, China.
Corresponding Author: Rui Yang, Email: yangrui@student.cumtb.edu.cn

Abstract: Considering the importance of global climate change mitigation, this paper focuses on the low-carbon transformation of China's coal-fired power industry. China's coal-fired power industry is large-scale. The geographical distribution of power plants is uneven, and the technical level shows an unbalanced pattern. The existing units are mainly those with capacities of 300-600MW and 600-1000MW, while most of the newly added units are advanced ones with high parameters. Although the proportion of coal-fired power installed capacity has decreased to 36.9% due to new energy, it still plays a crucial role in power supply. Clean coal technologies, such as ultra-supercritical units, have developed well, and technologies like green ammonia co-firing and CCUS have also made good progress. Coal-fired power is of vital importance in ensuring power security, system regulation, centralized heating, and reducing energy consumption costs. In terms of policies, the "1+N" system and local policies promote the low-carbon transformation.

Keywords: Coal-fired power; Power industry; China; Low-carbon transformation

1 INTRODUCTION

With the global high-level attention to climate change issues, the control of greenhouse gas emissions has become a consensus in the international community. As one of the world's largest energy consumers and carbon emitters, China shoulders significant responsibilities in addressing climate change. In the past few decades, China's economy has developed rapidly, and the energy demand has been continuously growing. Coal, as one of China's major energy sources [1], plays an important role in power. However, the traditional coal-fired power methods have problems such as low energy utilization efficiency and high carbon emissions, which run counter to the requirements of China's carbon neutrality goal [2].

Therefore, the low-carbon transformation of the coal-fired power industry is of utmost significance for China's sustainable energy development [3]. Achieving a low-carbon transformation can effectively reduce coal consumption and carbon dioxide (CO₂) emissions, mitigate the negative impact on the environment, and propel China's transition towards a green and low-carbon economy. Through technological innovation and industrial upgrading, the energy utilization efficiency of coal-fired power can be improved, power costs can be reduced, and the competitiveness of China's energy industry can be enhanced [4]. The low-carbon transformation of the coal-fired power industry can also drive the development of related industries, such as new energy, energy conservation, and environmental protection, injecting new impetus into economic growth.

The development status and trends of the low-carbon transformation of China's coal-fired power industry has important practical significance for formulating scientific and reasonable policies and measures, promoting the sustainable development of the coal-fired power industry, and achieving China's emission control goals [5]. Research on the low-carbon transformation of the coal-fired power industry can provide a basis for decision-making for China's departments, guiding them to formulate more effective policies to promote energy structure adjustment and energy conservation and emission reduction. For coal-fired power enterprises, understanding the trends and paths of low-carbon transformation can help enterprises make early arrangements, increase investment in technological research and development, and improve their own competitiveness. Research in this field can also provide references for the academic community, promoting the development and improvement of relevant theories.

2 THE CURRENT STATUS OF CHINA'S COAL-FIRED POWER INDUSTRY

2.1 Geographical Distribution of Power Plants

The current situations of coal-fired power units vary in different regions of China. In the Northeast region, units with a capacity of 300,000 kilowatts and above are dominant. Some of them need energy-saving and flexibility retrofits to adapt to the consumption of new energy and peak-shaving of the power grid. The North China region, being a major coal-producing province, has a huge installed capacity of coal-fired power. The proportion of cogeneration units exceeds 50%. However, there are many small and medium-sized units, which need to be upgraded, retrofitted, and backward production capacity phased out. Also, due to its proximity to Beijing and Tianjin, strict environmental protection requirements are in place. In the East China region, the scale of coal-fired power ranks first in the country. There are many self-supplied power plants, and the proportion of large-scale units is relatively high, but some small-

scale units need to be phased out or retrofitted. Some units have already undergone flexibility retrofits to meet the demand for new energy integration. In the Central China region, large-scale units with a capacity of 600,000 kilowatts and above are dominant. The region is actively promoting retrofit and upgrade and strengthening power grid interconnection. In the Northwest region, the installed capacity of coal-fired power is large and diverse in types. It is necessary to accelerate flexibility retrofits to ensure the power grid operation and new energy consumption. In the future, flexibility retrofits are needed to promote energy transformation. In the South region, the 1-million-kilowatt ultra-supercritical units along the coast of Guangdong Province are dominant. The region is promoting multi-energy complementarity to improve comprehensive utilization efficiency. In other provinces, clean energy will be the main focus in the future. Generally speaking, the distribution of coal-fired power plants in China is shown in Figure 1 and has the following characteristics.

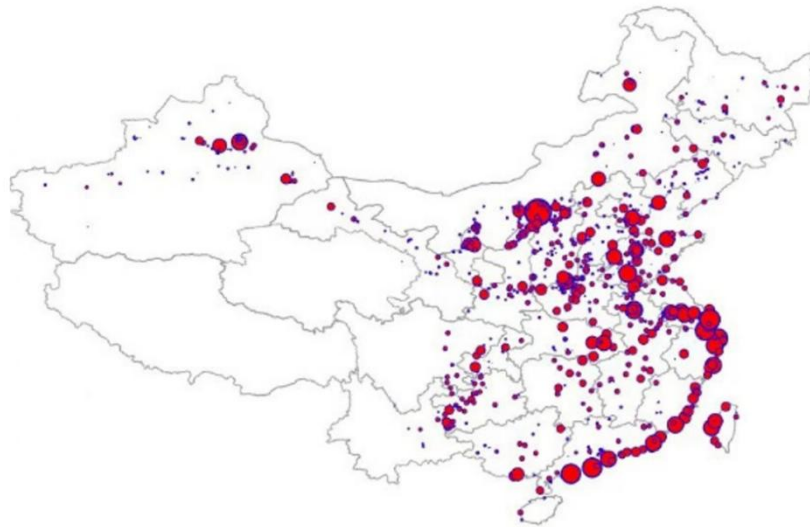


Figure 1 Distributions of all China's Coal-Fired Power Plants, with Capacity Sizes

Source: https://www.gov.cn/guoqing/2017-07/28/content_5043915.htm

First, the geographical distribution is unbalanced. The distribution of coal-fired power is significantly influenced by the distribution of coal resources. Coal-fired power is mainly concentrated in regions with abundant coal reserves. For instance, in China, Shanxi, Inner Mongolia, and Shaanxi are major coal-producing provinces. Besides resource-rich areas, coal-fired power also has a certain distribution in regions with developed economies and high electricity demand. Take the eastern coastal areas of China as an example. Although they are relatively scarce in coal resources, due to their developed industries and dense population, the demand for electricity is huge.

Secondly, the focus is close to the consumption centers, but there is still a need for power transmission from the west to the east. Some coal-fired power enterprises are located near energy consumption centers, which helps to reduce power losses during transmission. Excessively long power transmission distances will lead to increased power losses. Building coal-fired power facilities near consumption centers can effectively reduce such losses and improve energy utilization efficiency. However, coal-fired power in China is also supplied across regions. There is a mismatch between the coal-producing areas and the energy consumption centers. It is necessary to build high-voltage transmission lines to transport coal-fired power from the producing areas to regions with high demand. China's "West-to-East Power Transmission" project includes a large amount of coal-fired power transmission, transporting electricity from coal-rich areas in the west to the economically developed eastern regions.

Furthermore, the technical level shows a pattern of "higher in the south and lower in the north". In regions with a higher technical level and stronger economic strength, coal-fired power enterprises tend to adopt more advanced power-technologies. For example, ultra-supercritical coal-fired power-technology is mainly concentrated in some coastal areas with developed economies and high requirements for environmental protection and energy efficiency. In some relatively underdeveloped regions, traditional and less efficient coal-fired power technologies still dominate. These regions may find it difficult to quickly update their power-technologies due to limited funds and difficulties in technology introduction. This difference in technical level has led to uneven development quality and environmental protection levels of the coal-fired power industry in different regions, and also affects the overall pattern of coal-fired power distribution.

2.2 The Technical Levels of Current Power Units

Based on the cross-comparison between China's Coal-fired Power Unit-level Database and IEA statistical data [6-7], the capacity levels of existing coal-fired generator sets and incremental projects in China are shown in Figure 2. The existing capacity is approximately 1.109 billion kilowatts. There are still 94 million kilowatts and 202 million kilowatts of coal-fired power projects under construction and awaiting construction respectively. In particular, the planning and

construction of ultra-high-voltage power grids have become one of the key projects of the "new infrastructure". Regarding the structure of coal-fired power installed capacity, among the existing units nationwide, the two types of units with capacities of 300-600MW and 600-1000MW are dominant. The units under construction and awaiting construction are mainly large-scale units with higher parameters. The proportion of units with capacities of 600-1000MW and above 1000MW is much higher than that of other types. With the construction and commissioning of advanced incremental units and the improvement of the quality and efficiency of existing units, the power-efficiency of coal-fired power will be further enhanced.

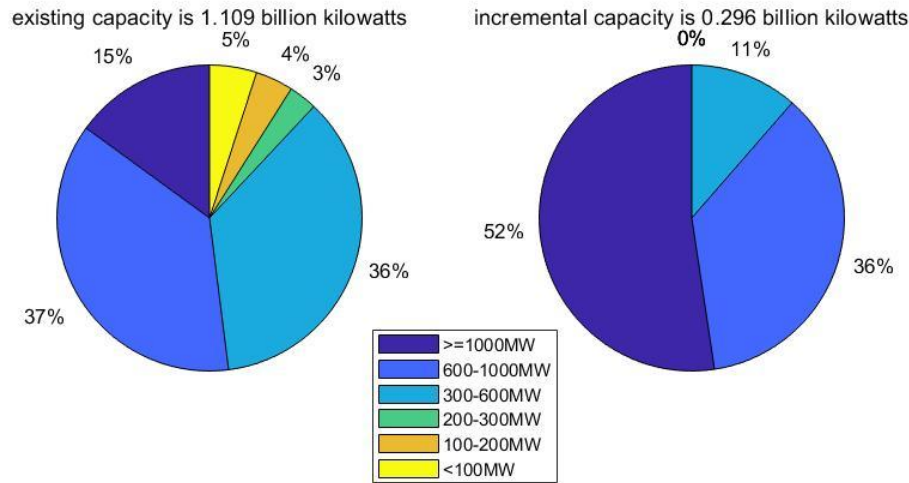


Figure 2 The Composition of China's Existing and Incremental Coal-Fired Power Units

In recent years, through measures such as "building large-scale units while phasing out small-scale ones", "equivalent replacement", and eliminating backward units, the energy efficiency of China's existing coal-fired power units has been effectively improved. The coal consumption per kilowatt-hour is approximately 305 grams of coal equivalent (gce/kWh), which is already better than that of developed economies such as the United States and Germany. At the same time, a large number of newly added coal-fired power projects are high-parameter coal-fired power units of 1000MW and above. The coal consumption per kilowatt-hour of units under construction and to be constructed is even as low as 276 gce/kWh. Therefore, the relatively short service life of China's coal-fired power units means that large-scale elimination in the short term is less feasible, and improper transformation may lead to higher risks.

With the rapid development of China, the electricity consumption of the whole society has been continuously increasing, putting forward higher requirements for power supply. To ensure the leapfrog development of China's power industry and provide affordable and stable electricity for the country's economic and social development, coal-fired power plays a crucial role. As shown in Figure 3, from 2009 to 2023, the installed capacity of coal-fired power continued to rise. However, with the increase in the installed capacity of new energy power, the proportion of coal-fired power installed capacity has dropped to 36.9%, a decrease of 23.4% over ten years.

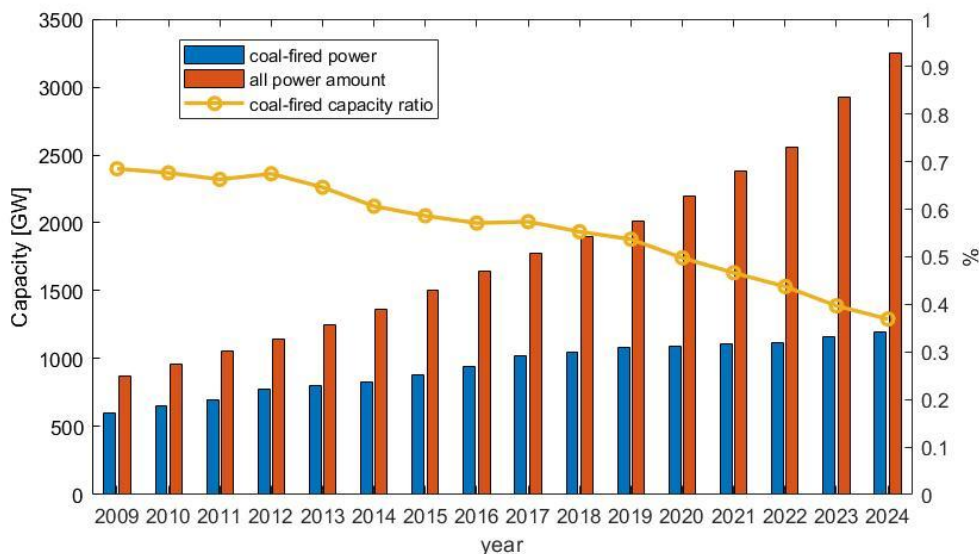


Figure 3 The Installed Capacity, Proportion and Growth Rate of Coal-Fired Power in China from 2009 to 2024

In terms of power amount, driven by the rapid growth of the installed capacity of new energy power, although China's coal-fired power reached 5.38 trillion kWh in 2023, accounting for 53.6% of the total power, this proportion has decreased by 16.2 percentage points over the past decade. This reflects the rapid growth of new energy power and the gradual optimization of the energy structure. Nevertheless, coal-fired power plays an irreplaceable role in ensuring national energy security and the stable operation of the economy. With the advancement of clean energy technologies and the promotion of policies, coal-fired power and new energy will form a more coordinated development pattern.

2.3 Low-carbon Technology Level and Development Trends

Among relevant low-carbon technologies, clean coal technology refers to the general term for new technologies in the whole process of coal development and utilization, including processing, combustion, conversion, and pollution control technologies that reduce pollutant emissions and improve utilization efficiency. It mainly includes two aspects: one is the clean technology for direct coal combustion, and the other is the technology for converting coal into clean fuels. Regarding coal-fired power, clean coal power technologies mainly refer to power-technologies with obvious emission-reduction effects, such as ultra-supercritical units, integrated gasification combined cycle (IGCC) power, green ammonia co-firing, carbon capture, utilization and storage (CCUS). Clean coal technology is one of the leading technologies in the world to solve environmental problems, and efficient and clean coal-fired power is the main focus of clean coal technologies in various countries.

Since 2007, the National Development and Reform Commission has required that all newly built coal-fired units must be supercritical and ultra-supercritical units. These two types of units have entered a fully commercial stage in China. Vigorously developing large-capacity, high-parameter supercritical and ultra-supercritical units can significantly reduce coal consumption, save coal resources, reduce carbon dioxide emissions, and lower the emission level per unit of electricity. Since 1978, with the progress and development of technology, China's standard coal consumption for power supply has been decreasing year by year, from 471 grams/kWh to the current 305 gce/kWh, and the gap with the coal consumption for power in developed countries is gradually narrowing.

In recent years, by digesting and absorbing advanced foreign IGCC technologies, China has improved its local design, manufacturing capabilities, and R & D levels, promoted the localization of gas turbines, with the localization rate reaching 85%. According to the IGCC projects under construction in China, the construction cost is 7,000-8,000 yuan/kW. With the maturity of technology, equipment optimization, especially the full-scale promotion of localization, IGCC is rapidly developing towards high-efficiency, low-carbon, large-scale, and commercialization.

Overall, clean coal power technology has good technical and economic characteristics, which is conducive to improving power-efficiency, saving resources, and reducing pollutant and carbon dioxide emissions. Vigorously developing clean coal power is an effective measure to optimize and upgrade coal-fired power technology, and it is also the main direction of low-carbon development of China's coal-fired power.

The carbon-reduction principle of the green ammonia co-firing technology is based on the green preparation process and clean combustion characteristics of green ammonia. In terms of application cases, the National Energy Group carried out a coal-ammonia co-firing combustion test under high-load power-conditions at the Taishan Power Plant in Guangdong. This is currently the largest-capacity unit that has completed the ammonia-co-firing combustion test verification at home and abroad. This test has provided valuable practical experience for the large-scale application of green ammonia in the coal-fired power field, and promoted the green ammonia co-firing technology towards commercial application.

CCUS technology refers to the process of separating carbon dioxide from industrial or related energy sources, transporting it to a storage site, and keeping it isolated from the atmosphere for a long time. The CCUS technology has a significant effect on greenhouse gas emission reduction. Research [8] shows that the contribution rate of CCUS to carbon dioxide emission reduction is expected to be more than 50% in the future. The first CCUS demonstration project jointly built by China and Australia, with an annual recovery capacity of 3,000 tons, the Huaneng Beijing Thermal Power Plant, has started operation. China Datang Corporation and Alstom jointly cooperate to develop two CCUS demonstration projects with an annual carbon dioxide capture capacity of over 1 million tons in Daqing, Heilongjiang, and Dongying, Shandong. The China Power Investment Corporation independently developed and fully adopted domestic equipment to build an annual 10,000-ton liquid carbon dioxide capture device at the Shuanghuai Power Plant in Chongqing, marking the development and breakthrough of domestic carbon dioxide capture technology in China, and laying a good foundation for China to achieve clean coal power and the low-carbon development of the coal-fired power industry.

3 DEVELOPMENT TRENDS OF CHINA'S COAL-FIRED POWER INDUSTRY

3.1 Ensuring Power Security

New energy power is characterized by randomness, volatility, and intermittency, with a low effective capacity, making it difficult to guarantee real-time electricity demand. The peak power load of the power grid generally occurs between 18:00-20:00. During this period, the power output of photovoltaic power is basically zero, and the power output of wind power is less than 10% of the installed capacity. If extreme weather conditions are added, such as continuous days of low wind or rainy and cloudy days, secondary disasters affecting energy security are likely to occur, triggering a chain reaction in the power system. For example, in early 2021, Texas in the United States was hit by rain, snow, and

freezing natural disasters. While the electricity load surged, the harsh weather caused pipeline ice blockages, gas source interruptions, and icing of wind power equipment. Gas-fired and wind-power units successively shut down, leading to a major power outage. The production and lives of nearly 4 million people were severely affected, causing immeasurable economic losses. Since China has insufficient flexible resources such as gas-fired units, and the energy storage system is in the initial development stage and is still difficult to play a significant role in power regulation, coal-fired power remains an important power source to support the stable and reliable operation of the power system under major accidents and extreme disasters, ensuring power supply security.

3.2 Providing System Regulation

With the accelerated development of new energy, the system's demand for flexible power sources will continue to increase. In China, most hydropower stations are run-of-river type. The regulation capacity is limited due to the lag in the construction of regulating and key hydropower stations. Pumped-storage power stations are restricted by site resources, and gas-fired power stations are limited by gas sources and gas prices, making large-scale construction unfeasible. Nuclear power is restricted by safety and economic factors and is not suitable for frequent regulation. Energy storage is affected by technical maturity and economy and does not yet have a competitive advantage. Coal-fired power units operate stably and reliably. After transformation, they can change their load over a wide range. Under the current technical conditions and energy resource endowment, coal-fired power is the most economical and reliable large-scale flexible regulating power source. The flexibility transformation of coal-fired power is a practical choice to improve the system's regulation capacity.

3.3 Undertaking Centralized Heating

For a long time, the power industry has been the main force in clean heating. Since the 1990s, combined heat and power (CHP) units have replaced highly polluting heating boilers, playing a huge role in solving heating problems in northern China and improving the environment. In China, hundreds of millions of tons of coal are burned for heating in a decentralized manner. At the present stage, it is difficult to completely replace them with gas or electricity. The most effective way is to replace them with CHP. Currently, the proportion of coal used for power and CHP heating in China accounts for 50% of total coal consumption. About half of the coal-fired power units are CHP units, and the proportion of heating units in the "Three North" regions is as high as 60%. Centralized heating by coal-fired power replacing scattered coal burning and undertaking clean heating in northern China in winter is an important measure to ensure people's livelihood under the premise of environmental friendliness.

3.4 Reducing Energy Consumption Costs

As new energy is a power source with low energy density, to meet electricity demand, it is necessary to significantly increase the installed capacity. In 2023, China added 290 million kW of new energy, reaching a record high of 89.2% [9]. Since the "14th Five-Year Plan" period, the average annual investment in power sources has reached 767 billion yuan [10], and the annual investment in power source projects has reached 967.5 billion yuan, of which non-fossil energy accounts for more than double the previous annual investment in power sources of 350-380 billion yuan. With technological progress, the cost of wind and solar power will decrease, but in the short term, it is still difficult to offset the increase in electricity costs caused by the rise in system costs due to changes in the power system structure. As the main supplier of electricity and heat, coal-fired power is an important guarantee for the whole society to use electricity and heat fairly at present and in the future.

4 POLICIES RELATED TO THE LOW-CARBON TRANSFORMATION OF COAL-FIRED POWER

It is extremely difficult for China's coal-fired power to withdraw in the short term. Its future development and the gradual withdrawal path are crucial for China to achieve the carbon peak and carbon neutrality goals. In 2021, the central supervision department established a working group for carbon peak and carbon neutrality, and began to construct a "1 + N" policy system. Here, "1" refers to one top-level design document, and "N" refers to a series of policy plans for key action areas. Due to China's coal-dominated energy structure, coal-fired power occupies the position of the main power source in the entire power system. However, recognizing the pollution and high-emission problems of coal-fired power plants, given the high-emission and high-pollution characteristics of coal-fired power, the Chinese supervision department formulated a series of measures related to mitigating the emissions of coal-fired power plants during the past four Five-Year Plan periods from 2001 to 2020, and achieved specific results.

First, regarding the high-pollution problem, for example, in 2007, in order to accelerate the elimination of obsolete coal-fired technologies, the National Development and Reform Commission put forward the "Opinions on Accelerating the Shutdown of Small Thermal Power Units". It required the closure of small and obsolete units, and gave priority to the development of efficient and large-scale coal-fired power plant units. This policy has been particularly successful in reducing various air pollutant emissions, especially carbon dioxide emissions, and has made a significant contribution to reducing the emissions of China's coal-fired power plants. In addition, to reduce the use of raw coal, the advocated coal-to-gas project plays a crucial role in reducing the inventory carbon emissions of coal-fired power plants. The implementation of this policy is expected to reduce emissions by 280-300 million tons by 2030. The supervision

department has also formulated a series of other plans and documents to address the issue of improving the energy efficiency of coal-fired power plants and dealing with emission reduction problems. In 2014, the "Opinions on Promoting the Clean and Efficient Utilization of Coal" was introduced, and in 2015, the "Implementation Plan for Ultra-low Emission and Energy-saving Reconstruction of Coal-fired Power Plants" was formulated. In addition, during the 13th Five-Year Plan period, significant progress was made in the implementation of the five-year power development plan. In 2020, China's coal-fired power installed capacity was less than 50% of the total national installed capacity for the first time, and the carbon emission factor in most provinces decreased by 3%-6%.

Carbon emission reduction of coal-fired power plants remains an important issue. Therefore, the Chinese supervision department has formulated the latest national 14th Five-Year Plan. At the beginning of the 14th Five-Year Plan, the supervision department issued the guiding "14th Five-Year Plan for the Modern Energy System" and the "Implementation Plan for the Transformation and Upgrading of National Coal-fired Power Units". These policies put forward specific clean-energy requirements for coal-fired power plants at the national level, and will guide the development, transformation, and decommissioning of all coal-fired power plant units until 2025. Subsequently, various provinces across the country have successively introduced relevant policies for energy conservation, emission reduction, and clean-up transformation of coal-fired power. For example, in July 2023, Henan Province introduced the "Three-year Action Plan for Promoting the Stable Improvement of the Ecological Environment Quality in Henan Province (2023-2025)". In August 2023, Shandong Province issued the "Action Plan for the Transformation and Upgrading of the Coal-fired Power Industry in the Province".

5 CONCLUSION

This paper elaborates in detail on the current situation of China's coal-fired power industry and the development of key energy-saving and emission-reduction technologies in the low-carbon transformation of coal-fired power. In the analysis of the current situation of the coal-fired power industry, first, based on regions, the distribution characteristics, installed capacity of coal-fired power units, and power of coal-fired power plants in China are summarized. Secondly, an analysis is conducted on the currently popular low-carbon technologies for coal-fired power, describing the current situation and development trends of these key energy-saving and emission-reduction technologies from multiple aspects. Then, the relevant policies for the low-carbon development of coal-fired power are sorted out, which can provide support for subsequent research. Overall, the low-carbon transformation and development of China's coal-fired power industry is showing a stable and positive trend, but there are still many difficulties that need to be overcome.

COMPETING INTERESTS

The authors have no relevant financial or non-financial interests to disclose.

REFERENCES

- [1] Gang He, Jiang Lin, Froylan Sifuentes, et al. Rapid cost decrease of renewables and storage accelerates the decarbonization of china's power system. *Nature Communications*, 2020, 11(2486): 441.
- [2] Jiankun He, Zheng Li, Xiliang Zhang, et al. Towards carbon neutrality: A study on china's long-term low-carbon transition pathways and strategies. *Environmental Science and Ecotechnology*, 2022, 9: 100134.
- [3] Jianjun Wang and Li Li. Sustainable energy development scenario forecasting and energy saving policy analysis of China. *Energy Policy*, 2016, 93: 264-272.
- [4] Guanyi Yu and Yueyang Guo. Development Status and Prospects of Clean and Efficient Coal-fired Power Technology in China. *E3S Web of Conferences*, 2019, 118: 02059.
- [5] Department of State Bulletin. For man and nature: Building a community of life together, 2021. https://www.gov.cn/gongbao/content/2021/content_5605101.htm.
- [6] Global Energy Monitor. Global coal plant tracker, July 2024. <https://globalenergymonitor.org/projects/global-coal-plant-tracker/download-data>.
- [7] IEA. Coal 2024, Analysis and forecast to 2027, 2024. <https://www.iea.org/reports/coal-2024>.
- [8] Pengchen Wang, Beibei Shi, Nan Li, et al. CCUS development in China and forecast its contribution to emission reduction. *Scientific Reports*, 2023, 13(1): 17811.
- [9] The State Council Information Office. China's energy transition, Aug 2024. https://www.gov.cn/zhengce/202408/content_6971115.htm.
- [10] China Electricity Council. China power industry annual development report 2024, July 2024. <https://www.cec.org.cn/detail/index.html?3-334911>.

SUPPLY AND DEMAND EVALUATION OF URBAN RECREATIONAL GREEN SPACES IN ZHAOQING CITY FROM THE PERSPECTIVE OF SUPPLY AND DEMAND BALANCE

HongJun Xie¹, SiRu Ye^{2*}

¹*School of Guangdong Technology College, Zhaoqing 526100, Guangdong, China.*

²*Zhaoqing Forestry Bureau, Zhaoqing 526040, Guangdong, China.*

Corresponding Author: SiRu Ye, Email: 1104652980@qq.com

Abstract: Urban recreational green spaces, as an important component of the urban ecosystem, are of significant value to study. This paper delves into the supply and demand conditions of urban recreational green spaces in Zhaoqing City. The study reveals that there are significant differences in the demand and satisfaction levels of recreational green spaces among different social groups. Moreover, the supply and demand conditions of urban recreational green spaces in Zhaoqing City exhibit a pronounced differentiation in spatial distribution, with the northern and southeastern areas being high-supply hotspots, while some regions experience insufficient supply. This imbalance between supply and demand, along with the spatial differentiation, not only exacerbates the unfairness in the allocation of green space resources but also affects the quality of life and happiness of urban residents. The findings of this study can provide practical references for the future optimization of urban recreational green space planning in Zhaoqing City, strengthening resource integration, and ensuring the equitable distribution of green space resources, with the aim of achieving a balance between supply and demand and sustainable development.

Keywords: Urban recreational green space; Supply and demand balance; Three-step floating catchment area method; Quantitative analysis

1 INTRODUCTION

Against the backdrop of rapid urbanization, urban recreational green spaces, as an important component of the urban ecosystem, not only carry the multiple ecological functions of beautifying the urban environment [1], regulating the urban climate [2], and protecting biodiversity [3], but also serve as significant venues for urban residents to relax and entertain, to get close to nature, and to engage in social activities [4, 5]. With the improvement of living standards and the shift in leisure concepts, the demand for recreational green spaces among urban residents is becoming increasingly diverse, ranging from simple strolls and fitness to parent-child activities and outdoor adventures, all of which pose higher demands on the planning and management of urban recreational green spaces [6]. The theory of supply and demand balance, a core concept in economics, has been widely applied in recent years in fields such as urban planning, resource allocation, and public service management [7-9]. This theory emphasizes achieving a dynamic balance between supply and demand through rational allocation and optimal utilization, under conditions of limited resources, to maximize the efficiency of resource use. In the planning of urban recreational green spaces, the application of the supply and demand balance theory means that it is necessary to comprehensively consider the supply capacity of the green spaces and the actual needs of residents, and through scientific and reasonable planning and management, to achieve effective allocation and efficient utilization of green space resources.

The core objective of this study is to deeply explore the supply and demand balance of urban recreational green spaces in Zhaoqing City, to comprehensively and deeply evaluate the supply and demand situation of its recreational green spaces, and to provide scientific basis and strategic suggestions for its sustainable development. The entry point of this study lies in, from the perspective of supply and demand balance, how is the supply and demand situation of urban recreational green spaces in Zhaoqing City? What are the problems of supply and demand imbalance? Specifically, this study will first understand the current supply situation of urban recreational green spaces in Zhaoqing City through field research and data collection, including the types, area, distribution, facilities configuration, and service quality of green spaces; secondly, through methods such as questionnaire surveys, interviews, and big data analysis, it will deeply collect and analyze the demand information of Zhaoqing City residents for urban recreational green spaces, to understand the actual situation of residents' preferences, frequency of use, preferences, and satisfaction with green spaces; finally, on the basis of fully mastering the information of both supply and demand, this study will further construct a scientific and reasonable supply and demand balance evaluation index system, which will comprehensively consider the supply capacity of green spaces and the actual needs of residents, to quantitatively evaluate the supply and demand balance status of urban recreational green spaces in Zhaoqing City. Therefore, this study can provide scientific basis and decision support for the planning and management of urban recreational green spaces in Zhaoqing City, promote the sustainable development and efficient utilization of urban recreational green spaces, on the other hand, it can also provide reference and reference for other cities in the evaluation of recreational green space supply and demand, and promote theoretical innovation and practical exploration in the field of urban planning and management. Based on the above analysis and evaluation, this study will be able to identify specific manifestations of supply and

demand imbalances, such as insufficient green space supply, uneven distribution, and excessive demand for certain types of green spaces in certain areas. It will also delve into the underlying reasons behind these imbalances, promoting the sustainable development of urban recreational green spaces in Zhaoqing City.

2 LITERATURE REVIEW

At present, there is an increasing interest in the academic community regarding the study of "urban park green space equity" [10]. Some researchers have calculated the distribution of per capita green space area within accessible areas and used spatial network analysis to estimate the accessibility of green and blue spaces, thereby evaluating the supply and service capacity of green spaces [11, 12]; others have approached the issue from the perspective of demand, using the supply and demand points of park green spaces and residential areas, employing Euclidean distance to analyze the phenomenon of spatial interaction weakening with increasing distance, and measuring the balance of supply and demand through the percentage difference in Poisson density [13]. Other researchers have adopted the gravity model to explore the fairness of urban green spaces, and then analyzed the spatial distribution of urban green spaces and their correlation with urbanization [14]. At the same time, there has been attention paid to the elderly population, proposing age-friendly green space design, and using the two-step floating catchment area method to measure the accessible area of park green spaces based on different modes of transportation, thereby evaluating the supply and demand situation [15-17]. However, when describing population distribution, it is usually dependent on census data or building volume rates to count the population in residential areas, and this assumption of uniform population distribution has certain limitations. Scholar Tan Chuandong has constructed a regression model between land cover types and census population, and inverted the results to obtain a more accurate spatial distribution of population, a method that more accurately addresses the issue of population quantity and distribution [18, 19]. Although this evaluation method can precisely reflect the population quantity at specific locations, using only such static data, due to the large time span and limited accuracy, it is not sufficiently powerful in describing the demand for park green spaces in that area.

In this digital era, the application of dynamic and static big data to assist in explaining the degree of spatial supply and demand has also subtly shifted, which has also effectively resolved the precise positioning of population spatial differentiation. Based on location big data (mobile signaling, POI data), from three dimensions of internal supply (infrastructure), external demand (population), and spatial linkage (regional transportation) to measure the potential factors affecting the use of park green spaces [20, 21], as well as from Weibo check-in data to reflect the usage status and supply capacity of existing parks in the region [22], quantitatively analyzing the distribution density of poi data to reflect the degree of public demand for park green spaces from two aspects, and then evaluating the fairness of the spatial distribution of green spaces [23]. The evaluation of the balance between green space supply and demand is also affected by factors such as travel mode and land use type, affecting the population's access to nearby public green space resources [24]. From the perspective of fairness and justice, there is a certain difference between green space acquisition and geographical distribution. Some scholars have analyzed the spatial and temporal differences in the supply and demand of park green spaces in the central urban area of Wuhan from 2000 to 2014 at the grid scale of two transportation modes (walking and driving), pointing out that the comprehensive impact of surrounding land use and socio-economic environment cannot be ignored [25].

From the perspective of the application method of the evaluation model, in addition to the per capita green space rate and per capita green space area, the measurement of the rationality of green space layout often takes accessibility and fairness as one of the indicators. The evaluation methods can be roughly divided into: (1) Analysis models that use bandwidth h as the radius to determine the time, transportation costs, and proximity of road network distances required to reach a space, such as GIS network analysis, buffer analysis, and the shortest path analysis method [26, 27]; (2) Measurement models that search for the area, quantity, density, and capacity of supply and demand points around the demand point search area [28]; (3) Gravity models that calculate spatial accessibility values using the distance between supply and demand points as a parameter [29]; (4) Evaluation models that are based on supply and demand relationships and comprehensively consider factors such as spatial quantity, area, population distribution, and street numbers, such as the 2SFCA and gravity model [30].

3 RESEARCH METHOD

3.1 Overview of the Study Area

Zhaoqing City consists of 3 districts, 4 counties, and administratively oversees 1 county-level city, with a total area reaching 14,897.45 square kilometers. As of 2023, the city's permanent population is estimated to be approximately 4.1317 million, of which 2.1937 million are urban residents, accounting for 53.09% of the total population. As a key node of the Guangdong-Hong Kong-Macao Greater Bay Area and the Pearl River-Xijiang Economic Belt, as well as a core member of the Guangfo-Zhaoqing Economic Circle and the Guangzhou Metropolitan Area, Zhaoqing City faces the dual pressures of urban development and the improvement of living environments. To address these challenges, in March 2023, Zhaoqing City introduced the "Implementation Plan for Promoting the Construction of the '15-Minute Community Life Circle' in Zhaoqing," aiming to optimize the allocation of community resources and create an efficient and convenient community service network. The community has thus become the core unit for building the community life circle. As an ecological city, Zhaoqing particularly emphasizes the service function of green space in the construction of the community life circle, highlighting walkability to enhance the overall quality of green leisure public

services and living environments. Given the broadness of the urban area, to ensure the concentration and depth of the research, this study limits its geographical scope to the Chengxi Subdistrict of Zhaoqing's Duanzhou District. This subdistrict is part of the old urban area of Zhaoqing Duanzhou, with a total area of 7.7 square kilometers, including 18 communities, a population density of approximately 20,922 people per square kilometer, and a permanent resident population of about 161,136. The study area is divided into research units within the range of a regular hexagon with an inscribed circle diameter of 500m ($S=93,750m^2$)(See Figure 1-2).

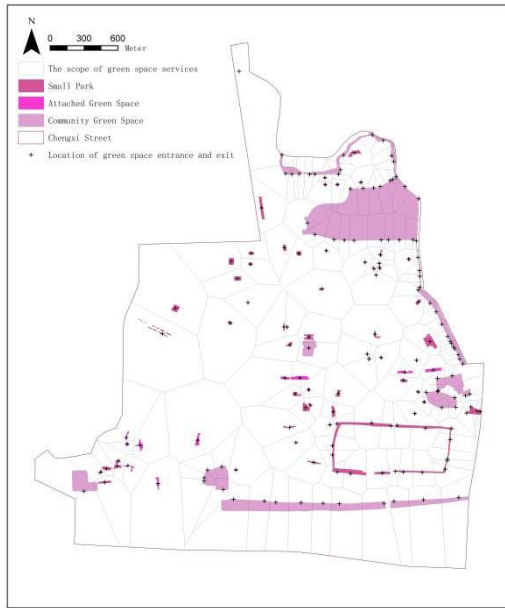


Figure 1 Current Status of Green Space

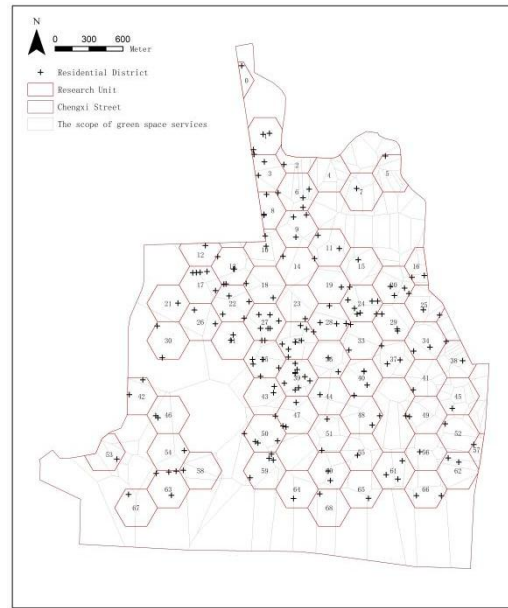


Figure 2 Research Unit

3.2 Data Source

The data used in this study includes:

- (1) Main park boundary data, sourced from AutoNavi Map Areas of Interest (AOI), with data collection time in April 2024.
- (2) City boundary and city road data, sourced from OpenStreetMap (OSM), with data collection time in April 2024.
- (3) Residential community data sourced from AutoNavi Map Points of Interest (POI) and Anjuke, with data collection time in December 2023. Each data entry includes the corresponding community name, latitude and longitude address, number of floors, and other information.
- (4) Population data, calculated based on data (3) in conjunction with the number of households published by the Real Estate Information Network of Zhaoqing City.

3.3 3SFCA Evaluation Model

Assuming an adult walks at a constant speed of 70 meters per minute, the travel distance for walking for 15 minutes is approximately 1050 meters. Step one, using the Network Analyst analysis module of the ARCGIS data processing platform, construct a three-level OD cost matrix for residential demand points and recreational green space supply points with search thresholds of 350m, 700m, and 1050m respectively. Considering that the distance to the recreational supply point affects residents' choice of recreational points, that is, the longer the distance from the demand point to the recreational supply point, the lower the willingness to travel, and the lower the probability of the recreational supply point being chosen, a distance decay function is referenced to calculate the Gaussian weight value of the recreational green space, as shown in formula (1). After calculating W_{ij} , substitute it into the 3SFCA formula (2) to obtain the recreational green space selection weight G_{ij} .

$$G(d_{ij}) = \begin{cases} \frac{e^{-\frac{1}{2} \times (\frac{d_{i,j}}{d_0})^2} - e^{-\frac{1}{2}}}{1 - e^{-\frac{1}{2}}}}, & d_{i,j} \leq d_0 \\ 0, & d_{i,j} > d_0 \end{cases} \quad (1)$$

$$G_{ij} = \frac{W_{ij}}{\sum_{j \in \{Dist(i, j) < d_0\}} W_j} \quad (2)$$

In equation (2), G_{ij} is the choice weight between residential demand point i and recreational green space point j , $Dist(i, j)$ is the travel cost from i to any recreational green space supply point j within the effective travel range, and d_0 is the size of the effective travel range. W_{ij} and W_j are the Gaussian weights of the pairwise relative between residential demand point i and recreational green space supply point j , and the sum of all weight values that residential demand point i obtains from recreational green space supply point j , respectively.

Step 2, substitute the G_{ij} and W_{ij} obtained in step one into equation (3), and calculate the supply-demand ratio within the limited search threshold range for residential demand points and recreational green space supply points.

$$D_j = \frac{S_j}{\sum_{i \in \{d_{i,j} < d\}} P_i W_{i,j} G_{i,j}} \quad (3)$$

In equation (3), S_j is the area of the recreational green space of j , W_i is the Gaussian weight value of the recreational green space of j , G_{ij} is the selection weight value between the recreational green space j and the residential point i , and P_i is the population size of i . D_j is the supply-demand ratio of recreational services for each recreational green space.

$$\begin{aligned} A_i &= \sum_{j \in \{d_{i,j} < d\}} D_j W_{ij} G_{ij} \\ &= \sum_{j \in D_1} G_{ij} D_j W_1 + \sum_{j \in D_2} G_{ij} D_j W_2 + \sum_{j \in D_3} G_{ij} D_j W_3 \end{aligned} \quad (4)$$

In equation (4), A_i represents the sum of the supply-demand ratios D_j of the recreational green space supply points j within the limited search threshold for demand point i . D_1 , D_2 , D_3 are the values of the recreational green space supply-demand service A_i summed under different search thresholds.

4 RESEARCH RESULTS

4.1 Questionnaire Distribution Results

A total of 1,770 questionnaires were distributed, and 1,679 valid questionnaires were collected, with a collection rate of 94.86%. The questionnaire reliability analysis (Alpha) is $0.717 > 0.600$, and the KMO test is $0.730 > 0.700$, indicating good validity coefficients. The research data can be used for the writing of this article. The results of the survey research are as follows:

4.2 Long-term Residents Have a Higher Satisfaction with the Environment and a Greater Variety of Choices

4.2.1 The longer the residence time, the higher the satisfaction with park green spaces

As shown in Figure 3, among residents who have lived in Zhaoqing for more than 20 years, 43.40% expressed that they are very satisfied with the demand for nearby park green spaces, while only 5.35% indicated dissatisfaction. In contrast, among residents who have lived there for less than a year, the proportion of those very satisfied is only 5.35%. This indicates that long-term residents have significantly higher adaptability and satisfaction with their surrounding environment compared to new residents who have recently moved in.

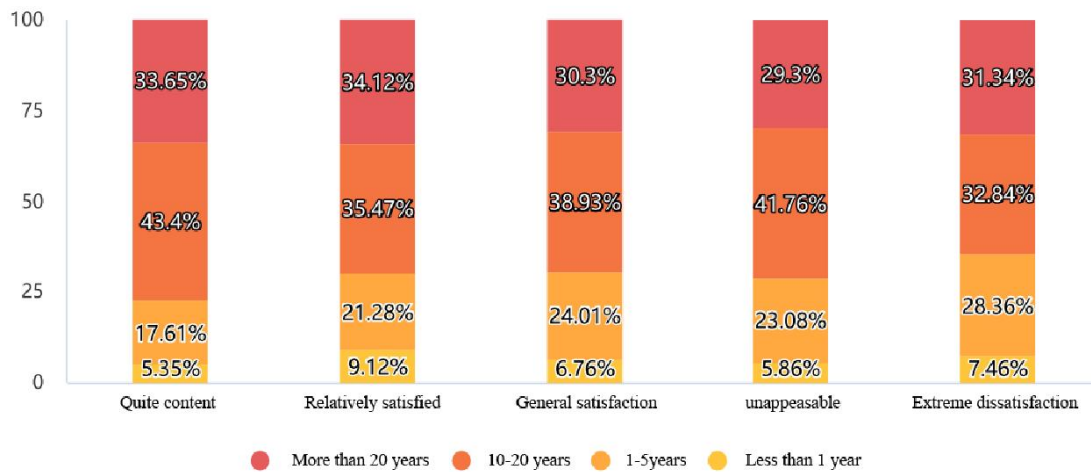


Figure 3 Can the Green Spaces Around the Residential Area Meet the Needs?

4.2.2 Long-term residents tend to choose other recreational facilities

According to the data presented in Figure 4, among the resident group that has lived in the area for over 20 years, more than one-third, specifically 31.42%, tend to choose other types of recreational facilities to spend their leisure time. In contrast, among residents who have lived there for less than 1 year, this percentage is significantly lower at only 7.02%. This comparative data reveals an important trend: residents who have lived in a community for a long time, when faced with insufficient traditional leisure facilities such as parks and green spaces, will actively seek out alternative recreational options to meet their entertainment and relaxation needs.

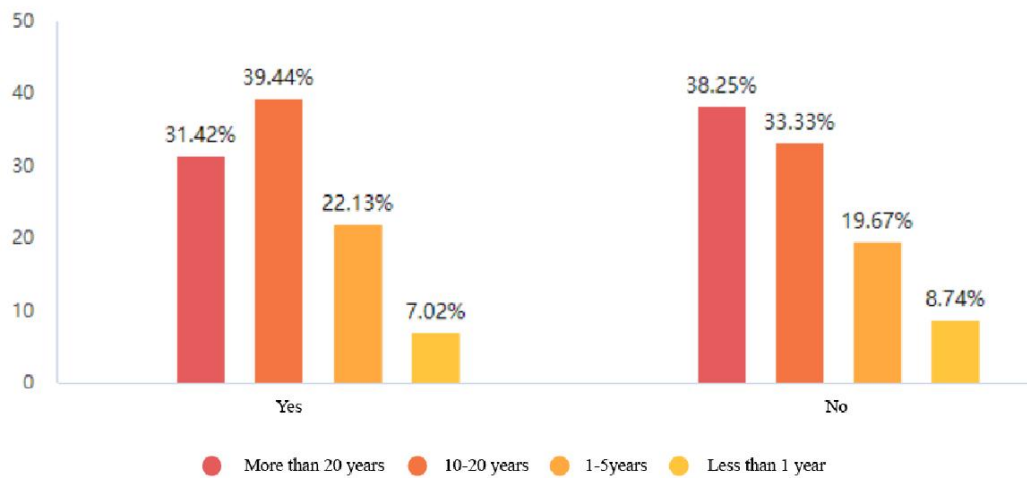


Figure 4 Whether the Lack of Green Space in Residential Areas Will Lead to Visiting Other Spaces Among Different Lengths of Residence

4.3 Age Influences Satisfaction with Park Green Spaces and Recreational Choices

4.3.1 The older the age, the lower the satisfaction with park green spaces

Among all age groups, the 41-50 age group has the highest level of satisfaction with park green spaces, with 31.13% expressing great satisfaction, whereas only 11.01% of those over 60 years old express great satisfaction. Overall, young people (19-30 years old) and middle-aged individuals (31-40 years old) have a higher level of satisfaction with park green spaces, while the satisfaction level of the elderly (over 60 years old) is significantly lower (See Figure 5).

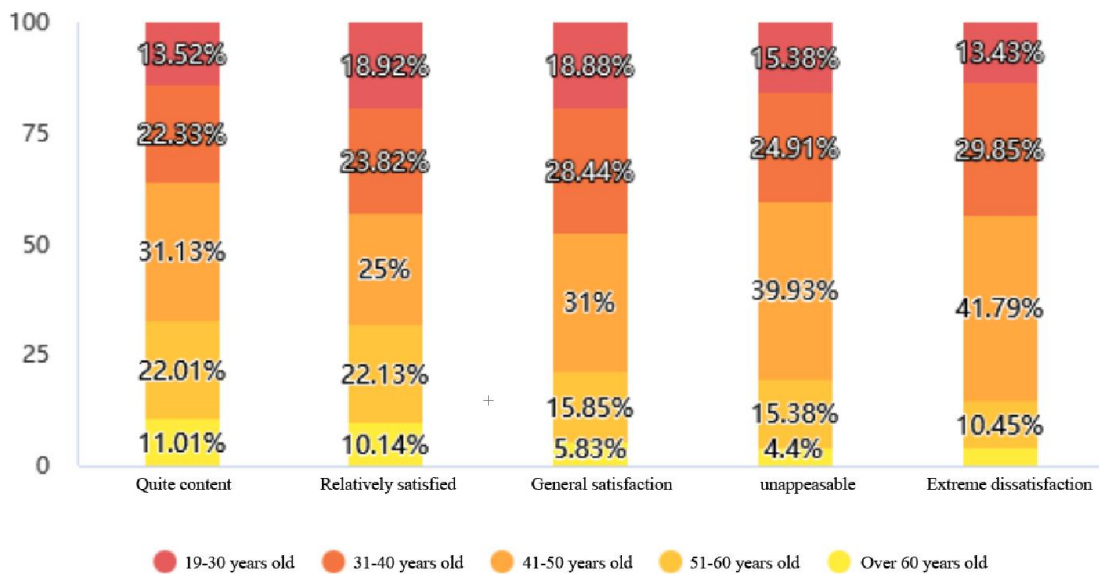


Figure 5 Residents' Satisfaction with the Green Spaces Around Their Residential Areas

4.3.2 Young people are more inclined to choose other recreational facilities

The data indicates that a higher proportion of individuals aged 19-30 and 31-40 choose other recreational facilities, with percentages of 17.51% and 26.47% respectively. In contrast, only 5.61% of individuals aged 60 and above opt for other recreational facilities, suggesting that younger people have a more active demand for recreational facilities (See Figure 6).

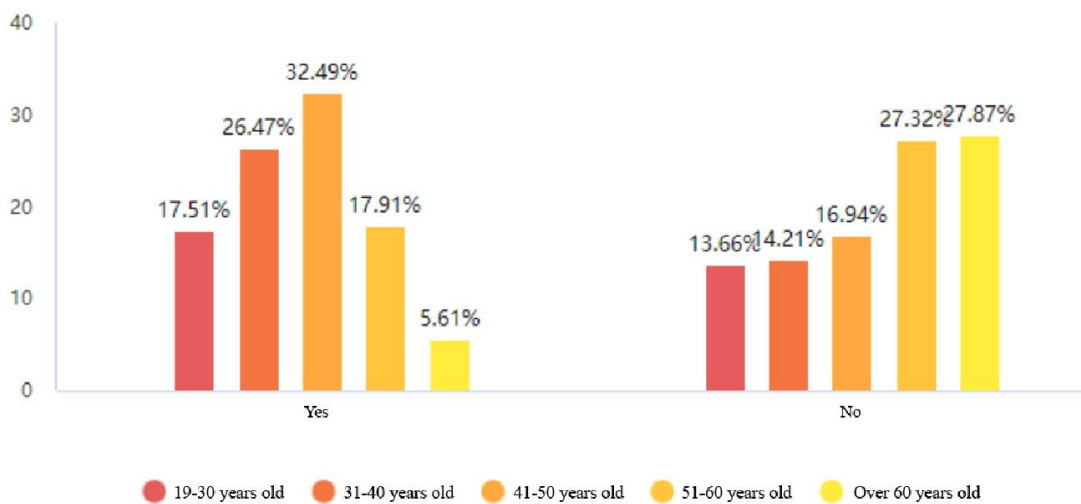


Figure 6 Whether the Lack of Residential Green Space is Associated with Visiting Other Spaces Across Different Age Groups

4.4 Gender Influence on Satisfaction with Urban Green Spaces and Alternative Choice Behavior

4.4.1 Men generally have higher satisfaction with urban green spaces than women

In each satisfaction level, the proportion of satisfied males is higher than that of females (See Figure 7). In the "very satisfied" option, males account for 62.26%, while females only account for 37.74%.

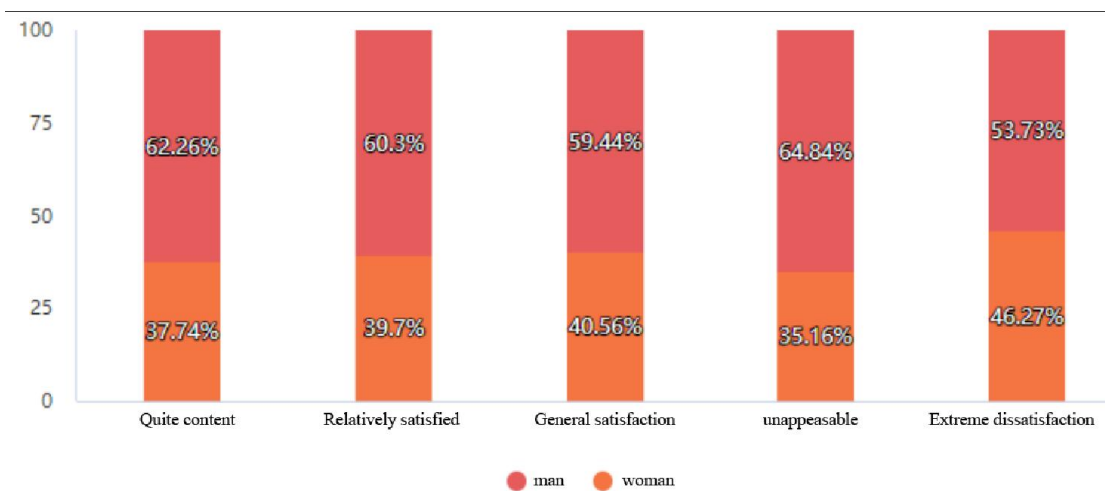


Figure 7 Satisfaction with Green Spaces by Gender

4.4.2 Men are more inclined to choose other recreational facilities

The survey indicates that 917 males (61.30%) would choose alternative recreational facilities, compared to 579 females (38.70%), showing a tendency for males to have more alternative options when park green spaces are lacking (See Figure 8).

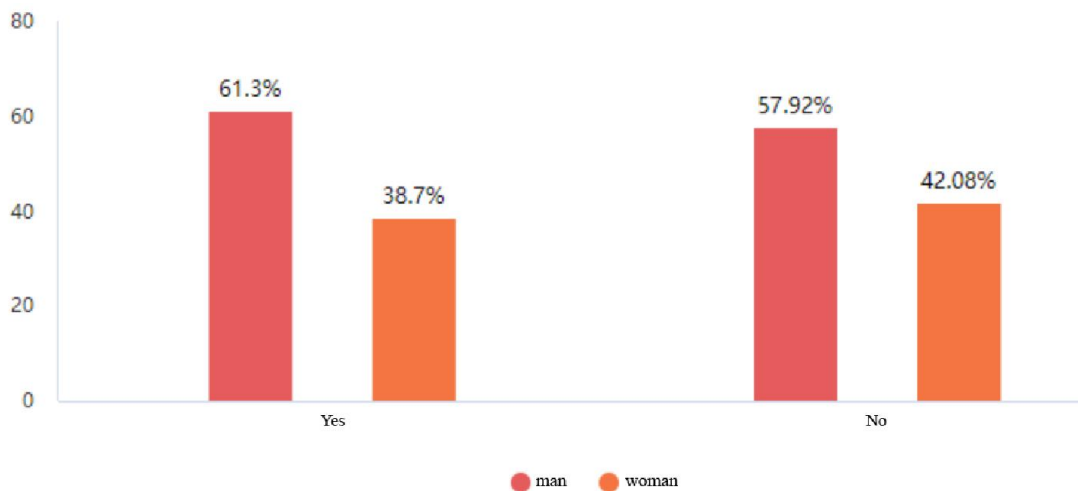


Figure 8 Whether the Lack of Residential Green Space is Associated with Visiting Other Spaces Among Different Genders

4.5 Analysis of Community Residents' Recreational Demands and Green Space Supply

Under the global assessment framework (Figure 9), there is a significant spatial differentiation in the supply and demand of recreational green spaces in Chengxi Street. Specifically, the northern and southeastern areas are hotspots of high supply for recreational green spaces, with the presence of local cold spots of low supply. The overall level of green space supply and demand shows a gradient decrease from east to west, and the current situation of insufficient and imbalanced spatial distribution of green space resources is quite evident. Based on the argument of spatial autocorrelation mentioned above, it further illustrates that the highly aggregated recreational green spaces, with their scale effects, have formed high supply hotspots in specific areas, effectively meeting the recreational needs of the surrounding residents. On the contrary, the small and scattered green spaces within the urban area, limited by their scale and distribution, have a supply capacity that is difficult to match the strong demand of high-density population areas, thus constituting cold spots of green space supply, which further exacerbates the unfairness of green space resource allocation.

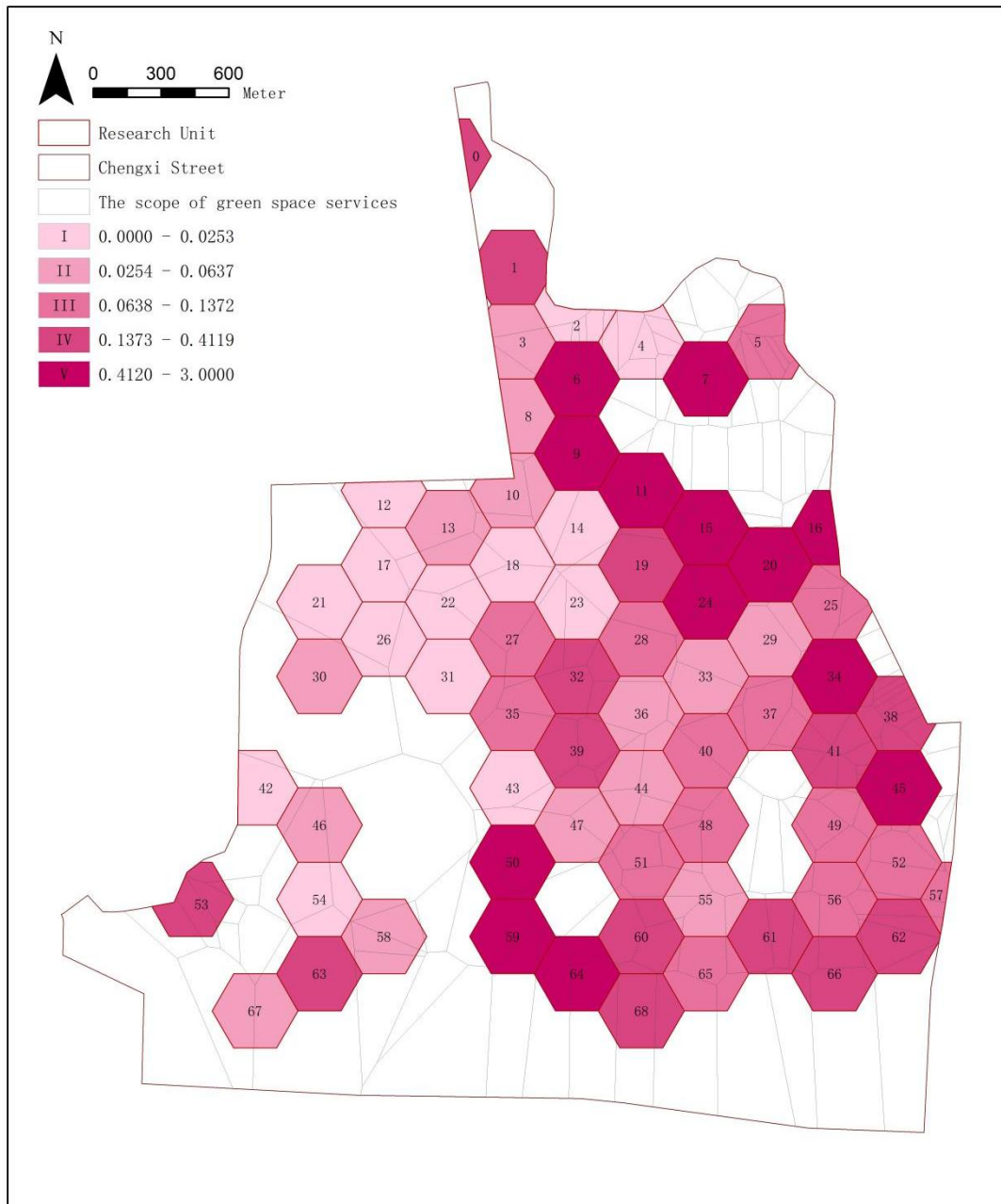


Figure 9 Global Evaluation of Green Space Supply and Demand Services

5 DISCUSSION

This study, from the perspective of supply and demand balance, conducted an in-depth analysis of the supply and demand situation of urban recreational green spaces in Zhaoqing City. The main research findings are summarized as follows:

5.1 Length of Residence Has a Significant Impact on Recreational Green Space Satisfaction

The length of residence is an important factor affecting residents' satisfaction with recreational green spaces. Long-term residents, due to their stronger adaptability and sense of belonging to the surrounding environment, have a significantly higher level of satisfaction with park green spaces than newly arrived residents. At the same time, long-term residents also demonstrate a stronger ability to make alternative choices when facing insufficient green spaces, and are more inclined to seek out other types of recreational facilities.

5.2 Age Factors Have an Impact on the Satisfaction with Park Green Spaces and Recreational Choices

Age also significantly affects residents' demand and satisfaction with recreational green spaces. Young people have a

more active demand for recreational facilities and are more inclined to choose a variety of recreational activities, while older people have a higher level of satisfaction with park green spaces, but a relatively lower proportion choose other recreational facilities. This age difference reflects the preferences and needs characteristics of different social groups for recreational activities.

5.3 Gender Differences Affect Satisfaction with Park Green Spaces and Alternative Choice Behavior

Gender differences are also an important factor affecting residents' satisfaction with recreational green spaces and alternative choice behavior. Men generally have higher satisfaction with park green spaces than women, and they are more inclined to have alternative choices when green spaces are lacking. This gender difference may be related to the different characteristics of men and women in leisure activities, social needs, and other aspects.

5.4 There is a Significant Spatial Differentiation in the Supply and Demand of Urban Recreational Green Spaces in Zhaoqing City

From the perspective of spatial distribution, there are significant spatial differentiation characteristics in the supply and demand situation of urban recreational green spaces in Zhaoqing City. The northern and southeastern areas are hotspots for high supply of recreational green spaces, while there is a shortage of supply in some areas. This spatial differentiation exacerbates the unfairness in the allocation of green space resources and affects the quality of life and happiness of urban residents. Therefore, in the future urban recreational green space planning of Zhaoqing City, the characteristics of the needs of different social groups should be fully considered, the spatial layout and resource integration of green spaces should be strengthened, in order to achieve a balance between supply and demand and sustainable development.

FUNDING

This study was supported by the:

1. 2024 Zhaoqing City Philosophy and Social Science 14th Five-Year Plan Project (24GJ-209);
2. 2024 Guangdong Technology College's University-level Research Platforms and Projects (2024YBZK003).

COMPETING INTERESTS

The authors have no relevant financial or non-financial interests to disclose.

REFERENCES

- [1] Hanson H I, Eckberg E, Widenberg M, et al. Gardens' contribution to people and urban green space. *Urban Forestry & Urban Greening*, 2021, 63: 127198.
- [2] Graça M, Cruz S, Monteiro A, et al. Designing urban green spaces for climate adaptation: A critical review of research outputs. *Urban Climate*, 2022, 42: 101126.
- [3] Sen S, Guchhait S K. Urban green space in India: Perception of cultural ecosystem services and psychology of situatedness and connectedness. *Ecological indicators*, 2021, 123: 107338.
- [4] Reyes-Riveros R, Altamirano A, De La Barrera F, et al. Linking public urban green spaces and human well-being: A systematic review. *Urban forestry & urban greening*, 2021, 61: 127105.
- [5] Ha J, Kim H J, With K A. Urban green space alone is not enough: A landscape analysis linking the spatial distribution of urban green space to mental health in the city of Chicago. *Landscape and Urban Planning*, 2022, 218: 104309.
- [6] Semeraro T, Scarano A, Buccolieri R, et al. Planning of urban green spaces: An ecological perspective on human benefits. *Land*, 2021, 10(2): 105.
- [7] Wang K, Wang W, Li T, et al. Optimizing living service amenities for diverse urban residents: A supply and demand balancing analysis. *Sustainability*, 2023, 15(16): 12392.
- [8] Wu H, Wang L, Zhang Z, et al. Analysis and optimization of 15-minute community life circle based on supply and demand matching: A case study of Shanghai. *PloS one*, 2021, 16(8): e256904.
- [9] Li P, Wang Z, Wang N, et al. Stochastic robust optimal operation of community integrated energy system based on integrated demand response. *International journal of electrical power & energy systems*, 2021, 128: 106735.
- [10] Huang Y, Hong X, Zheng Y, et al. Assessment and optimization of spatial equity for urban parks: A case study in Nanjing, China. *Ecological Indicators*, 2024, 166: 112449.
- [11] Liu B, Tian Y, Guo M, et al. Evaluating the disparity between supply and demand of park green space using a multi-dimensional spatial equity evaluation framework. *Cities*, 2022, 121: 103484.
- [12] Wolff M. Taking one step further—Advancing the measurement of green and blue area accessibility using spatial network analysis. *Ecological indicators*, 2021, 126(5): 107665.
- [13] Liu W, Chen W, Dong C. Spatial decay of recreational services of urban parks: Characteristics and influencing factors. *Urban Forestry & Urban Greening*, 2017, 25: 130-138.

- [14] Zhu Z, Li J, Chen Z. Green space equity: Spatial distribution of urban green spaces and correlation with urbanization in Xiamen, China. *Environment, Development and Sustainability*, 2023, 25(1): 423-443.
- [15] Rao Y, Zhong Y, He Q, et al. Assessing the equity of accessibility to urban green space: a study of 254 cities in China. *International Journal of Environmental Research and Public Health*, 2022, 19(8): 4855.
- [16] Ali M J, Rahaman M, Hossain S I. Urban green spaces for elderly human health: A planning model for healthy city living. *Land Use Policy*, 2022, 114: 105970.
- [17] Wang S, Wang M, Liu Y. Access to urban parks: Comparing spatial accessibility measures using three GIS-based approaches. *Computers, environment and urban systems*, 2021, 90: 101713.
- [18] Teng F, Wang Y, Wang M, et al. Monitoring and analysis of population distribution in China from 2000 to 2020 based on remote sensing data. *Remote Sensing*, 2022, 14(23): 6019.
- [19] Sun L, Wang J, Chang S. Population spatial distribution based on Luojia 1–01 nighttime light image: A case study of Beijing. *Chinese Geographical Science*, 2021, 31: 966-978.
- [20] Zhu J, Lu H, Zheng T, et al. Vitality of urban parks and its influencing factors from the perspective of recreational service supply, demand, and spatial links. *International journal of environmental research and public health*, 2020, 17(5): 1615.
- [21] Chen Z, Liu Q, Li M, et al. A New Strategy for Planning Urban Park Green Spaces by Considering Their Spatial Accessibility and Distributional Equity. *Forests*, 2024, 15(3): 570.
- [22] Chen D, Long X, Li Z, et al. Exploring the determinants of urban green space utilization based on microblog check-in data in Shanghai, China. *Forests*, 2021, 12(12): 1783.
- [23] Ma G, Pellegrini P, Wu H, et al. Impact of land-use mixing on the vitality of urban parks: Evidence from big data analysis in Suzhou, Yangtze River Delta region, China. *Journal of Urban Planning and Development*, 2023, 149(4): 4023045.
- [24] Ma G, Pellegrini P, Wu H, et al. Impact of land-use mixing on the vitality of urban parks: Evidence from big data analysis in Suzhou, Yangtze River Delta region, China. *Journal of Urban Planning and Development*, 2023, 149(4): 4023045.
- [25] Xing L, Liu Y, Liu X, et al. Spatio-temporal disparity between demand and supply of park green space service in urban area of Wuhan from 2000 to 2014. *Habitat International*, 2018, 71: 49-59.
- [26] Yang J. Research on optimization strategies for urban park green space planning in Nanjing based on GIS from the perspectives of network analysis and Thiessen polygon theory. *International Journal of Modern Physics C*, 2024, 2441002.
- [27] Xiao Y, Piao Y, Pan C, et al. Using buffer analysis to determine urban park cooling intensity: Five estimation methods for Nanjing, China. *Science of the Total Environment*, 2023, 868: 161463.
- [28] Chen J, Wang C, Zhang Y, et al. Measuring spatial accessibility and supply-demand deviation of urban green space: A mobile phone signaling data perspective. *Frontiers in Public Health*, 2022, 10: 1029551.
- [29] Chen P, Wang W, Qian C, et al. Gravity-based models for evaluating urban park accessibility: Why does localized selection of attractiveness factors and travel modes matter?. *Environment and Planning B: Urban Analytics and City Science*, 2024, 51(4): 904-922.
- [30] Zhang D, Ma S, Fan J, et al. Assessing spatial equity in urban park accessibility: An improve two-step catchment area method from the perspective of 15-minute city concept. *Sustainable Cities and Society*, 2023, 98: 104824.

NEW DEVELOPMENT OF BIOLOGICAL NITROGEN AND PHOSPHORUS REMOVAL PROCESSES FOR MUNICIPAL WASTEWATER

ZouTing Sun

Bohai college, Agricultural University Of Hebei, Cangzhou 061000, Heibei, China.

Corresponding Email: sunzouting@126.com

Abstracts: In recent years, with the acceleration of urbanization, surface water eutrophication caused by excessive nitrogen and phosphorus content in sewage has become increasingly serious, and highly efficient nitrogen and phosphorus removal technology has become a key demand for urban wastewater treatment. In this paper, we systematically sorted out the traditional and emerging technologies of biological nitrogen and phosphorus removal, and compared and analyzed their advantages and disadvantages. Firstly, the basic principles of biological nitrogen removal and phosphorus removal are introduced respectively, and the A_2/O process with nitrification-denitrification as the core is elaborated in detail. Secondly, for the emerging technologies, low energy consumption processes such as BCFs, SHARON-ANAMMOX combined process and Dephanox process were introduced. Finally, the advantages and disadvantages of traditional and novel processes are compared by observing the activity of microflora and other indicators. The results show that the traditional technology is mature and stable but less economical, while the new technology has significant potential for energy saving and consumption reduction, but needs to further solve the stability problem of engineering application. The multi-dimensional comparison framework and process optimization path proposed in this paper can provide theoretical references for the technological upgrading and process selection of urban wastewater treatment plants, and has positive significance in promoting the technological innovation and sustainable development of water environment treatment.

Keywords: Municipal wastewater; Biological nitrogen and phosphorus removal; New technology; New process

1 INTRODUCTION

With the acceleration of global urbanization, the discharge of urban wastewater has increased dramatically, in which the excess of nutrient salts such as nitrogen and phosphorus has become the main cause of eutrophication of surface water[1]. According to the statistics of the United Nations Environment Program (UNEP), about 40% of lakes and rivers around the world have been degraded due to eutrophication over the past decade, and the nitrogen and phosphorus loads in the tail water of municipal wastewater treatment plants have contributed as much as 30%-50%. Traditional biological nitrogen and phosphorus removal technologies (e.g. A_2/O process) achieve nitrogen and phosphorus removal through nitrification-denitrification and metabolism of phosphorus-aggregating bacteria, but their high carbon consumption, operational energy consumption, and process stability problems make it difficult to meet the demand for sustainable development under the "dual-carbon" goal[2]. In this context, it is urgent to develop new biological nitrogen and phosphorus removal technologies with high efficiency and low consumption.

In recent years, various improvement strategies have been proposed by the academic community to address the limitations of traditional technologies. For example, van Loosdrecht's team alleviated the sludge age contradiction between nitrifying bacteria and phosphorus aggregating bacteria by optimizing the sludge reflux ratio of the A_2/O process. Meanwhile, new autotrophic denitrification technologies represented by anaerobic ammonia oxidation (ANAMMOX) and short-range nitrification denitrification (SHARON) have attracted much attention due to the characteristics of no organic carbon source and low energy consumption[3]. Denitrification phosphorus removal technology achieves synchronous nitrogen and phosphorus removal through a "one carbon dual-use" mechanism, which has been proven to reduce carbon source demand by more than 30%.

This article systematically reviews and compares the advantages and bottlenecks of traditional and new technologies, aiming to provide theoretical support for the upgrading of urban sewage treatment plant processes, promote the transformation of biological nitrogen and phosphorus removal technology towards high efficiency and low-carbon direction, and assist in the sustainable development of water environment governance.

2 TRADITIONAL BIOLOGICAL DENITRIFICATION TECHNIQUES

2.1 Principles of Traditional Biological Nitrogen Removal

2.1.1 The principle of nitrogen removal

The biological denitrification process can be divided into three steps.

The first step is ammonification, which refers to the process of converting organic nitrogen compounds in water into

ammonia nitrogen under the action of ammonifying bacteria. The process of ammonification is very fast, and no special measures need to be taken.

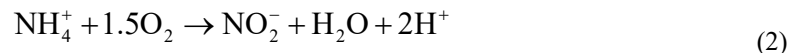
The second step is nitrification, which refers to the process under aerobic conditions where ammonia in water is first oxidized to nitrite by nitrite bacteria, and then further oxidized to nitrate by nitrate bacteria. During the reaction process, a long sludge age is required to ensure the activity and presence of nitrite and nitrate bacteria.

The third step is denitrification, which refers to the process in which denitrifying bacteria reduce nitrite and nitrate to nitrogen under anaerobic conditions, and add a carbon source to the reaction system to provide energy, causing nitrogen to be released from the water. Denitrifying bacteria are facultative anaerobic bacteria that can only undergo denitrification under anaerobic or anaerobic conditions, so it is necessary to create an anaerobic or anaerobic environment for them[4]. The reaction equation is as follows:

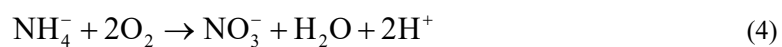
(1) Ammonification reaction



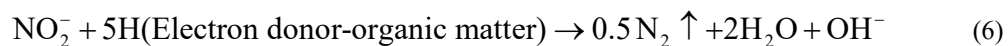
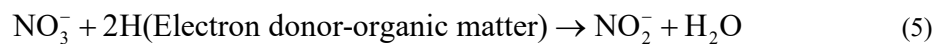
(2) Nitrification reaction



The overall reaction equation for nitrification is



(3) Denitrification



2.1.2 The principle of phosphorus removal

It refers to the process of releasing phosphorus using polyphosphate accumulating bacteria under anaerobic conditions; Under aerobic conditions, a large amount of phosphorus is absorbed from the external environment until there is an excess of phosphorus in the reaction system. The quantity is too large to meet the physiological needs of polyphosphate accumulating bacteria for reaction, so phosphorus can only be stored in the form of aggregates within the bacterial body. At the same time, it acts to form sludge with high phosphorus content and discharges it out of the system. At this point, the phosphorus content in the sewage is greatly reduced, achieving the expected results of phosphorus removal from the sewage. The process of biological phosphorus removal can be divided into the following three steps:

(1) Phosphorus uptake by phosphorus-colonizing bacteria

In a certain space and under sufficient oxygen conditions, the phosphorus removal bacteria oxidize and decompose the BOD or accumulated acids in the water, releasing energy that is mostly used to ingest phosphorus from the wastewater.

(2) Phosphorus Release by Polyphosphorus Bacteria

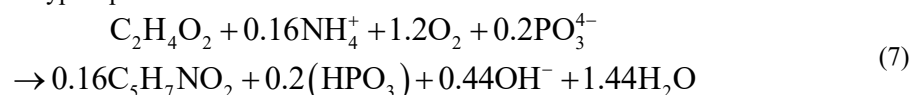
In a certain space and under anaerobic conditions, the phosphate removing bacteria break down large quantities of polyphosphates in the body by oxidation, accompanied by the production of large quantities of ATP. It consumes ATP, takes in organic matter from external sewage, and stores it inside the cell in the form of poly-B-hydroxybutyric acid, for example. At the same time the phosphoric acid produced is excreted from the body, reducing cell damage.

(3) Release of phosphorus-rich sludge

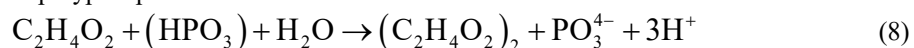
In a given space and under aerobic conditions, more phosphorus is taken in and stored than is released under otherwise identical conditions but with insufficient oxygen. The wastewater biological phosphorus removal process, in order to achieve the goal of efficient phosphorus removal, needs to utilize this characteristic of the phosphorus removing bacteria to discharge the excess remaining sludge out of the system.

The reaction equations involved in the process are as follows.

(1) Phosphorus uptake by Polyphosphorus bacteria



(2) Phosphorus release from polyphosphorus bacteria



2.2 Traditional Biological Nitrogen and Phosphorus Removal Process

Traditional biological denitrification and phosphorus removal process, based on the principle of microbial denitrification and phosphorus removal, to achieve the requirements of the environmental conditions for the growth of microorganisms can be denitrified, phosphorus removal-environmental conditions for aerobic, anaerobic and anoxic sewage treatment. Adjustment and combination of processes applicable to different situations (different sludge contents, different amounts and methods of reflux of mixed liquids, different forms of wastewater intake) to form a variety of different biological denitrification and removal of phosphorus process combinations applicable to the actual

situation[5].

A₂/O process is based on the A/O process, anaerobic structures are added before the process. The formation of an anaerobic tank-anoxic tank-aerobic tank structure combination form, is by far the simplest and most realize the synchronization of nitrogen and phosphorus removal process. A₂/O process flow, as shown in Figure 1.

First, the sewage and return sludge are passed into the anaerobic tank. Return sludge carries a small amount of nitrate nitrogen, then part of the nitrogen can first be converted into N₂ by denitrification. At this time, the organic matter in the mixture is initially degraded, while the phosphorus release by the phosphorus bacteria for the subsequent reaction to provide a biochemical reaction ATP. Then, the sewage into the anoxic tank, denitrification bacteria to the nitrate nitrogen salts brought in by the return of the mixture, as well as the organic matter of the influent water to denitrify denitrogenation. Finally, the ammonia and nitrogen in the water in the aerobic pool, nitrification reaction to generate nitrate nitrogen. The phosphorus-concentrating bacteria absorb part of the phosphorus from the water, which is separated in the sedimentation tank and discharged from the system as phosphorus-rich sludge[6].

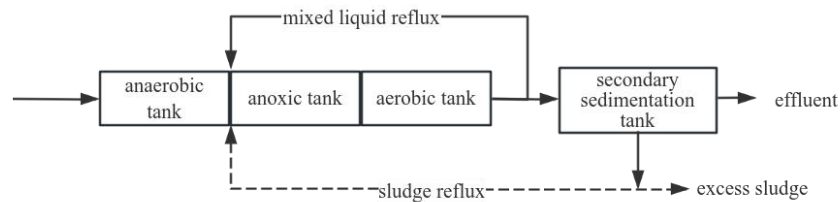


Figure 1 A₂/O Process Flow Chart

3 NEW TECHNOLOGY AND PROCESS OF BIOLOGICAL NITROGEN REMOVAL AND PHOSPHORUS REMOVAL

3.1 New Technology for Nitrogen Removal and Phosphorus Removal

3.1.1 Redenitrification and phosphorus removal

Comeau et al. discovered a new class of phosphorus-polymerizing bacteria that can remove both nitrogen and phosphorus from wastewater in the presence of insufficient oxygen. It is different from the traditional phosphorus removal process in the polyphosphorus bacteria, which was later named denitrifying polyphosphorus bacteria[7]. Macromolecular organic matter is hydrolyzed and acidified into small molecules of volatile fatty acids(VFA) by acidic anaerobes under anaerobic conditions, and denitrifying polyphosphate-oxidizing bacteria (DPAOs) take up the VFA from the environment into the body in an active transport mode, assimilating them into the endocarbon source storage PHA; while in the anoxic segment, DPAOs can use NO₃⁻ or NO₂⁻ as electron acceptors under anoxic conditions to oxidatively decompose PHA stored in the body during the anaerobic stage to generate energy from PHA stored in the body[8]. Part of this energy is used for the growth and reproduction of its own cells, and the other part is used to overdose on inorganic phosphates from the environment and stored in the body as polyphosphate. At the same time, the NO₃-N or NO₂-N in the system is reduced to N₂, realizing: two uses of one carbon. There are DEPHANOX process, A₂N-SBR process and BCFS process, which have high application value[9].

3.1.2 Simultaneous nitrification and denitrification

Simultaneous nitrification denitrification is a new type of nitrification denitrification technology found in the treatment of sewage leaching process. The main application method of this technology is to utilize the same reactor to deal with both nitrification and denitrification processes. Combined with relevant evidence, the theory is feasible and can reduce carbon demand and sludge production by 30%[10]. Developed to date, simultaneous nitrification denitrification has become a more efficient denitrification technology for wastewater treatment in major cities. There are many examples of successful applications of SND, such as SBR, biological rotor, CAST, oxidation ditch and other processes.

3.1.3 Anaerobic ammonia oxidation

It is a biological process in which microorganisms use nitrite as an electron acceptor and biochemical reactions occur under anaerobic conditions to directly convert ammonia nitrogen to nitrogen [11]. This process was discovered by Mulder et al. of Delft Technology, the Netherlands, when treating effluent water. The traditional nitrification-denitrification process requires an external carbon source in order to carry out the reaction properly, while the new technology does not require an external carbon source during the reaction, but also consumes low energy, has less operating costs, and avoids the secondary pollution that may be caused by a variety of chemicals to the water and the environment. Studies have demonstrated that the best overall performance under fully anaerobic conditions is achieved when the temperature reaches about 30°C and the pH is 8. In addition, Blum et al. showed that the environmental factors affecting anaerobic ammonia oxidizing bacteria (AnAOB) also include dissolved oxygen (DO), organic matter concentration, and C/N ratio. Therefore, efficient enrichment of AnAOB requires changing the process operating conditions according to the water quality to provide optimal growth conditions[12].

3.1.4 Short-range nitrification and denitrification

Partial-denitrification(PD) can ensure a stable supply of Anammox electron acceptors by controlling the end product in

conventional denitrification to $\text{NO}_2\text{-N}$ and inhibiting its further reduction[13]. The main consideration of the short-range denitrification process is to achieve a stable conversion of nitrate to nitrite for sustained nitrite accumulation. It nitrifies the ammonia and nitrogen in the effluent through the action of microorganisms first to nitrate, and then denitrifies the nitrate to nitrogen emission. Compared with the traditional nitrification-denitrification process, the short-range nitrification-denitrification technology has a higher nitrogen treatment efficiency and can complete the nitrogen conversion in a smaller reactor, which saves the footprint of the treatment facility, improves the nitrogen removal efficiency, and better meets the requirements of nitrogen emission indexes[14]. Currently, based on the basic principle of short-range nitrification denitrification for nitrogen removal, there are Sharon-Anammox combined process and Sharon process, etc.

3.2 New process of Nitrogen Removal and Phosphorus Removal

3.2.1 Dephanox technology

Dephanox process, which is the basis of denitrification denitrification and phosphorus removal process, the theory and application of the process to further resolve the contradiction between nitrogen and phosphorus, the process is shown in Figure 2. In Dephanox process, the sludge rich in DPAOs directly enters the anoxic tank without passing through the aerobic tank, so it does not consume PHA in the aerobic stage, but almost all of it is used as the internal carbon source material to realize the excess phosphorus absorption in the anoxic section; at the same time, the post-aeration section can remove the residual phosphorus and make the PHA in the body of the DPAOs to consume completely, so as to create the conditions for the next anaerobic stage to synthesize and renew the PHA[15]. Dephanox process can maximize the advantages of denitrification to remove phosphorus, while saving carbon source and aeration energy consumption, nitrifying bacteria and DPAOs are in their optimal growth environments, which solves the problem of differences in the age of the bacterial sludge.

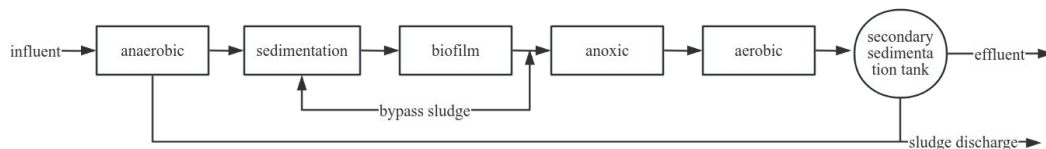


Figure 2 Dephanox Process Flow Chart

3.2.2 SHARON-ANAMMOX Joint process

Sharon process is a high nitrogen removal technology formed on the basis of the principle of short-range nitrification denitrification, which has the characteristics of effective, low energy consumption, low reaction time, no need to add foreign carbon and no secondary pollution. The difference between this principle and the traditional denitrification is that Shraon can control the ammonia nitrogen oxidation in the nitrosation stage by controlling certain conditions such as temperature and dissolved oxygen content, and at the same time denitrify it directly.

The Sharon-Anammox combined process is the process of removing ammonia and nitrogen from the effluent after a series of reactions by introducing the effluent from the preliminary formation of the Sharon process directly into the Anammox reactor[16].

3.2.3 BCFs

The BCFs process was developed by the Delft University of Technology in the Netherlands based on the principles of Pasveersloot and UCT during relevant experiments. This new process has a wide range of applications and can make full use of the efficient denitrification and phosphorus removal carried out by denitrifying phosphorus removing bacteria under anoxic conditions. In this process, up to 50% of the phosphorus is removed by this feature, and the treatment effect is very high.

The BCFs process consists of 5 reactors(anaerobic, selective, anoxic, anoxic/aerobic, and aerobic), each with a relatively specialized function. The processing flowchart of BCFs is shown in Figure 3 below. The survival environment of bacteria in each reactor can be optimized by controlling the 3 cycles. In this process reaction, the effect of nitrogen and phosphorus removal is improved, and the complete removal of phosphorus and the optimal removal of nitrogen are realized[17]. Since phosphorus bacteria have an affinity for phosphate, phosphorus-rich supernatant can be drawn from the end of the anaerobic tank to recover the phosphorus therein, improving resource utilization and maximizing environmental and economic benefits.

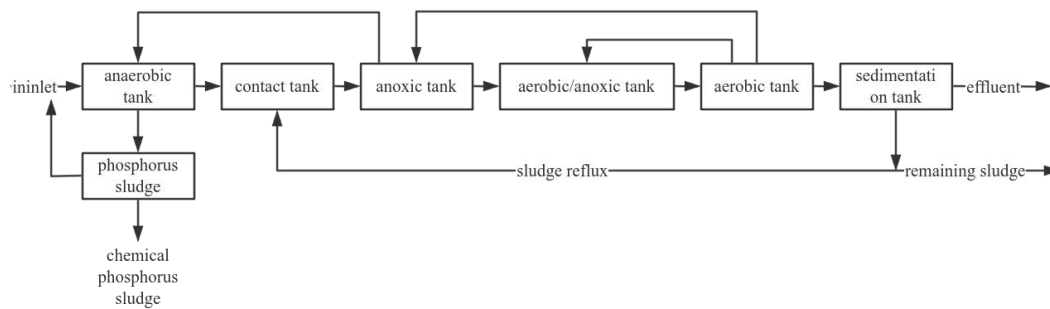


Figure 3 BCFs Process Flow Chart

4 COMPARISON OF NITROGEN REMOVAL AND PHOSPHORUS REMOVAL TECHNOLOGY

At present, the advantages and disadvantages between the new wastewater biological nitrogen and phosphorus removal technology comparison (Table 1 below). As can be seen from the table, on the whole, the different technologies can reduce the carbon source, sludge production, faster reaction rate, and then in the treatment of low C/N sewage process has a certain adaptability, and in all kinds of operating conditions, including pH, temperature, sludge age, aeration, etc., also reflects a strong tolerance, to meet the requirements of stable operation. Several technical advantages proposed in the article can be very good to improve the effect of urban wastewater denitrification and phosphorus removal treatment, although the existing research also has certain limitations, and the actual engineering application conditions are not mature enough, but in the future development of these new technologies are put into use, and many of the problems will be solved naturally. Comprehensive analysis of these new wastewater biological denitrification and removal of phosphorus technology to achieve the principle is not difficult to find, strengthen the control of the advantage of microbial flora has become an important premise to ensure the effectiveness of the process and the basis, but due to the control of the conditions required for more, hindering the new technology to further promote the application of practice.

Table 1 Advantages and Disadvantages of Nitrogen and Phosphorus Removal Technologies

Technical approach		Advantages	Disadvantages
Traditional method	biological	Easy to achieve the application, the overall stability is good, the technology is basically mature	The effect did not meet the expectation, the carbon source requirements, can not apply special water quality
Anaerobic oxidation	ammonia	Sludge has a small yield, high nitrogen removal efficiency, fast reaction speed, small carbon source demand, and good effect in low C/N sewage	The slow growth rate, the cell yield, the reaction process is easily affected by environmental factors and difficult to control
Synchronous nitrification and denitrification	nitrification	Integrated nitrogen removal and phosphorus removal can treat low C/N sewage, reduce the demand for carbon source and sludge production	Dissolved oxygen is difficult to control due to different biological reactions within one reactor
Short-range nitrification and denitrification	nitrification	It can save the consumption of oxygen, carbon source and alkalinity, reduce the sludge production; and reduce the faster denitrification rate, and reduce the HRT of the system	High requirements for bacteria, the need for seed enrichment, and has high requirements for oxygen environment
Redenitrification and phosphorus removal	and	The realization of "one carbon dual use" can save aeration and carbon source, reduce sludge production, and realize the reduction of energy consumption	Bacteria must be enriched to achieve, and subsequent sludge production is small but difficult to treat, increasing additional costs

5 SUMMARIZE

Traditional biological denitrification and phosphorus removal technology has been unable to meet the needs of modern urban sewage purification and environmental characteristics, coupled with the high standard of nitrogen and phosphorus emission requirements put forward by the state, forcing major cities in the sewage treatment process must improve the level of technology to ensure the sustainable development of sewage treatment. Through the article on the sewage treatment process of nitrogen, phosphorus removal of new technology research and comparative analysis is not difficult to find that these new wastewater biological denitrification and phosphorus removal technology (synchronous nitrification denitrification, denitrification phosphorus, anaerobic ammonia oxidation, short-range nitrification denitrification) are based on the principle of the traditional biological nitrogen removal and phosphorus removal process on the basis of further research and development of new technologies, in order to improve the economy, high efficiency, low-consumption sustainable development and the formation of new biological denitrification and phosphorus removal technologies. In order to improve the economy, high efficiency, low consumption and sustainable development and the formation of a new biological denitrification and phosphorus removal technology. It can be applied to sewage treatment

to further improve the biological denitrification and phosphorus removal process and promote urban construction and development.

The future urban wastewater treatment process for biological nitrogen and phosphorus removal should deeply integrate biotechnological innovation, digital empowerment, and the concept of resource recycling to promote the transformation of sewage treatment into a sustainable development model characterized by "low-carbon efficiency and intelligent collaboration." It is essential to continue focusing on low-consumption processes such as shortcut nitrification, anaerobic ammonium oxidation, and denitrifying phosphorus removal, while combining innovative technologies from various fields to specifically enhance the activity of functional microbial communities. Overcoming issues such as carbon source limitations and sludge production bottlenecks, continuous innovation of new biological nitrogen and phosphorus removal processes should be pursued to achieve deep removal of nitrogen and phosphorus.

COMPETING INTERESTS

The authors have no relevant financial or non-financial interests to disclose.

REFERENCES

- [1] Jordi P, Ferran R, Albert B, et al. Enhancement of biological nutrient removal process with advanced process control tools in full-scale wastewater treatment plant. *Water Research*, 2021, 200:117212-117212.
- [2] Kamonwan K, Heewon J, Rahul K, et al. Bioelectrochemical system for nitrogen removal: Fundamentals, current status, trends, and challenges. *Chemosphere*, 2023, 339:139776-139776.
- [3] Gan R, Zhang K. Enhanced nitrogen and phosphorus removal by iron-manganese mediated autotrophic denitrification in electrochemical system and the underlying mechanisms. *Process Safety and Environmental Protection*, 2024, 190(PA):545-559.
- [4] Jianmin L, Wei Z, Hong L, et al. Achieving deep autotrophic nitrogen removal in aerated biofilter driven by sponge iron: Performance and mechanism. *Environmental Research*, 2022, 213:113653-113653.
- [5] Tanwar P, Nandy T, Khan R, et al. Intermittent cyclic process for enhanced biological nutrient removal treating combined chemical laboratory wastewater. *Bioresource Technology*, 2006, 98(13):2473-2478.
- [6] Wang Y, Tang T, Wu J, et al. Succession of nitrogen and phosphorus removal functions of sludge and biofilm in low-temperature sewage treatment. *Journal of Water Process Engineering*, 2024, 58:104836.
- [7] Peng W, Xingxing Z, Yuguang W, et al. Development of a novel denitrifying phosphorus removal and partial denitrification anammox (DPR + PDA) process for advanced nitrogen and phosphorus removal from domestic and nitrate wastewaters. *Bioresource Technology*, 2021, 327:124795-124795.
- [8] Xiu-Zhen G, De-Shuang Y, Meng-Fei Y, et al. Denitrification and Phosphorus Removal from Low C/N Urban Sewage Based on a Post-Partial Denitrification AOA-SBR Process. *Huanjing Kexue*, 2019, 40(1):360-368.
- [9] Ronghua X, Fuqiang F, Qining L, et al. Overlooked Ecological Roles of Influent Wastewater Microflora in Improving Biological Phosphorus Removal in an Anoxic/Aerobic MBR Process. *Environmental Science & Technology*, 2021, 55(9).
- [10] Drawbridge M, Huo Y, Fanning E, et al. Growth, productivity and nutrient removal rates of sea lettuce (*Ulva lactuca*) in a land-based IMTA system with white seabass (*Atractoscion nobilis*) in Southern California. *Aquaculture*, 2024, 587:740836.
- [11] Wei Q, Lv D, Huang H M, et al. Research on Treatment of Domestic Sewage with Aerobic Denitrifying Bacteria Immobilized by Carbon Fiber. *Applied Mechanics and Materials*, 2014, 3547(675-677):627-632.
- [12] Weiqing J, Yunguang M, Zebing N, et al. Improving nitrogen and phosphorus removal and sludge reduction in new integrated sewage treatment facility by adjusting biomass concentration. *Journal of Water Process Engineering*, 2022, 50.
- [13] Chuansheng Y, Yongzhen P, Jiantao J, et al. Advanced nitrogen and phosphorus removal from municipal wastewater via simultaneous enhanced biological phosphorus removal and semi-nitrification (EBPR-SN) combined with anammox. *Bioprocess and Biosystems Engineering*, 2020, 43(11):1-14.
- [14] Du S, Yu D, Zhao J, et al. Achieving deep-level nutrient removal via combined denitrifying phosphorus removal and simultaneous partial nitrification-endogenous denitrification process in a single-sludge sequencing batch reactor. *Bioresource Technology*, 2019, 289:121690.
- [15] Peng C, Junkang W, Xiwu L, et al. Denitrifying phosphorus removal and microbial community characteristics of two-sludge DEPHANOX system: Effects of COD/TP ratio. *Biochemical Engineering Journal*, 2021:108059.
- [16] Zhuwu J, Zhongjian Z, Mengfan W, et al. Full-scale operation of an integrated aerated biofilter-denitrification shallow biofilter system for simultaneous nitrogen and phosphorus removal from low-carbon domestic sewage: Influencing parameters, microbial community and mechanism. *Chemical Engineering Journal*, 2023, 471.
- [17] Xiao H, Kai Y, Jianghua Y, et al. Nitrogen removal performance and microbial characteristics during simultaneous chemical phosphorus removal process using Fe₃. *Bioresource Technology*, 2022, 363:127972-127972.

CURRENT STATUS AND PROSPECTS OF ADVANCED COMPRESSED AIR ENERGY STORAGE IN CHINA

YanPeng Li^{1,2}, HaoRan Zhou^{1*}, RiPeng Cong¹, TianChen Rao¹

¹*School of Urban Geology and Engineering, Hebei GEO University, Shijiazhuang 050031, China.*

²*Hebei GEO University, Hebei Province Underground Artificial Environment Smart Development and Management Technology Innovation Center, Shijiazhuang 050031, China.*

Corresponding Author: HaoRan Zhou, Email: 1780849928@qq.com

Abstract: Under the "dual carbon" target, the intermittency and fluctuation of renewable energy generation pose challenges to grid stability, making energy storage technologies crucial for enhancing energy utilization efficiency and ensuring power system security. Among these, compressed air energy storage (CAES) has emerged as a key large-scale storage solution due to its advantages in scalability, longevity, and cost-effectiveness. This paper analyzes the fundamental principles, technological classifications, and application status of CAES in China. Studies indicate that China has successfully developed multiple hundred-megawatt-scale non-combustion CAES demonstration projects, with system efficiency reaching 65%–70%, and has achieved breakthroughs in salt cavern storage, supercritical compression, and phase-change thermal storage technologies. However, CAES in China still faces challenges such as geographical limitations, high investment costs, and an underdeveloped market mechanism. Future advancements can be driven by technological optimization, large-scale deployment, and policy incentives, ultimately establishing CAES as a core technology for renewable energy integration and grid peak shaving, thus contributing significantly to the realization of the "dual carbon" target.

Keywords: Compressed air energy storage; Energy storage technology; Current status and prospects

1 INTRODUCTION

Guided by the "dual carbon" strategic objective, renewable energy sources such as solar and wind power have been rapidly expanding, accelerating the transition toward a low-carbon energy structure in China. However, their inherent intermittency and instability pose significant challenges to the stable operation of power grids. Large-scale energy storage technologies provide an effective and economical means to mitigate curtailment of wind and solar power and facilitate peak shaving and valley filling for power grids. [1] Energy storage solutions include CAES, electrochemical storage, pumped hydro storage, and flywheel storage [2]. Among them, pumped hydro storage currently dominates due to its low cost and high efficiency. However, its application is constrained by geographical and hydrological conditions. As a large-scale physical energy storage technology with significant development potential, CAES offers advantages such as scalability, long lifespan, and cost efficiency, making it widely applicable in smart grid peak shaving and large-scale renewable energy integration. It serves as a critical solution for addressing the mismatch between energy supply and demand. Additionally, CAES enables the storage and conversion of multiple energy forms, including cold, heat, and electricity, facilitating integration with various thermal systems, thereby enhancing operational flexibility and overall efficiency [3]. This paper introduces the fundamental principles and classifications of CAES, discusses its application in China, and examines future challenges and prospects for CAES technology development in the country.

2 WORKING PRINCIPLE OF COMPRESSED AIR ENERGY STORAGE SYSTEMS

CAES is a technology that converts electrical energy into compressed air and releases it for power generation when needed. As illustrated in Figure 1, during periods of low electricity demand or excess renewable energy generation, the system uses electrical energy to drive a compressor, compressing air to high-pressure conditions for storage in underground caverns, gas tanks, or high-pressure containers. The compression process generates substantial heat, which traditional systems typically dissipate. Advanced systems, however, incorporate thermal storage technologies to recover this heat, thereby improving overall efficiency.

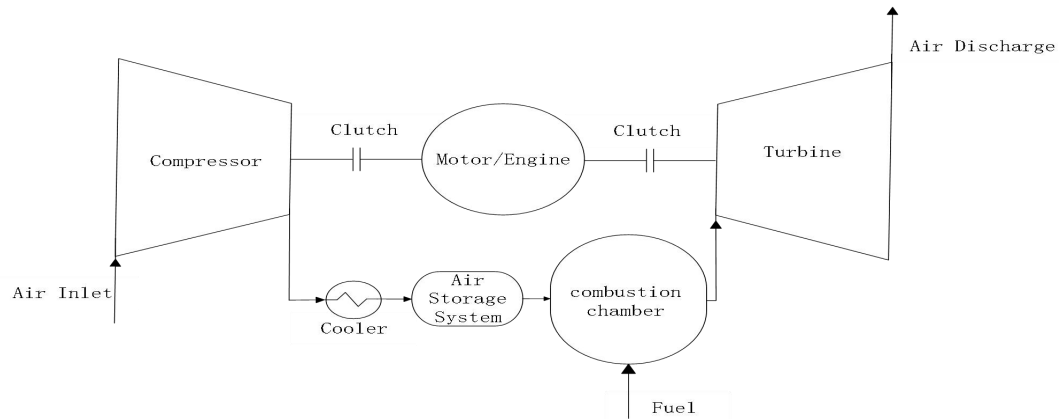


Figure 1 Schematic Diagram of Compressed Air Energy Storage

When electricity demand rises or grid peak shaving is required, the stored high-pressure air is released and expanded through turbines to drive a generator for electricity production. Traditional CAES requires preheating of the air before expansion, often achieved through natural gas combustion to enhance expansion efficiency. In contrast, advanced CAES recovers the previously stored thermal energy to provide sufficient heat for expansion, eliminating the need for additional fuel, making the system more efficient and environmentally friendly.

This process involves energy conversion and management across multiple stages, including air compression, storage, thermal management, and expansion for power generation. CAES is well-suited for large-scale, long-duration energy storage, effectively balancing grid loads, improving renewable energy utilization, and serving as an emergency backup power source. While traditional CAES systems suffer from efficiency losses due to heat dissipation, advancements in thermal energy recovery and isothermal compression have significantly improved modern CAES efficiency, positioning it as a pivotal technology in the large-scale energy storage market. The typical lifespan of CAES systems ranges from 30 to 40 years, depending on the engineering quality of the facility [4].

3 TECHNOLOGICAL CLASSIFICATION OF COMPRESSED AIR ENERGY STORAGE SYSTEMS

Since the 1940s, extensive research has been conducted on CAES technology, leading to multiple classifications based on working medium, thermodynamic processes, and system structures. The existing CAES technologies can be broadly categorized into two main branches [5]:

3.1 Classification Based on Thermal Management

3.1.1 Advanced adiabatic compressed air energy storage

AA-CAES is a closed-loop energy storage technology that achieves high-efficiency thermal energy recovery, encompassing three primary stages: compression, storage, and energy release (Figure 2). The system utilizes heat exchangers to capture the thermal energy generated during compression and later reuse it to preheat the air entering the turbine, enabling heat exchange throughout the storage and release processes. The key feature of AA-CAES lies in its adiabatic process and thermal energy reutilization.

Compared to traditional CAES, where compression heat is typically dissipated and air must be reheated via natural gas combustion during expansion, resulting in energy loss and carbon emissions, AA-CAES optimizes this process to enhance efficiency and sustainability.

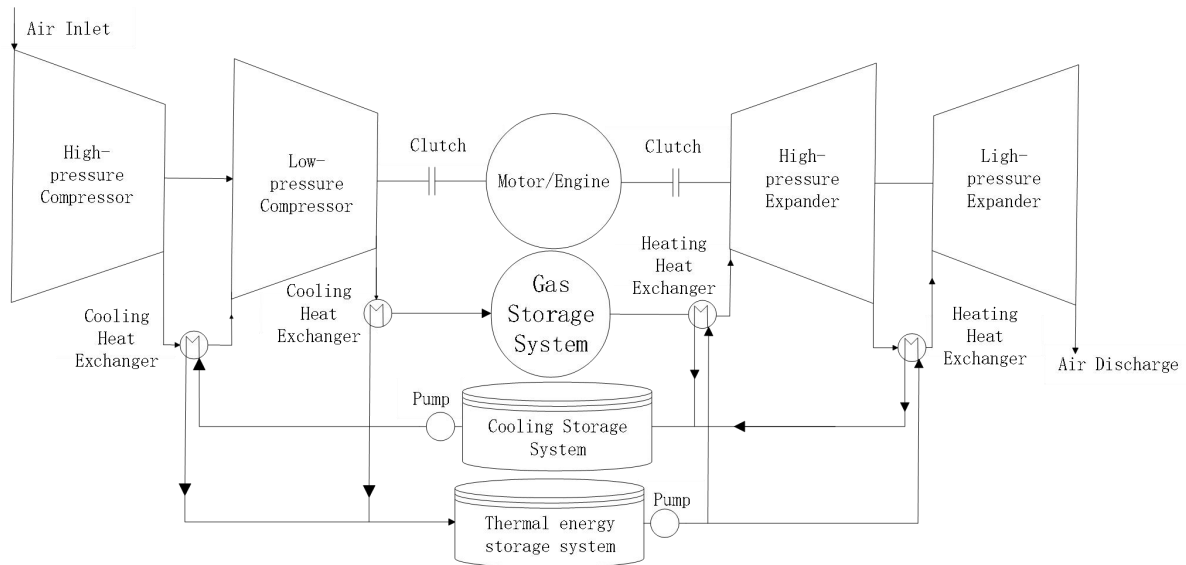


Figure 2 Schematic Diagram of Advanced Adiabatic Compressed Air Energy Storage

3.1.2 Traditional diabatic compressed air energy storage

D-CAES, also known as combustion-based CAES, is a traditional CAES technology that operates through charging and discharging processes. During charging, external electrical energy drives a compressor to compress air, which is then stored in underground caverns or high-pressure containers. The heat generated during compression may be stored or released [6]. During discharge, when power is needed, the compressed air is released, expanded through turbines to generate electricity. If thermal energy was previously stored, it can be used to preheat the air before expansion, improving power generation efficiency.

Compared to conventional gas-fired power plants, D-CAES reduces fuel consumption, making it suitable for large-scale grid peak shaving and renewable energy regulation. However, it faces challenges such as geographical constraints, efficiency limitations, and reliance on natural gas. Early CAES projects, such as Germany's Huntorf power station [7], achieved an average efficiency of only 42% due to heat dissipation losses (Figure 3). The McIntosh power station in the U.S. improved efficiency to approximately 54% by integrating gas and steam turbines in a combined cycle approach (Figure 4).

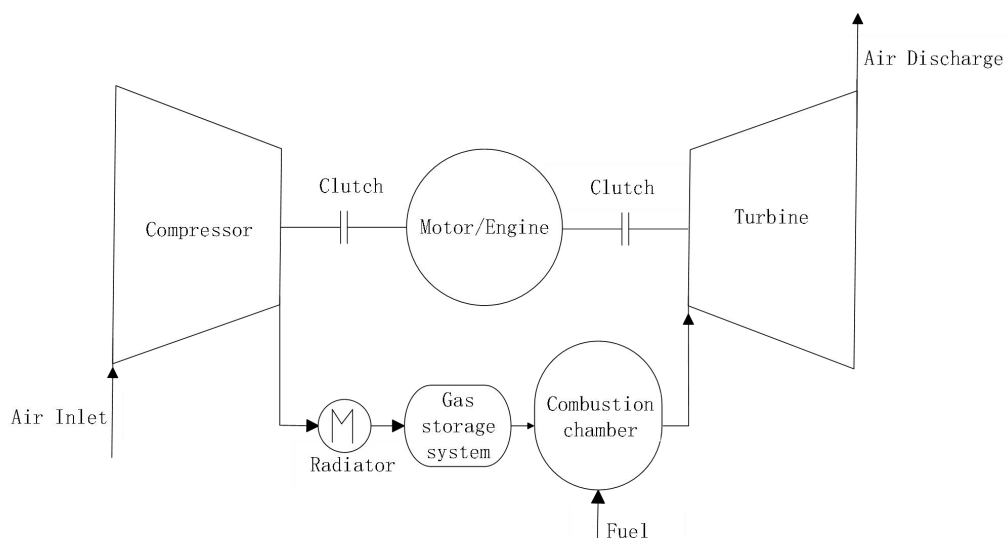


Figure 3 The Huntorf Principle of Germany

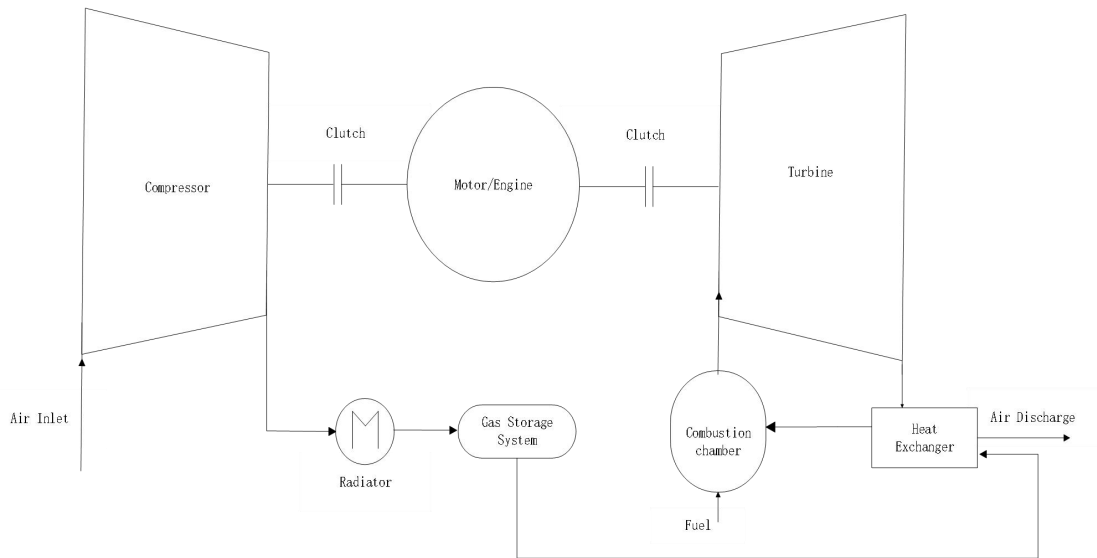


Figure 4 The McIntosh Principle of the United States

3.2 Classification Based on Medium Coupling

3.2.1 Closed-cycle Liquid-Piston Compressed Air Energy Storage

LP-CAES is an innovative CAES technology that incorporates liquid pistons (typically water or oil) in the gas compression and expansion process, enhancing energy storage efficiency while reducing environmental dependencies (Figure 5).

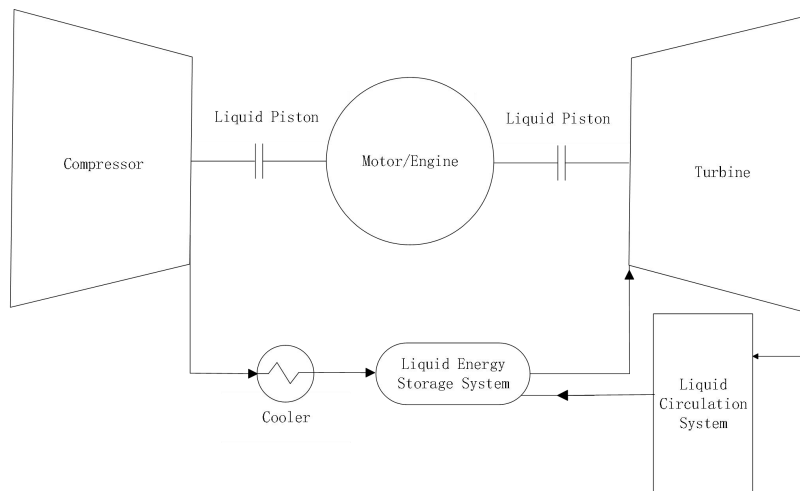


Figure 5 Closed-cycle Liquid-Gas Compressed Air Energy Storage

3.2.2 Open-cycle Liquid-Gas Compressed Air Energy Storage

OC-CAES integrates conventional CAES with liquid piston technology. The process involves air liquefaction, cryogenic storage, and expansion for power generation [8]. During charging, compressed and purified air is cooled to -196°C , transforming into liquid air for storage in insulated tanks to minimize thermal losses. During discharge, the liquid air absorbs ambient or industrial waste heat, rapidly vaporizing into high-pressure air to drive turbines, enhancing overall system efficiency (Figure 6).

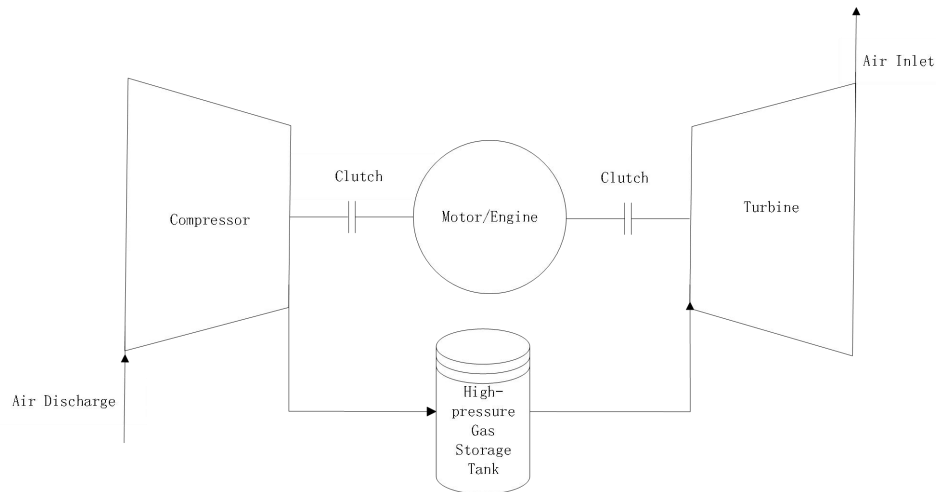


Figure 6 Open-cycle Liquid-Gas Compressed Air Energy Storage

3.3 Comparison of CAES Technologies

Different CAES technologies exhibit variations in efficiency, carbon emissions, application scenarios, and fundamental design philosophies, as shown in Table 1.

From a thermodynamic optimization perspective, AA-CAES achieves energy recycling through thermal storage devices, addressing the second law of thermodynamics by reducing entropy increase, thereby improving system efficiency. In contrast, D-CAES discards compression heat, representing a "thermodynamic compromise" that prioritizes engineering simplicity but results in lower efficiency and higher carbon emissions.

Liquid-air coupled systems introduce innovations in cross-medium energy transfer. The closed-cycle system enforces near-isothermal processes through the incompressibility of liquids, effectively controlling the polytropic exponent (n) in gas compression. The open-cycle system leverages natural geological formations as "natural pressure vessels," integrating CAES with geophysical environments. These design differences lead to distinct advantages: closed-cycle systems rely on advancements in material science and engineering, while open-cycle systems depend on geological exploration technologies.

Table 1 Technical Comparison of Compressed Air Energy Storage Technologies

Technology Type	Efficiency (%)	Carbon Emissions	Application Scenario	Core Challenge
AA-CAES	65-75	Low	Large-scale grid peak shaving	High cost of thermal storage materials
D-CAES	40-52	High	Retrofitting conventional power plants	Dependence on fossil fuels
Closed-cycle LP-CAES	60-70	Low	Distributed energy storage	Sealing and circulation stability
Open-cycle LP-CAES	55-65	Low	Geographically adaptive storage	Dependence on specific geological conditions

4 APPLICATION OF CAES TECHNOLOGY IN CHINA

In recent years, China has increasingly focused on CAES technology, with early explorations centered around demonstration projects, as shown in Table 2. The Institute of Engineering Thermophysics at the Chinese Academy of Sciences proposed a supercritical CAES system combining liquid air storage and traditional CAES in 2009, which led to the construction of a 1.5 MW pilot system in Langfang in 2013. This project validated the feasibility of a non-combustion CAES approach, marking China's transition from laboratory research to engineering verification. Following this, several large-scale projects emerged. In 2017, the Bijie 10 MW non-combustion CAES demonstration

project was commissioned, introducing salt cavern storage and achieving 60% efficiency. In 2021, the 10 MW commercial CAES power plant in Feicheng, Shandong, demonstrated economic feasibility, followed by the commissioning of the 60 MW Jintan salt cavern storage project in Jiangsu, which achieved 60% efficiency and significantly reduced gas storage costs.

By 2024, China entered a phase of large-scale CAES deployment. The Feicheng 300 MW salt cavern storage project was commissioned, boasting a 65% efficiency rate and a 100% domestically produced equipment supply chain. Concurrently, the 300 MW "Energy Storage No. 1" project in Yingcheng, Hubei, pioneered a "salt-electricity joint operation" model, enhancing local renewable energy consumption. By 2025, China's total planned CAES capacity is expected to exceed 7.5 GW, covering key regions such as Northwest and East China, marking a rapid expansion from kilowatt-scale prototypes to hundred-megawatt-scale commercial operations.

Table 2 Typical Domestic Compressed Air Energy Storage Development in Recent Years

Year	Project Name	Location	Capacity	Project Highlights
2022	Jintan Salt Cavern CAES	Jiangsu Changzhou	60MW/300MWh	First non-combustion commercial project, 60% efficiency, annual coal savings of 40,000 tons
2023	Haixi CAES Project	Qinghai Haixi	200MW/800MWh	Largest non-combustion CAES, target efficiency 65–70%, supports Northwest renewable energy base
2024	Feicheng Salt Cavern CAES	Shandong Tai'an	350MW(under construction)	First 300MW-class CAES project, optimized thermal management, expected efficiency 65-70%
2025	Wulanchabu Cold-Climate CAES	Inner Mongolia	50MW/200MWh	First cold-climate CAES, -30°C operational capability, 65% efficiency
2025	Zhangjiakou Supercritical CAES	Hebei Zhangjiakou	100MW	Ground storage alternative to salt caverns,

				supercritical
				compression for
				flexible siting
2025	Yunnan Energy Investment CAES	Yunnan	TBD	Integrating with solar resources for hybrid renewable energy utilization

5 CHALLENGES AND FUTURE PROSPECTS OF CAES TECHNOLOGY

5.1 Challenges

Compressed air energy storage (CAES) is currently undergoing large-scale development and has broad application prospects as an energy storage technology. It plays a crucial role in the construction of future intelligent energy systems and in enhancing the regulation capacity of power systems. CAES is expected to provide significant support for future power grids, though there is still room for further development [9].

(1) Geographical Constraints and Gas Storage Bottlenecks

China's salt cavern resources are concentrated in Jiangsu and Shandong, limiting national deployment. Non-salt cavern regions require artificial storage or ground tanks, which are costly and technologically immature.

(2) Economic Viability

While localization has reduced equipment costs by 30%, investment costs must decrease further from ¥5000/kW to ¥2500–3500/kW through scale-up and modular design. Market incentives such as capacity pricing and auxiliary service subsidies remain inconsistent across provinces.

(3) Competition from Other Technologies

Lithium-ion batteries dominate short-duration storage, and hydrogen storage is more suitable for ultra-long-duration applications. CAES must solidify its position as the most cost-effective long-duration storage solution.

(4) Policy and Market Mechanism Gaps

Standardized safety regulations and efficiency benchmarks are lacking. Some provinces mandate energy storage integration but lack clear financial incentives, increasing investment risks.

5.2 Future Prospects

(1) Technological Advancements

Non-combustion CAES efficiency is expected to exceed 70% with advanced heat management and supercritical storage.

(2) Cost Reduction and Localization

Full localization of CAES equipment is expected to further reduce costs to ¥2500–3500/kW by 2025. Expansion in salt cavern storage could lower gas storage costs to ¥0.5/m³.

(3) Diverse Applications

Projects such as Haixi CAES will support large-scale renewable energy bases, while Zhangjiakou integrates CAES with hydrogen production.

(4) Policy and Market Expansion

Subsidies and capacity pricing mechanisms in pilot regions like Shandong and Jiangsu are expected to be nationally implemented, improving project IRR to 8–10%.

6 CONCLUSION

This study analyzes the current status and development prospects of CAES technology in China. Research findings indicate that domestic CAES technology has achieved breakthroughs in hundred-megawatt-scale projects, with system efficiency increasing to 65%–70%, localized equipment costs reduced by 30%, and salt cavern gas storage costs lowered to ¥0.5/m³, demonstrating the scalability and feasibility of non-combustion CAES technology. Compared to pumped hydro storage, CAES offers advantages in geographical adaptability, long lifespan, and multi-energy system integration, making it suitable for grid peak shaving and renewable energy consumption. However, CAES still faces challenges, including uneven distribution of salt cavern resources, high unit investment costs, and competition from lithium-ion and hydrogen storage technologies. Future advancements in supercritical compression and phase-change thermal storage materials are expected to further improve efficiency beyond 70%. Combined with policy support and expanded application scenarios, CAES is poised to become a mainstream long-duration energy storage solution. By

2025, China's total installed CAES capacity is projected to exceed 2 GW, contributing significantly to the achievement of the "dual carbon" target.

COMPETING INTERESTS

The authors have no relevant financial or non-financial interests to disclose.

REFERENCES

- [1] Liu Xiaochi, Mei Shengwei, Ding Ruocheng, et al. Current Status, Development Trends, and Application Prospects of Compressed Air Energy Storage Engineering. *Power Automation Equipment*, 2023, 43(10): 38-47+102. DOI: 10.16081/j.epae.202309005.
- [2] Xiong Fujun, Huang Shenghua. Application of Energy Storage Technologies in Photovoltaic and Wind Power Systems under New Situations. *Light Sources and Lighting*, 2025, (01): 150-152.
- [3] Guo Dingzhang, Yin Zhao, Zhou Xuezhi, et al. Research Status and Development Trends of Gas Storage Devices in Compressed Air Energy Storage Systems. *Energy Storage Science and Technology*, 2021, 10(05): 1486-1493. DOI: 10.19799/j.cnki.2095-4239.2021.0356.
- [4] Qin Chaokui, Yuan Jing. Development Status and Application Prospects of Compressed Air Energy Storage Technology. *Shanghai Gas*, 2017, (06): 35-41.
- [5] Li Saren Gaowa, Yuan Xin, Chen Heng, et al. Introduction and Key Development Direction Prediction of Compressed Air Energy Storage Technology. *Energy Technology*, 2024, 22(06): 56-60.
- [6] Han Zhonghe, Zhou Quan, Wang Yingying, et al. An Optimization Scheme for Advanced Adiabatic Compressed Air Energy Storage (AA-CAES) Systems. *Acta Energetica Solaris Sinica*, 2016, 37(03): 629-635.
- [7] Ji Lv, Chen Haisheng, Zhang Xinjing, et al. Research and Application Prospects of Compressed Air Energy Storage Technology. *High Technology and Industrialization*, 2018, (04): 52-58.
- [8] Li Chengchen, He Xin, Tao Feiyue, et al. A New Hybrid Energy Storage System Coupling Compressed Air and Pumped Storage, and Its Thermodynamic Analysis. *Journal of Xi'an Jiaotong University*, 2022, 56(04): 40-49+71.
- [9] Li Ji, Huang Enhe, Fan Rendong, et al. Research Status and Prospects of Compressed Air Energy Storage Technology. *Turbine Technology*, 2021, 63(02): 86-89+126.

PREPARATION OF HIGH-TOUGHNESS THERMOPLASTIC STARCH FILMS VIA ENZYMATIC HYDROLYSIS AND CROSS-LINKING MODIFICATION

Hao Wang, ChuanWei Zhang*

College of Mechanical and Electrical Engineering, Qingdao University, Qingdao 266071, Shandong, China.

Corresponding Author: ChuanWei Zhang, Email: zhangchuanwei3722@163.com

Abstract: Unlike traditional petroleum-based thermoplastic films, starch-based films rely on solvent systems and cannot be processed thermally, resulting in low production efficiency and hindering large-scale industrial applications. This study developed a dual-modification method combining enzymatic hydrolysis, dual cross-linking, and plasticizers to prepare enzyme-crosslinked thermoplastic starch (ECSS). High-toughness and transparent films were fabricated via hot-pressing technology. Enzymatic hydrolysis reduced starch crystallinity and molecular chain entanglement, facilitating subsequent cross-linking reactions. Citric acid (CA) and sodium trimetaphosphate (STMP) synergistically constructed a dense molecular cross-linked network through esterification and phosphorylation, respectively. With the assistance of plasticizers, the tensile strength of the film increased by 62.3%, and the elongation at break reached 348.7%. Thermogravimetric analysis (TGA) confirmed that dual cross-linking significantly enhanced thermal stability. Differential scanning calorimetry (DSC) revealed a reduced glass transition temperature (T_g), indicating improved thermoplasticity. X-ray diffraction (XRD) demonstrated that cross-linking effectively disrupted the crystalline structure of starch, forming a stable amorphous network.

Keywords: Thermoplastic starch; Enzymatic hydrolysis; Cross-linking; High-toughness film

1 INTRODUCTION

Petroleum-derived materials are widely used in industries such as plastics, synthetic fibers, and coatings due to their cost-effectiveness and superior performance [1]. However, their environmental impacts, including pollution due to non-biodegradability, resource depletion, and carbon emissions, are undeniable [2]. The finite nature of petroleum resources, coupled with their ecological drawbacks, has spurred the search for sustainable alternatives. In recent years, significant efforts have been directed towards the development of biodegradable materials. Starch, a renewable natural polysaccharide derived from various crops, has emerged as one of the most promising feedstocks for biodegradable plastics [3]. Unlike petroleum-based polymers, starch molecules contain abundant hydroxyl groups that form strong intermolecular hydrogen bonds [4], resulting in a melting temperature that exceeds the thermal decomposition threshold. This inherent property renders native starch non-thermoplastic and unsuitable for melt processing [5].

To enhance the processability of starch-based materials, enzymatic modification using α -amylase has been explored to reduce molecular weight and crystallinity, thereby enabling thermoplastic behavior [6,7]. While enzymatically hydrolyzed starch exhibits improved adsorption capacity and delayed degradation, it suffers from inferior shear resistance compared to native starch [8]. To address this limitation, dual modification strategies combining enzymatic and chemical treatments have been proposed. For instance, Karim et al. [9] employed a hybrid approach involving fungal α -amylase/glucoamylase-mediated hydrolysis followed by hydroxypropylation with propylene oxide. The modified starch demonstrated enhanced functionality compared to unmodified counterparts. These findings underscore the potential of dual modification to overcome the mechanical deficiencies of enzymatically treated starch [10].

Chemical modifications, including oxidation, esterification, ionization, grafting, and cross-linking, are commonly employed to tailor starch properties for diverse applications [11]. Among these, cross-linking is the most prevalent technique, aimed at replacing hydrogen bonds in crystalline regions with covalent bonds (e.g., ether, phosphodiester, or organic ester linkages) to stabilize molecular networks [12]. Enzymatic hydrolysis disrupts starch chains, reducing molecular weight and disentangling helical structures [13], while subsequent cross-linking reconnects adjacent chains via ester/ether bonds [14], thereby enhancing structural integrity and restricting chain mobility. Conventional cross-linkers such as epichlorohydrin (EPI) [15], glucose-malonaldehyde [16], glutaraldehyde [17], and polyurethanes [18] face challenges including high cost, toxicity, or inefficiency. In contrast, citric acid (CA) and sodium trimetaphosphate (STMP) [19, 20] offer eco-friendly alternatives. CA enables esterification with starch hydroxyl groups under sub-gelatinization [21, 22] or heat-moisture conditions [23], forming multi-chain cross-linked networks. STMP introduces phosphate ester bonds, improving mechanical strength, thermal resistance, and water stability [24]. Their non-toxic nature, high efficiency, and compatibility with enzymatic pretreatment make CA/STMP ideal for green manufacturing of thermoplastic starch with enhanced toughness and tensile strength [25].

Cross-linking efficiency and starch properties are highly dependent on reaction parameters such as temperature, duration, pH, additive concentration, and moisture content [26]. While dry/semi-dry methods achieve satisfactory cross-linking, their high energy demands (120–160 °C) limit scalability [27]. Wet cross-linking at 40–70 °C offers a low-energy, facile alternative with precise process control. Additives further optimize reactions by activating starch

binding sites. For example, Xie et al. [28] utilized Na_2SO_4 to suppress hydrolysis and stabilize active sites, albeit generating saline wastewater. Environmentally benign additives like urea and glycerol are preferred: urea enhances plasticity through hydrophobic interactions[29], while glycerol prevents chain hardening during cross-linking [30]. Their synergistic effects improve reaction efficiency, flexibility, and thermal stability. This study aims to resolve the trade-off between thermoplastic processability and mechanical robustness in starch films. We developed a dual-modified starch (ECSS) via α -amylase-assisted hydrolysis followed by CA/STMP cross-linking, with urea/glycerol as plasticizers. Comparative analyses of native starch (NS), enzymatically hydrolyzed starch (ES), and single-crosslinked starches (ECS: CA; ESS: STMP) were conducted to elucidate the superiority of dual cross-linking. The films were characterized through macroscopic observation, mechanical testing (tensile strength, elongation), thermal analysis (DSC, TGA), melt flow rate (MFR), and microstructural techniques (FTIR, XRD, SEM). These investigations provide mechanistic insights into the fabrication of high-toughness, transparent starch-based films.

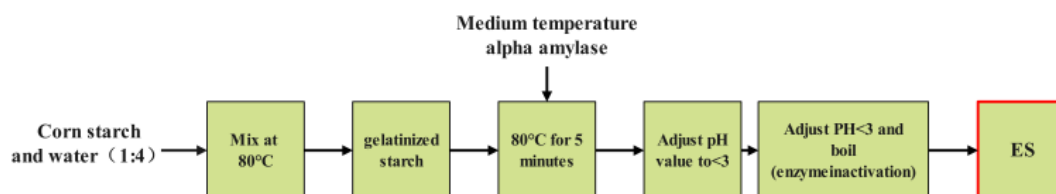


Figure 1 Process Diagram of Enzymatic Hydrolysis of Starch

2 EXPERIMENTAL MATERIALS AND METHODS

2.1 Experimental Materials

The starch used in this study was ordinary corn starch. Other chemicals and reagents included medium-temperature α -amylase (2U/mg), hydrochloric acid, sodium hydroxide, urea, citric acid, sodium tripolyphosphate, and montmorillonite, all purchased from Macklin Company (Shanghai, China). Glycerol was obtained from Shanghai Hushi.

2.2 Preparation of ES, ECS, ESS, and ECSS

The general preparation process for ES, ECS, ESS, and ECSS is outlined in Figure 1. The preparation method for ES is as follows: 20 g of corn starch was added to 80 mL of deionized water in a round-bottom flask and stirred rapidly in a water bath at 80 °C until the starch was completely gelatinized. Then, 0.05 g of medium-temperature α -amylase was dissolved in 10 mL of water and added to the gelatinized starch. The mixture was stirred for an additional 5 minutes to obtain a liquefied starch solution. This solution was then rapidly cooled in ice water to halt the enzymatic reaction. To adjust the pH of the solution below 3, 1 mol/L hydrochloric acid was added dropwise. The mixture was heated in a boiling water bath for 5 minutes and then cooled again in ice water. Once the solution reached room temperature, 1 mol/L sodium hydroxide was added to neutralize the hydrochloric acid, deactivating the enzyme. The enzymatic solution was then poured into a Teflon dish and dried in a vacuum oven at 70 °C for 24 hours to obtain ES.

For ECS, 30 g of enzymatically modified starch was mixed with 100 mL of deionized water in a round-bottom flask, and 9 g of citric acid was added. The mixture was stirred for 5 minutes. Sodium hydroxide (1 mol/L) was added dropwise to adjust the pH to 5.5. Next, 2 g of citric acid and 1 g of glycerol were added, and the mixture was stirred at 70 °C for 2 hours. After washing and drying, the product was placed in a Teflon dish with a PTFE sheet and dried in a vacuum oven at 40 °C for 48 hours to obtain ECS.

For ESS, 30 g of enzymatically modified starch was mixed with 100 mL of deionized water in a round-bottom flask, and sodium hydroxide (1 mol/L) was added to adjust the pH to 10. Then, 2 g of urea and 1 g of glycerol were added, followed by 9 g of sodium tripolyphosphate. The mixture was stirred in a water bath at 40 °C for 2 hours. After washing and drying, the product was placed in a Teflon dish with a PTFE sheet and dried in a vacuum oven at 40 °C for 48 hours to obtain ESS.

To prepare ECSS, the methods for ECS and ESS were combined. 30 g of enzymatically modified starch was mixed with 100 mL of deionized water, and 9 g of citric acid was added and stirred for 5 minutes. Sodium hydroxide (1 mol/L) was added to adjust the pH to 5.5, followed by 2 g of citric acid and 1 g of glycerol. The mixture was stirred at 70 °C for 2 hours. Sodium hydroxide (1 mol/L) was then added to adjust the pH to 10, and 9 g of sodium tripolyphosphate was added. The mixture was stirred in a water bath at 40 °C for 2 hours. After washing and drying, the product was placed in a Teflon dish with a PTFE sheet and dried in a vacuum oven at 40 °C for 48 hours to obtain ECSS.

2.3 Preparation of Modified Films

The modified starch prepared in Section 2.2 was used to produce films. An appropriate amount of dried starch was selected and compressed using a hot press at 0.5 MPa pressure and 40 °C for 2 minutes. After cooling for 5 minutes, starch-based films were obtained.

2.4 Optical Observation and Scanning Electron Microscopy

The prepared films were visually examined under bright light to assess their appearance, light transmittance, and transparency. The films were gold-coated and observed using a scanning electron microscope (JEOL-JSM6400, Tokyo, Japan) to examine their internal structure.

2.5 Microstructural Characterization of Modified Starch Molecules

2.5.1 FTIR Analysis

Fourier transform infrared spectroscopy (FTIR; Nicolet iS20, Thermo Fisher Scientific, USA) was employed to analyze the chemical structure of the modified starch films. FTIR spectra were recorded in the range of 400 to 4000 cm^{-1} for each sample.

2.5.2 XRD

X-ray diffraction (XRD; MiniFlex 600, Rigaku, Japan) was used to analyze the powders of NS and other samples. The samples were prepared with uniform thickness, and their surfaces were aligned parallel to the glass frame. The scan was conducted at a speed of 2 $^\circ/\text{min}$ for angles ranging from 10 $^\circ$ to 60 $^\circ$. Before testing, the samples were dried at 50 $^\circ\text{C}$ for 12 hours to prepare an anhydrous sample.

2.6 Mechanical Performance Testing

Mechanical testing was performed using a universal testing machine (Instron 3367, Illinois Tool Works Inc.) to measure the tensile strength and elongation at break of the hot-pressed films. Each sample, cut to a length of 35 mm and a thickness of 1 mm, underwent five tests at room temperature, and the average value was recorded.

2.7 Thermal Performance Analysis

2.7.1 Thermogravimetric Analysis (TGA)

Thermogravimetric analysis (TGA) was conducted using a TASDT650 synchronous thermal analyzer to assess the thermal stability of the films. Samples weighing approximately 5 mg were heated from room temperature to 450 $^\circ\text{C}$ at a heating rate of 10 $^\circ\text{C}/\text{min}$.

2.7.2 Differential Scanning Calorimetry (DSC)

Differential scanning calorimetry (DSC) was used to evaluate the thermal stability of the materials. Each sample was heated from room temperature to 150 $^\circ\text{C}$ at a rate of 10 $^\circ\text{C}/\text{min}$.

2.7.3 Melt Flow Rate (MFR)

The Melt Flow Rate (MFR) of the samples was tested according to the standard GB/T 3682.1-2018 D method. The tests were conducted at different temperatures and loading conditions to analyse the thermoplasticity and processing adaptability of the materials.

Two standard loading conditions were set for this experiment:

Standard test force No. 2: 1.2 kg, corresponding to approximately 11.77 N (formed by a base load of 0.325 kg plus a counterweight of 0.875 kg);

Standard test force No. 3: 2.16 kg, corresponding to approximately 21.18 N (base load 0.325 kg plus 1.835 kg counterweight).

The test temperatures were set at 120 $^\circ\text{C}$ and 150 $^\circ\text{C}$, which, in combination with the two pressure conditions, constituted four sets of experimental conditions. The samples were heated to soften under the set conditions and then extruded through a die of specified diameter. During the extrusion process, the melt strip was truncated every 20 seconds. For each set of conditions, five homogeneously truncated melt sample strips were selected and weighed, and their average mass was calculated. The resulting data were entered into a calculating device that automatically converted the melt flow rate (in $\text{g}/10\text{min}$). The test was repeated five times for each sample and the average value was taken to ensure the stability and representativeness of the experimental data.

2.8 Water Contact Angle Testing

The films were placed horizontally on the experimental platform, and 50 μL of distilled water was added each time. Once the value stabilized, the water contact angle was recorded using software. Each sample was tested five times, and the average value of the five measurements was calculated.

2.9 Water Vapour Transmission (WVT)

The water vapour transmission rate of the samples is measured using a modified version of the 'cup method' of ASTM E96-95. The test was carried out at constant temperature and humidity to evaluate the water vapour barrier properties of the films.

Firstly, the prepared starch-based films were cut into standard circles with a diameter of 65 mm and laid flat on a test cup previously filled with distilled water, making sure that the edges were sealed tightly to prevent lateral permeation. The test device was then pre-treated in a constant temperature and humidity environment with a relative humidity of

50% and a temperature of 23 ± 2 °C until the samples reached a constant state of mass, ensuring that water vapour transport occurred predominantly in the vertical direction of the film.

During the experiment, the mass change of the cup assembly was recorded every 30 minutes, and the water vapour transmission rate was calculated by monitoring the mass loss due to water evaporation. The WVT value was calculated using the following formula:

$$\text{WVT} = \frac{\Delta_m}{\Delta_t \cdot S} \quad (1)$$

Δ_m Weight loss for water, Δ_t is the experimental time, S is the film area.

3 RESULTS AND DISCUSSION

3.1 Film Morphological Analysis

Figure 2 presents both macroscopic images and cross-sectional scanning electron microscope (SEM) images of the films, which were prepared from various modified starches using hot pressing. These images are used to characterize the morphology of the films. The ECS film shows moderate transparency and a rough texture, with numerous voids and bubbles, as depicted in Figure 2a. The ESS film appears opaque, featuring a smooth surface with some internal bubbles and cracks, as shown in Figure 2b. In contrast, the ECSS film has a smooth surface, free from cracks or bubbles, and demonstrates excellent transparency, as shown in Figure 2c. These results suggest that the ECSS-modified starch films exhibit favorable morphology, confirming that the preparation method is viable.

Following enzymatic hydrolysis, the issue of molecular chain entanglement was resolved, allowing for improved thermal processing. Figures 2d, e, and f display the internal structures observed under SEM. After hot pressing, the films show no distinct starch granules, and the integrity of the starch granules is reduced. This indicates that the films possess thermoplastic properties. Compared to Figures 2d and e, Figure 2f shows a more uniform internal structure, suggesting that the ECSS film has superior thermoplastic properties.

From the SEM images, clear differences in the internal structure and bonding states of the starch films can be observed. Figure 2g (ECS film) displays surface layering and cracking, which suggests a relatively loose network structure and insufficient uniformity. Figure 2h (ESS film) shows a loose internal structure with more cracks, likely due to the high crosslinking density resulting from the crosslinking process, but without adequate flexible regulation. In contrast, Figure 2i (ECSS film) exhibits a smooth and uniform surface with no visible cracks or pores, and the internal structure is dense and consistent. This observation fully demonstrates the synergistic effect of citric acid and sodium tripolyphosphate double crosslinking, as well as the enhancement of material flexibility and uniformity through the use of plasticizers. These findings indicate that ECSS significantly outperforms the other two materials in terms of internal structure and bonding state.

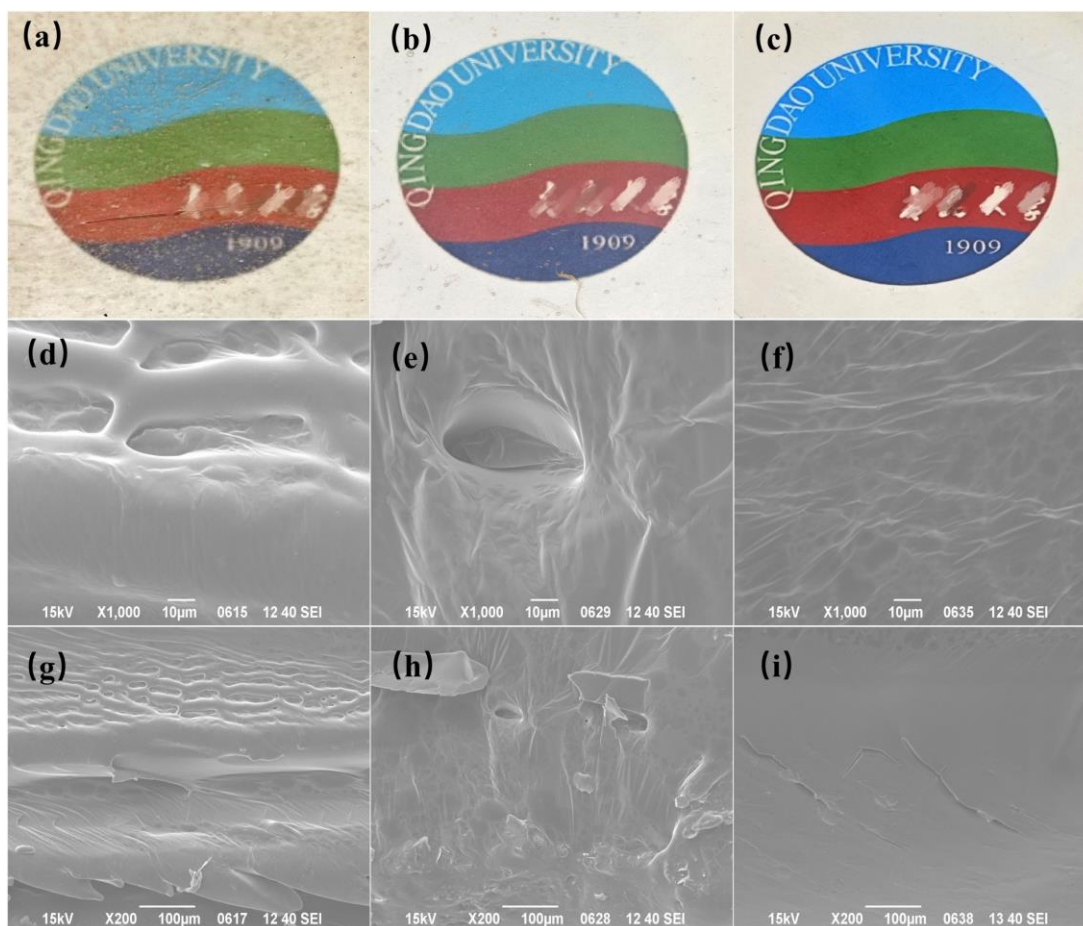


Figure 2 (a, b, c) Macroscopic Images Showing Starch Films after Hot Pressing with the Internal Structure of Different Starch Films under Electron Microscopy. (a, d, g) ECS, (b, e, h) ESS, (c, f, i) ECSS

3.2 Molecular Change Analysis

3.2.1 FTIR analysis

The Fourier transform infrared (FTIR) absorption spectra of native starch (NS), enzymatically hydrolyzed starch (ES), citric acid-crosslinked starch (ECS), sodium tripolyphosphate-crosslinked starch (ESS), and double-crosslinked starch (ECSS) are shown in Figure 3. In the FTIR spectra, NS exhibits a broad peak at 3314 cm^{-1} , corresponding to the O-H stretching vibration, which indicates the abundance of hydroxyl groups in the starch molecules. After enzymatic hydrolysis and crosslinking modifications, the O-H stretching vibration peaks of the modified samples (ES, ECS, ESS, ECSS) gradually shift to lower wavenumbers (e.g., ECSS at 3267 cm^{-1}). This shift suggests that crosslinking and plasticizing reactions enhance intermolecular hydrogen bonding while reducing the number of free hydroxyl groups. This implies that the introduction of citric acid, sodium tripolyphosphate, and plasticizers (such as glycerol and urea) significantly alters the intermolecular interactions in starch.

In the $1550\text{-}1700\text{ cm}^{-1}$ region, a new C=O stretching vibration peak appears in ECS, which is a characteristic feature of ester bond formation between citric acid and the hydroxyl groups of starch molecules, confirming the crosslinking effect of citric acid. In ESS, enhanced peaks in the $900\text{-}1200\text{ cm}^{-1}$ region (particularly around 1150 cm^{-1} and 1040 cm^{-1}) correspond to the vibrations of P=O and P-O-C bonds, indicating the presence of phosphoester crosslinking introduced by sodium tripolyphosphate. Additionally, the reduced intensity of the O-H peak in ESS suggests that some hydroxyl groups are involved in forming phosphoester bonds.

The FTIR spectrum of the double-crosslinked sample (ECSS) shows a combination of features from both the single-crosslinked materials. The C=O esterification vibration peak in the $1550\text{-}1700\text{ cm}^{-1}$ region and the phosphoester characteristic peak in the $900\text{-}1200\text{ cm}^{-1}$ region are both significantly enhanced, indicating that citric acid and sodium tripolyphosphate collaboratively participate in the crosslinking reaction, forming a denser intermolecular crosslinked network. Furthermore, the O-H vibration peak in ECSS shifts further to 3267 cm^{-1} compared to the other samples, suggesting that the double-crosslinking system significantly strengthens the intermolecular hydrogen bonding, thereby enhancing the structural stability of the starch material.

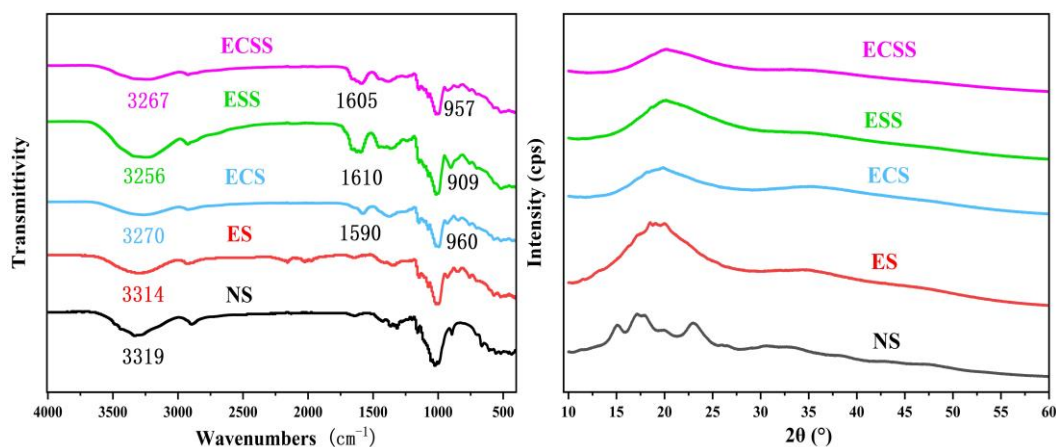


Figure 3 FTIR Absorption Spectra and XRD Spectra of NS, ES, ECS, ESS, ECSS

3.2.2 XRD analysis

The X-ray diffraction (XRD) spectra reveal significant changes in the crystal structure of the starch samples during the modification process. Native starch (NS) shows typical A-type crystal diffraction peaks at 15°, 17°, 20°, and 23°, indicating a high degree of crystallinity. However, after enzymatic hydrolysis (ES), these characteristic diffraction peaks are noticeably weakened, indicating that the enzymatic treatment disrupted part of the ordered crystalline structure in the starch molecules. Further crosslinking modifications (ECS and ESS) cause the diffraction peaks to weaken and broaden, suggesting that the crosslinking effects of citric acid and sodium tripolyphosphate significantly disrupt the molecular chain order, rendering the material more amorphous. Notably, for the double-crosslinked sample (ECSS), the diffraction peaks almost disappear, indicating a highly amorphous structure. This suggests that the double-crosslinking reaction not only disrupts the crystalline regions but also creates a denser amorphous network.

This trend of decreasing crystallinity is consistent with the changes observed in the FTIR spectra. For instance, the -OH stretching vibration peaks (3256 cm⁻¹ and 3267 cm⁻¹) in ECS and ESS are significantly reduced, suggesting that the crosslinking reaction consumes hydroxyl groups, thereby decreasing the hydrogen bonding between molecular chains. This change in chemical bonds further disrupts the ordered structure of the crystalline regions, leading to the weakening of the diffraction peaks in the XRD analysis. Therefore, by combining the XRD and FTIR analyses, it is evident that the synergistic effects of enzymatic hydrolysis and crosslinking modifications drive the starch material's transition from a crystalline to an amorphous state. This transition 'imparts enhanced mechanical properties and processability to the starch-based films.

3.3 Thermal Performance Analysis

3.3.1 Thermogravimetric Analysis (TGA)

The thermogravimetric analysis (TGA) spectra highlight significant variations in the thermal decomposition behaviors of the starch samples treated under different conditions. Native starch (NS) exhibits the lowest onset temperature for thermal decomposition, approximately 250 °C. This can be attributed to its molecular structure, where hydrogen bonding predominates and there is an absence of chemical crosslinking, which contributes to its relatively poor thermal stability. The enzymatically modified starch (ES) shows a slight increase in the onset temperature of decomposition, around 260 °C. This improvement is likely due to the partial breaking of molecular chains during enzymatic hydrolysis, which reduces the crystalline regions and moderately enhances thermal degradation properties. However, the overall thermal stability is still limited since no substantial crosslinking network is formed within the structure.

In contrast, the citric acid-crosslinked starch (ECS) demonstrates a notable increase in the thermal decomposition onset temperature, reaching above 270 °C. This indicates that citric acid induces the formation of stable chemical crosslinking bonds through esterification, thereby enhancing the structural integrity and thermal stability of the starch. The sodium tripolyphosphate-crosslinked starch (ESS) further elevates the decomposition onset temperature to around 300 °C. This enhancement is attributed to the formation of phosphoester bonds, which increase the crosslinking density between the molecules, thus further improving thermal stability. The double-crosslinked sample (ECSS) exhibits the highest thermal decomposition onset temperature, exceeding 300 °C. This suggests that the synergistic effect of citric acid and sodium tripolyphosphate, through the formation of a dense double-crosslinked network, significantly boosts molecular stability and resistance to thermal degradation.

As shown in Figure 4, the weight loss curves during thermal decomposition reveal that NS and ES undergo rapid, single-stage decomposition, exhibiting relatively straightforward degradation behavior. Conversely, the weight loss curves for ECS, ESS, and ECSS show multi-stage decomposition, indicating that crosslinking modifications have enhanced the complexity of the molecular chains, thereby delaying the onset of primary decomposition. Additionally, the ECSS sample retains the highest residual char content at elevated temperatures (>350 °C), further confirming that the double-crosslinked structure improves both thermal stability and the material's ability to undergo carbonization.

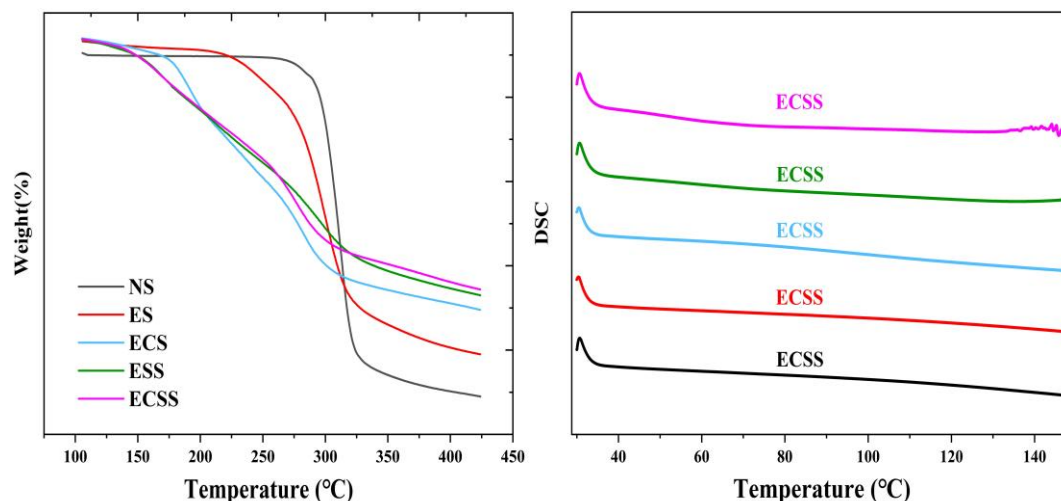


Figure 4 TGA (a) and DSC (b) Mapping of NS, ES, ECS, ECS, ECSS

3.3.2 Thermal Melt Performance (DSC)

The differential scanning calorimetry (DSC) spectra reveal distinct differences in the thermal properties of the starch samples in the temperature range of 40 °C to 150 °C. These variations primarily reflect the relationship between molecular chain arrangements, the formation of the crosslinked network, and the resulting thermal stability. The ECSS sample demonstrates the most gradual heat flow curve, suggesting significantly superior thermal stability compared to the other samples. This improvement in thermal stability is primarily attributed to the formation of the double-crosslinked network. Citric acid and sodium tripolyphosphate, by forming ester and phosphoester bonds, respectively, work synergistically to increase the crosslinking density between starch molecules. The crosslinked network not only limits the thermal motion of the molecular chains but also enhances overall thermal stability. Moreover, the addition of glycerol and urea as plasticizers optimizes the flexibility and distribution of the molecular chains, resulting in better heat resistance.

In contrast, the DSC curves of the ECS and ESS samples demonstrate relatively lower thermal stability, slightly inferior to that of the ECSS sample. Although single crosslinking modifications can increase bonding strength and crosslinking density, the limited number of crosslinking sites results in a weaker network structure and lower stability. Among these, the ESS sample shows better thermal stability in the medium-to-high temperature range compared to ECS, likely due to the more stable chemical structure provided by the phosphoester bonds formed by sodium tripolyphosphate in specific temperature ranges. The ES sample, however, exhibits a more pronounced decline in the heat flow curve, indicating poor thermal stability. The absence of chemical crosslinking support between the molecular chains—relying only on physical interactions—leads to easier decomposition when heated. Furthermore, the DSC curve of NS shows the most significant decrease in heat flow, indicating that the unmodified starch structure is more loosely organized, with weak intermolecular cohesion, making it highly susceptible to thermal degradation.

3.3.3 MFR

Melt flow rates of different samples under DIFFERENT TEMPERATURE and pressure conditions can be seen in table 1 and the melt flow rates of NS, ES, TPS, and ETPS measured under standard test forces at different temperatures and adaptability levels (120 ° C and 150 ° C) with adapta can be seen in figure 5.

Table 1 Melt Flow Rates of Different Samples under DIFFERENT TEMPERATURE and Pressure Conditions

Materials	Solute flow rate (g/10 min)			
	120°C和 11.77N	120°C N and21.18	150°C and 11.77 N	150°Cand21.18N N
NS	0	0	0	0
ES	0	0	0	0
ECS	0.88 (±0.21)	5.09 (±0.34)	1.38 (±0.16)	5.74 (±0.49)
ESS	1.43 (±0.23)	8.27 (±0.49)	2.24 (±0.35)	9.33 (±0.76)
ECSS	1.87 (±0.35)	10.81 (±0.87)	2.93 (±0.31)	12.2 (±0.88)

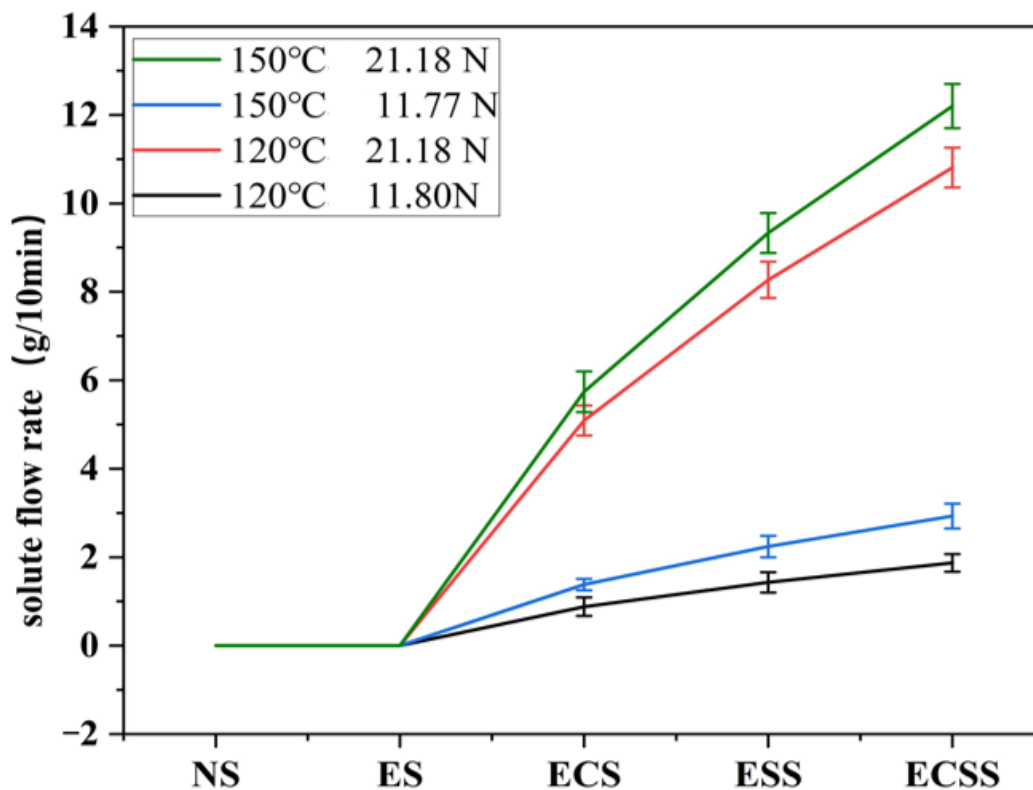


Figure 5 The Melt Flow Rates of NS, ES, TPS, and ETPS Measured under Standard Test Forces at Different Temperatures and Adaptability Levels (120 °C and 150 °C) with Adapta

3.4 Starch Film Mechanism Analysis

As illustrated in Figure 6, the crosslinking reaction between sodium tripolyphosphate (STMP) and citric acid influences the starch structure through distinct mechanisms. Sodium tripolyphosphate reacts with the hydroxyl groups in the starch molecules, forming phosphoester bonds. These bonds create a dense network structure that enhances the overall stability of the film. In contrast, citric acid undergoes esterification, where its carboxyl group forms ester bonds with the hydroxyl groups in the starch. This further strengthens the crosslinking effect while imparting some flexibility to the material.

Glycerol and urea serve as plasticizers, providing additional support. Glycerol, with its multi-hydroxyl structure, forms hydrogen bonds with the starch molecular chains, while urea, through its amino and carbonyl groups, interacts with the hydroxyl groups in starch. This interaction not only prevents excessive hardening of the chains during the crosslinking process but also enhances the flexibility and toughness of the material. Furthermore, this combination improves the overall flowability and ductility of the starch-based films.

In conclusion, the synergistic effects of these components result in starch films that demonstrate both flexibility and strength. This combination of properties makes the films more adaptable and resilient, thereby improving their suitability for various applications.

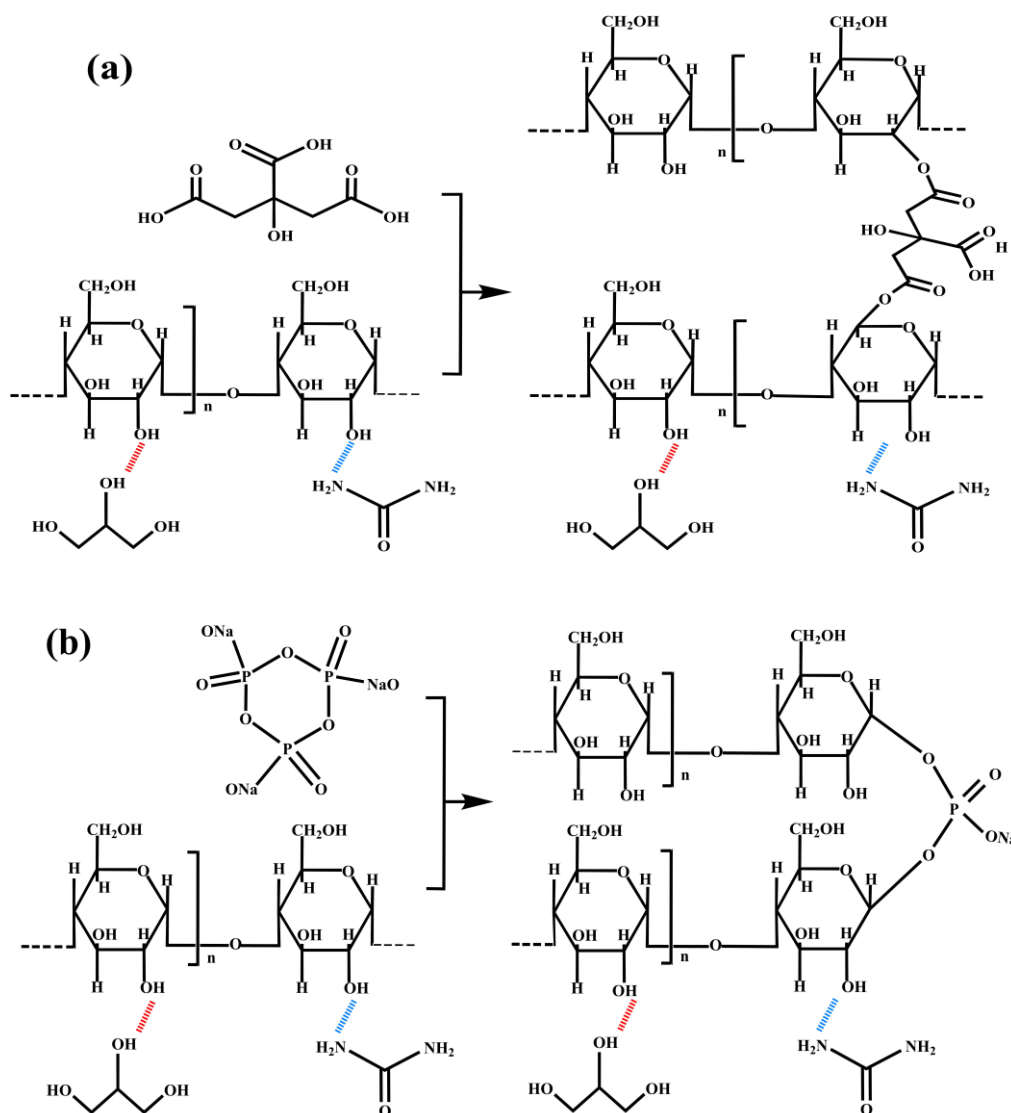


Figure 6 Crosslinking Mechanism Diagram, (a) Citric acid Crosslinking Mechanism Diagram, (b) Sodium Tripolyphosphate Crosslinking Mechanism Diagram

3.5 Mechanical Performance Analysis

As shown in the mechanical performance chart (Figure 7), the ECSS film demonstrates significantly superior tensile strength and elongation at break compared to the other samples. The tensile strength of ECSS is 1.61 MPa, substantially higher than that of the single-crosslinked ESS (1.02 MPa), ECS (0.63 MPa), and the unmodified enzymatically hydrolyzed starch ES (0.12 MPa). This considerable improvement is attributed to the formation of a double-crosslinked network, where the esterification reaction of citric acid and the phosphoester bonds formed by sodium tripolyphosphate work synergistically to increase the crosslinking density between molecules, leading to a substantial enhancement in the material's strength.

Despite its high tensile strength, the ECSS film also exhibits a remarkable elongation at break of 351.45%, which is significantly higher than the values observed for ESS (175.39%) and ECS (210.64%). This phenomenon suggests that the synergistic effect of the double-crosslinking not only increases the rigidity of the molecular chains but also enhances their flexibility. The plasticizers, glycerol and urea, form hydrogen bonds with the starch molecular chains, reducing intermolecular cohesion and increasing the flexibility of the chains. Additionally, the increased proportion of amorphous regions further facilitates the mobility of the molecular chains, which in turn improves the elongation at break.

The X-ray diffraction (XRD) spectra of the ECSS sample reveal the weakest diffraction peaks, indicating that the double-crosslinking reaction significantly disrupts the crystalline structure of the starch, resulting in a material that is almost entirely amorphous. This observation aligns with the high elongation at break seen in the mechanical performance, as the amorphous structure enhances the material's toughness, making it more ductile during stretching.

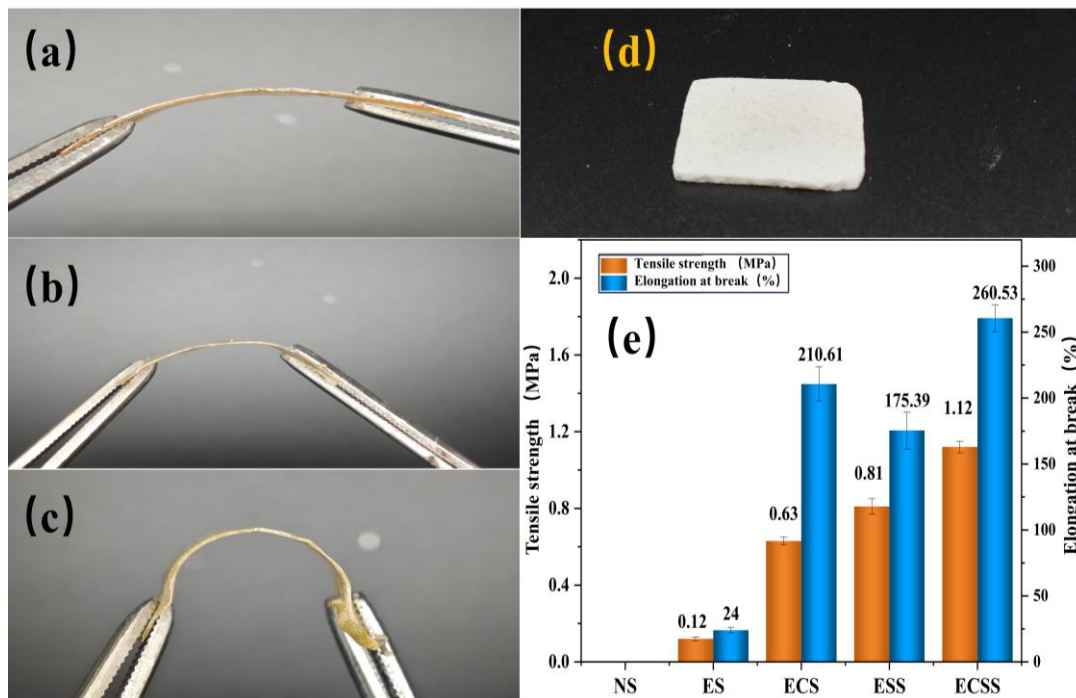


Figure 7 Comparison of Mechanical Properties of Hot Pressed Specimens with Different Modified Specimens, (a) ECS Hot Pressed Specimens (b) ESS Hot Pressing Specimen (c) ECSS Hot Pressing Specimen, (d) Comparison of Tensile Strength and Elongation at Break of Different Specimens

3.6 Water Contact Angle Analysis

The water contact angles of different film samples are shown in Figure 8. Starch is inherently hydrophilic; however, its water resistance can be significantly enhanced through modification. The results of the water contact angle tests, presented in the figure, reveal notable differences in water resistance among the ECS, ESS, and ECSS films. The water contact angle for the ECS film is 33.14° , indicating that the citric acid-crosslinked film retains some hydrophilic properties. This is attributed to the polar groups introduced by the carboxyl and ester bonds formed during the esterification reaction of citric acid, which increases the film's ability to absorb water molecules.

The water contact angle for the ESS film is 29.06° , which is lower than that of ECS. This reduction is likely due to the higher hydrophilicity of the phosphoester bonds formed by the sodium tripolyphosphate crosslinking, resulting in increased water absorption on the film surface. In contrast, the water contact angle for the ECSS film increases substantially to 51.02° , demonstrating its superior water resistance compared to the single-crosslinked films. This enhanced performance is attributed to the double-crosslinking effect of citric acid and sodium tripolyphosphate, which creates a denser crosslinked network between molecules, thereby reducing the surface free energy of the material. Additionally, the incorporation of plasticizers reduces the exposure of polar groups within the film.

In conclusion, the double-crosslinking system significantly improves the water resistance of starch-based films, offering reliable support for enhancing their water-resistant performance in practical applications.

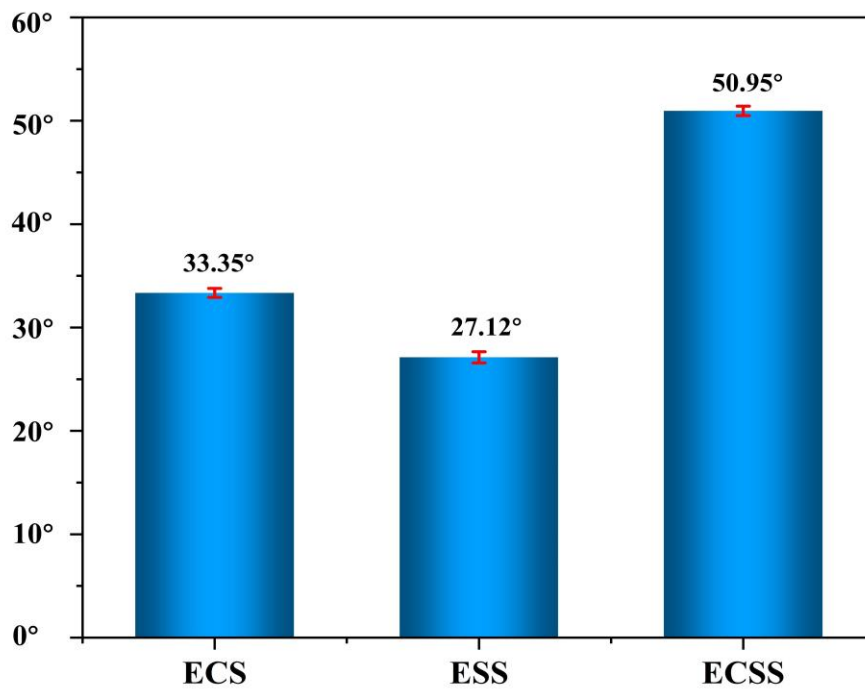


Figure 8 Water contact Angle of Different Film Samples: (a) ECS Film、(b) ESS、Film、(c) ECSS Film

3.7 Water Vapour Transmission (WVT)

The water vapour transmission rate values of the different samples are shown in Figure 9. As shown in the figure, the water vapour transmission rate values of all the three samples are high and the water repellency is not considered to be excellent. The water vapour transmission rate of the ECS film is the highest among the three samples at 14.5×100 ($\text{g}^2/\text{m} \times 24\text{h}$), which is due to the fact that the single citric acid cross-linking (ECS), although it improves the densification of the film to a certain extent, fails to inhibit the water vapour permeation effectively due to the high number of flexible chain segments. The WVT value of the sample ESS film was reduced by 13.8×100 ($\text{g}^2/\text{m} \times 24\text{h}$) to whereas the introduction of sodium trimetaphosphate for crosslinking (ESS) led to the formation of phosphate bonds in the system and the network structure was further strengthened, which made the water molecule penetration pathway more complex, thus reducing the WVTR value. The WVT value of the ECSS film is 12.9×100 ($\text{g}^2/\text{m} \times 24\text{h}$), which is the lowest among the three films. This is because the double cross-linking leads to the construction of a denser three-dimensional cross-linking network structure between the molecules, which effectively fills up the free volume between the polymer chains, and enhances the shielding effect of the film against water vapour.

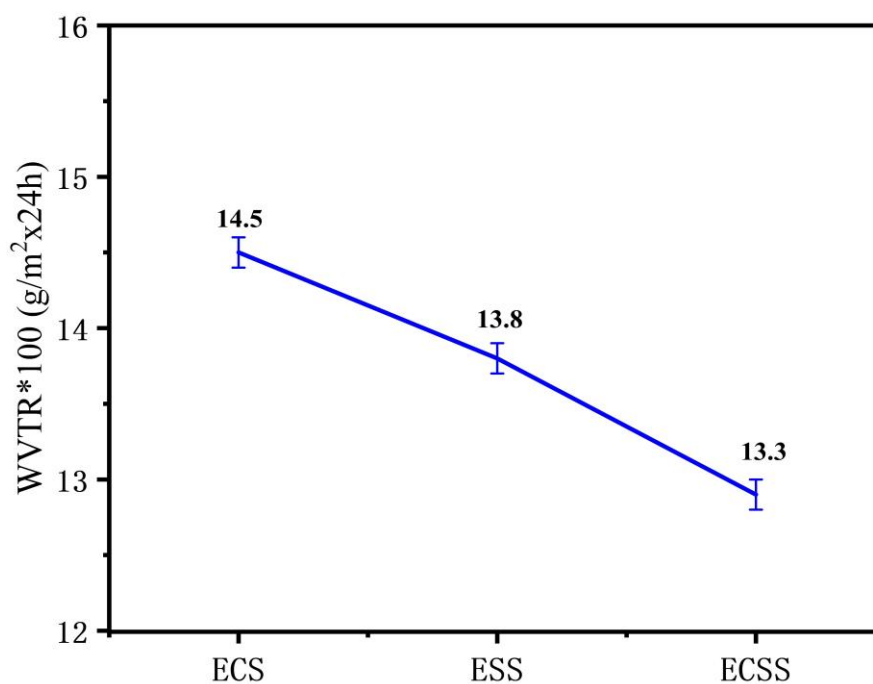


Figure 9 Water Vapor Permeability of Different Samples

4 CONCLUSIONS

This study successfully developed a double-crosslinked modified starch (ECSS) with enhanced thermoplastic properties by employing a synergistic modification strategy involving enzymatic hydrolysis, citric acid esterification, and sodium tripolyphosphate crosslinking. The resulting films demonstrated high toughness and transparency. The structural changes and performance enhancement mechanisms during the modification process were systematically investigated. Enzymatic hydrolysis significantly reduced the length and crystallinity of the starch molecular chains, minimized chain entanglement, and greatly improved the mobility of the molecular chains, thus providing a foundation for subsequent chemical modifications.

The esterification of citric acid and phosphoesterification of sodium tripolyphosphate formed a stable, three-dimensional crosslinked network between starch molecules, imparting the material with superior mechanical properties, thermal stability, and water resistance. Additionally, the incorporation of glycerol and urea as plasticizers enhanced the starch's flexibility and toughness, while effectively preventing the closure of hydroxyl active sites and improving the uniformity and efficiency of the crosslinking reaction.

After thermal processing, the modified starch films exhibited excellent thermal stability and mechanical strength. The results confirmed that the double-crosslinking modification significantly improved the material's thermal stability and mechanical strength, enabling the films to retain better shape stability at high temperatures. Mechanical performance testing revealed outstanding flexibility and tensile properties.

The enzymatic double-crosslinking modification strategy proposed in this study offers a novel solution to overcome the limitations of starch-based materials in thermoplastic processing. Furthermore, it provides both theoretical and practical foundations for the development of green, biodegradable, and high-performance starch-based thermoplastic materials. This approach holds considerable promise for applications in packaging, coatings, and functional composite materials.

COMPETING INTERESTS

The authors have no relevant financial or non-financial interests to disclose.

REFERENCES

- [1] X Luan, M Kumar, H Wang, et al. Dynamic material flow analysis of plastics in China from 1950 to 2050. *Resources, Conservation and Recycling*, 2021, 327: 129492.
- [2] M Kumar, S Sharma, Y Zhang, et al. Current research trends on micro- and nano-plastics as an emerging threat to global environment: A review. *Journal of Hazardous Materials*, 2021, 409: 124967.
- [3] W Ning, Y Zhao, C Liu, et al. The influence of citric acid on the properties of thermoplastic starch/linear low-density polyethylene blends. *Carbohydrate Polymers*, 2007, 67(3): 446–453.
- [4] B-T Wang, Q Zhang, Y Wang, et al. Studies of cellulose and starch utilization and the regulatory mechanisms of related enzymes in fungi. *Journal of Fungi*, 2020, 12(3): 530.
- [5] M Xu, Y Liu, J Wang, et al. Fabrication high toughness poly(butylene adipate-co-terephthalate)/thermoplastic starch composites via melt compounding with ethylene-methyl acrylate-glycidyl methacrylate. *Composites Part B: Engineering*, 2023, 250: 126446.
- [6] LZ Li, F Zhang, X Chen, et al. The effect of starch concentration on the gelatinization and liquefaction of corn starch. *Starch/Stärke*, 2015.
- [7] S Wang, J Liu, M Zhao, et al. Treatment and mechanism for hot melting starch by reducing the molecular chain winding and crystallinity. *International Journal of Biological Macromolecules*, 2024, 325: 121574.
- [8] H Xiao, Q Lin, G-Q Liu. Effect of cross-linking and enzymatic hydrolysis composite modification on the properties of rice starches. *Molecules*, 2012, 17(7): 8136–8146.
- [9] A Karim, Y Nadiha, O Nazuni, et al. Dual modification of starch via partial enzymatic hydrolysis in the granular state and subsequent hydroxypropylation. *Carbohydrate Polymers*, 2008, 56(22): 10901–10907.
- [10] B Kaur, D Ariffin, A Bhat, et al. Progress in starch modification in the last decade. *Food Hydrocolloids*, 2012, 26(2): 398–404.
- [11] A Gilet, T Martin, C Lefèvre, et al. Synthesis of 2-hydroxydodecyl starch ethers: Importance of the purification process. *Carbohydrate Polymers*, 2018, 58(7): 2437–2444.
- [12] W S Ratnayake, D S Jackson, et al. Phase transition of cross-linked and hydroxypropylated corn (*Zea mays* L.) starches. *LWT - Food Science and Technology*, 2008, 41(2): 346–358.
- [13] H Kong, Z Li, J Zhang, et al. Fine structure impacts highly concentrated starch liquefaction process and product performance. *Food Chemistry*, 2021, 164: 113347.
- [14] J Compart, A Schmidt, H Gruber, et al. Customizing starch properties: A review of starch modifications and their applications. *Polymers*, 2023, 15(16): 3491.
- [15] JN BeMiller. Effect of hydrocolloids on normal and waxy maize starches cross-linked with epichlorohydrin. *Food Hydrocolloids*, 2021, 112: 106260.
- [16] X Wang, L Chen, Y Li, et al. Crosslinking effect of dialdehyde starch (DAS) on decellularized porcine aortas for tissue engineering. *Acta Biomaterialia*, 2015, 79: 813–821.
- [17] B S Scopel, L B Silva, D S Andrade, et al. Starch-leather waste gelatin films cross-linked with glutaraldehyde. *Journal of Polymers and the Environment*, 2020, 28: 1974–1984.

- [18] R Lubczak, D Szczęch, et al. Polyurethane foams with starch. *Journal of Chemical Technology and Biotechnology*, 2019, 94(1): 109–119.
- [19] I Lipatova, A Yusova. Effect of mechanical activation on starch crosslinking with citric acid. *International Journal of Biological Macromolecules*, 2021, 185: 688–695.
- [20] Y Zhao, X Zheng, T Hu, et al. Cross-linked modification of tapioca starch by sodium trimetaphosphate: An influence on its structure. *Carbohydrate Polymers*, 2024, 23: 101670.
- [21] A S Babu, R Kumar, V Patel, et al. Chemical and structural properties of sweet potato starch treated with organic and inorganic acid. *Carbohydrate Polymers*, 2015, 52: 5745–5753.
- [22] P C Martins, L C Gutkoski, V G Martins. Impact of acid hydrolysis and esterification process in rice and potato starch properties. *International Journal of Biological Macromolecules*, 2018, 120: 959–965.
- [23] P Van Hung, T N Dung, T M Cuong, et al. Physicochemical characteristics and in vitro digestibility of potato and cassava starches under organic acid and heat-moisture treatments. *Food Chemistry*, 2017, 95: 299–305.
- [24] K Noulis, G Drosou, E Papadopoulou, et al. Sodium trimetaphosphate crosslinked starch films reinforced with montmorillonite. *Polymers*, 2023, 15(17): 3540.
- [25] H-S Kim, J H Lee, M S Park, et al. Cross-linking of corn starch with phosphorus oxychloride under ultra high pressure. *Carbohydrate Polymers*, 2012, 130(4): 977–980.
- [26] N Hu, F Zhang, J Li, et al. Synthesis and evaluation of microstructure of phosphorylated chestnut starch. *Starch/Stärke*, 2014, 37(1): 75–85.
- [27] Y Xie, Z Li, W Wang, et al. Effects of cross-linking with sodium trimetaphosphate on structural and adsorptive properties of porous wheat starches. *Food Chemistry*, 2019, 289: 187–194.
- [28] J Hu, X Wang, R Liu, et al. Dissolution of starch in urea/NaOH aqueous solutions. *Carbohydrate Polymers*, 2016, 133(19).
- [29] P Liu, H Zhang, M Fang, et al. Effects of different ratios of water and glycerol on the physicochemical properties of starch-based straws. *International Journal of Biological Macromolecules*, 2025, 466: 142215.
- [30] P Cheviron, F Gouanvé, E Espuche. Preparation, characterization and barrier properties of silver/montmorillonite/starch nanocomposite films. *Journal of Membrane Science*, 2016, 497: 162–171.

THE DEVELOPMENT OF THE INCLUSION OF THE SHIPPING INDUSTRY IN EMISSION TRADING SYSTEMS AND ITS IMPACT ON THE SHIPPING SECTOR

Cong Xu

Shipping Management and Law, Shanghai Maritime University, Shanghai 201308, China.
Corresponding Email: cc_19951215@hotmail.com

Abstract: With the growing global demand to address climate change, emission trading systems have gradually become a core tool for reducing greenhouse gas emissions in various regions. Shipping is an essential part of global trade, and several regions are either already including or planning to include the sector in their emission trading systems. Given the varying levels of development of ETS across different regions, the management approaches for incorporating shipping into these systems differ significantly. The incorporation of shipping will have widespread implications for shipowners, international cargo owners, ship operators, and the shipbuilding industry. As the shipping sector takes on the responsibility of transporting international goods, its integration into ETS will drive significant changes across various industries. These changes include increased compliance costs, new regulatory requirements, and a shift toward cleaner technologies and fuels. The paper discusses the impacts of these changes, focusing on how shipping's inclusion in ETS is reshaping the sector globally and driving its transition towards sustainability.

Keywords: Emission trading system; Shipping industry; Decarbonization; Energy efficiency; Green shipping corridors

1 INTRODUCTION

As the core way of transport supporting global trade, the shipping industry is responsible for over 90% of international cargo transportation. Its total carbon emissions account for 2.89% of global anthropogenic emissions, being significant negative externality characteristics. Currently, there are three main types of measures being implemented in the shipping industry to reduce carbon emissions: technological measures, operational measures, and market-based measures.

Technological measures primarily involve improving ship energy efficiency, using clean fuels, and replacing old, high-emission ships with newer vessel. Operational measures include reducing ship speed, optimizing routes based on weather conditions, improving logistics management, enhancing loading and unloading efficiency, and maintaining ship hulls. These measures focus on management efficiency and operations to reduce greenhouse gas emissions. Market-based measures refer to incorporating the shipping industry into emission trading system(ETS)and carbon taxes, using market-based regulatory tools to actively engage the shipping industry in emission reduction efforts. Essentially, an ETS is a market-based incentive mechanism that controls the cost of emissions in the shipping industry by adjusting the total emission allowance, allocation methods, and prices. It encourages industries to upgrade their technologies and operational methods to reduce greenhouse gas emissions. Theoretically, there are two types of ETS: the *Cap and Trade* system and the Baseline system. However, discussions and research on ETS typically refer to the *Cap and Trade* system. The key difference between these two mechanisms lies in their approach to setting emission limits. The *Cap and Trade* system sets a fixed upper limit on the total emissions within the system, while the Baseline system establishes a reduction target or carbon debt based on the entity's performance relative to the baseline. Under both mechanisms, emission reductions or surplus allowance can be traded between companies. However, the Baseline system is more complex and typically incurs higher costs for regulators. Baseline system requires setting emission baselines for each covered emission activity or industry, and emissions from each entity are measured against these baselines. In contrast, the *Cap and Trade* system does not require baseline calculations, as the total emissions cap is the key factor driving the emission reduction goals. Some Baseline systems set specific emission targets for different facilities to determine the credit-generating emission baselines.

The emission reduction in the shipping sector reflects a typical multilateral regulatory predicament: On one hand, the shipping industry actively responds to global emission reduction trends, making breakthroughs in technology and operations. However, the potential for technological improvements, such as in fuel consumption, is constrained by the long economic life cycle of ships, making it difficult to achieve emission reductions in a short term. It means that the shipping industry cannot solely rely on incremental technological advancements to meet the goal of net-zero emissions. On the other hand, carbon pricing mechanisms are rapidly developing globally. While the International Maritime Organization (IMO) coordinates global shipping emission reduction efforts, the approaches adopted by different regions are subject to regional limitations. Due to the international nature of shipping, carbon pricing mechanisms implemented by different regions face issues of overlap and conflict during their implementation.

2 CHALLENGES OF INTERNATIONAL SHIPPING EMISSION TRADING SYSTEM

According to the Convention on the International Maritime Organization under the International Convention for the

Prevention of Pollution from Ships (MARPOL), IMO, as a specialized agency of the United Nations responsible for global shipping emissions reduction, has proposed the establishment of a global shipping ETS market. This initiative aims to cover international shipping carbon emissions through a unified system of allowance allocation and trading rules, with the core objective of supporting the maritime industry's commitment to achieving net-zero emissions by 2050[1].

IMO suggests that regional carbon trading mechanisms that incorporate shipping into carbon trading systems have a negative impact on global emissions reduction efforts. Therefore, IMO prefers to lead the establishment of a global carbon trading market for shipping. However, the *no more favorable treatment* principle established under the MARPOL Convention requires equal application of technical standards to all ships, which creates a normative conflict with the *common but differentiated responsibilities* principle under the UNFCCC framework. This is especially apparent in the allocation of carbon emission allowance, where developing countries advocate for differentiated management based on *per capita emission equivalents*, while developed countries emphasize that the *stateless emissions* nature of shipping should apply a uniform standard. As a result, it is difficult to reach a consensus on a unified plan.

Currently, countries and regions such as China, the European Union, New Zealand, South Korea, and the United States have established carbon emissions trading systems. However, most carbon emissions trading systems remain limited to sectors like energy, electricity, and road transportation. Only China (Shanghai), the EU, the UK, and South Korea have already included or plan to include shipping within the scope of carbon emissions trading.

3 PROGRESS OF EMISSION TRADING SYSTEMS IN AREAS INCORPORATING SHIPPING

3.1 The Korean Emissions Trading Scheme (K-ETS)

As the first Asian country to commit to carbon neutrality, South Korea has a detailed and proactive plan for establishing a carbon trading system. South Korea's carbon market, commonly referred to as K-ETS, was launched in 2015 with a government-operated carbon credit market that allocates emission allowances for businesses. Through policies and regulations such as the *Framework Act on Carbon Neutrality and Green Growth to Address the Climate Crisis* and the *Greenhouse Gas Emissions Trading Act*, the government has set carbon reduction targets and strategies for the country.

The carbon trading mechanism has had a significant impact on South Korea's industries, as it requires high-emission companies to purchase allowances or reduce emissions. This has increased operational costs for energy-intensive sectors such as steel, chemicals, and shipbuilding. It may lead to a decrease in profit margins and drive companies to seek energy-saving and emission-reduction technologies. South Korea's export-oriented industries may also face risks of reduced international competitiveness, particularly in cases where global carbon prices vary significantly.

Overall, the development of South Korea's carbon market can be divided into three stages: the first stage (2015–2017), the second stage (2018–2020), and the third stage (2021–2025)[2]. Each stage involves adjustments and upgrades in areas such as the market's coverage, allowance allocation, and offset mechanisms. As the market evolved from the first to the third stage, the sectors covered by the carbon market gradually expanded. In December 2014, the South Korean government officially included the shipping sector in the national carbon allowance allocation plan for the third phase of the K-ETS.

In principle, South Korea allocates different amounts of carbon allowances depending on the industry. However, for industries or businesses with special greenhouse gas emission characteristics (such as transition industries), separate industry-specific allowances may be calculated. The shipping industry is one such exception, and it receives fully free carbon emission allowances. South Korea's shipping industry is heavily supported by its shipbuilding sector. The three major conglomerates—Hyundai Heavy Industries, Samsung Heavy Industries, and Hanwha Ocean—account for 80% of global LNG carrier orders and 60% of orders for ultra-large container ships, with the growth rate for eco-friendly ship orders reaching 17% annually. The shipping industry contributes more than 7% of South Korea's domestic manufacturing output, and its upstream and downstream industries cover over 15 sectors, including steel, electronics, and new energy materials.

3.2 The UK ETS after Brexit

Before Brexit, the UK's carbon emissions were regulated under the EU Emissions Trading System (EU ETS). As a member of the EU, the UK participated in the EU ETS from its launch in 2005 until January 31, 2020, when it officially left the EU. Subsequently, the UK established an independent carbon trading system, which replaced the EU ETS framework on January 1, 2021.

According to a 2022 UK government survey, the UK Emissions Trading Scheme (UK ETS) covers about 25% of the UK's territorial carbon emissions. The UK ETS covers the electricity sector, energy-intensive industries, and domestic flights, as well as flights between the UK and the European Economic Area (EEA), Switzerland, and flights between the UK and the Strait of Gibraltar. The main program of the UK ETS involves 678 fixed installations and 369 aviation operators. Additionally, the scheme includes 250 facilities that participate through the *Hospital and Small Emitters Opt-out Mechanism*, and 110 *Ultra-small Emitters*[3]. Under the terms of the Windsor Framework, five power generation facilities in Northern Ireland continue to participate in the EU ETS.

The UK plans to include shipping in the carbon trading market starting in 2026, and the UK ETS management is actively exploring the possibility of extending the scheme to the maritime industry. Public consultations have already been launched regarding this policy. Shipping is one of the pillar industries in the UK, a nation with a long maritime

history, and 95% of the UK's imported goods are transported by sea. The shipping industry also creates numerous jobs in the UK, including in shipbuilding and port operations.

Under the current proposal, emissions included in the UK ETS mainly pertain to domestic maritime emissions, which cover emissions from voyages that begin and end at the same UK port, voyages between two UK ports, and emissions from anchoring and mooring during these voyages (including offshore facilities). The scope also includes emissions generated at berth in UK ports, including emissions from vessels arriving at or departing for international destinations. The consultation report also suggests that domestic maritime emissions should include emissions generated while vessels are moored at UK ports, even if the ship is leaving the port to travel to a foreign port.

3.3 Regional Emission Trading System and National Emission Trading System of China

China's carbon trading market was initially established through pilot cities. Since 2011, China has launched carbon emission trading pilot programs in seven regions: Beijing, Tianjin, Shanghai, Chongqing, Hubei, Guangdong, and Shenzhen. In December 2016, Fujian Province started its carbon trading market, becoming the eighth pilot region. In 2017, China marked the beginning of establishing a nationwide carbon trading market. On July 16, 2021, the national carbon market officially launched trading, while regional carbon trading markets continued to run. China's carbon trading market primarily focuses on energy-intensive industries, such as electricity and steel.

Due to this development model, the operation of China's carbon trading market varies between cities, with different regulations in place. Regional government departments are allowed to make the rules for their respective regional carbon trading markets.

According to a document released by the Shanghai Municipal Bureau of Ecology and Environment in 2024, 31 shipping companies have now been included in the carbon emission monitoring and trading market. This is currently the only carbon emission trading market in China that includes shipping. According to the *Shanghai Shipping Industry Greenhouse Gas Emissions Accounting and Reporting Method (Trial)* issued by the Shanghai Development and Reform Commission in 2016, enterprises engaged in waterborne freight and passenger transport in Shanghai are required to monitor, account for, and regularly report the amount of carbon dioxide emissions generated during their operations.

3.4 EU ETS

The *European Climate Law* legally commits the European Union to achieve climate neutrality by 2050, with the first milestone being a reduction in net greenhouse gas emissions to at least 55% below 1990 levels by 2030.

As the most ambitious sustainable roadmap globally, the European Green Deal, proposed in 2019, aims to drive Europe's economic sustainable development through systemic transformation and plans to achieve the world's first carbon-neutral region by 2050[4]. It regulates emissions from power and heat generation, industry, and aviation, which account for about 40% of the EU's total emissions. The EU Emissions Trading System (EU ETS) is a key pillar in implementing *the European Green Deal*.

Since its launch in 2005, the EU ETS has developed into one of the largest carbon trading markets globally. Its coverage has gradually expanded from power and industrial sectors to other energy-intensive industries.

In December 2022, the European Parliament and the EU Council reached a political agreement to revise the EU Emissions Trading System, contributing to achieving more ambitious climate goals for 2030. Compared to 2005 levels, emissions under the EU ETS will be reduced by 62% by 2030. Stricter reduction measures will start taking effect from 2024, and the cumulative reductions over the next seven years will significantly increase. Taking action across the economy to address climate change is crucial. This agreement contributes to achieving this goal by extending the EU ETS to include its fair share of emissions from maritime transport[5].

3.4 New Zealand ETS

New Zealand's carbon trading system, which began in 2008, is the only mandatory carbon emissions trading market in Oceania after the Australian carbon tax was repealed and its national carbon market plan was not implemented. The New Zealand carbon market is the first national carbon pricing system in the world to comprehensively cover agricultural emissions[6]. The system integrates six greenhouse gases, including carbon dioxide, methane, and sulfur hexafluoride, under the *Cap and Trade* principle. By 2023, the covered emissions reached 27.9 MtCO_{2e}, accounting for 38% of the total emissions of New Zealand.

In the early stages of the New Zealand emissions trading system, its broad coverage and low entry thresholds had limited effectiveness, as no emissions cap was initially set. The turning point came with the *2020 Climate Change Response (Emissions Trading Reform) Amendment*, which established an emissions cap for the system and introduced a allowance auction mechanism.

Although domestic aviation and coastal shipping emissions make up a small portion of transportation emissions, accounting for about 8% of total national greenhouse gas emissions, maritime transport and supply chains are key drivers of New Zealand's economy. New Zealand is actively implementing decarbonization strategies in these sectors to better manage supply chain emissions and maintain the competitiveness of upstream and downstream industries in international markets.

From 2008 to 2015, New Zealand's emissions trading system allowed participants to obtain emissions allowances through trading in international emissions markets. However, this provision was later removed, and the New Zealand

emissions trading system became a domestic market with no special connection to other regional trading systems. As one of the most comprehensive trading systems, New Zealand's emissions trading system included the transport sector, including shipping, from the outset, and mandates that the transportation sector report and surrender emissions units.

4 DISCUSSION AND CONCLUSION

4.1 Increasing Management and Operational Costs in the Shipping Industry

Regardless of whether shipping companies obtain emission allowances through free allocation or auction, the ultimate goal of an emissions trading system is to reduce overall emissions through a cap-and-trade mechanism. Under the incentives of market regulation, shipping companies will adopt ways to maximize profits while reducing carbon emissions.

This typically results in increased operational costs for the shipping industry, as companies need to either purchase additional emission allowances to cover their emissions or invest in technologies that reduce emissions[7]. The costs involved include not only the price of allowances but also expenses related to monitoring, reporting, and verifying emissions, as well as additional costs for upgrading equipment and ensuring compliance with emissions reduction targets[8].

4.2 Stricter Emissions Disclosure Requirements and Improved Transparency of Emissions

In June 2024, the Sea Cargo Charter released its 2024 Disclosure Report, highlighting positive progress in reducing the environmental impact of chartered shipping activities and improving the transparency of emissions reporting in the shipping industry. The report also emphasizes the gap between current emissions levels and the IMO 2050 net-zero emissions target. The Sea Cargo Charter is one of the three major environmental initiatives supported by the Global Maritime Forum, along with the Poseidon Principles and the Poseidon Principles for Marine Insurance. These initiatives share the common goal of improving emissions reporting transparency and contributing to the reduction of carbon emissions.

The report targets charterers engaged in bulk cargo transportation. These charterers must have signed time or voyage charter agreements that include mechanisms for allocating ballast voyage emissions. The reported data covers voyages by dry bulk carriers, chemical tankers, oil tankers, liquefied gas carriers, and voyages involving one or more ships in international trade. In April 2024, Sea Cargo Charter expanded its scope to include pure shipowners. In this report, 35 companies engaged in transporting various goods, including agricultural products, aluminum, chemicals, oil and gas, energy, metals, mining, cement, and timber, disclosed their 2023 chartering activities and the alignment of their emissions with the revised IMO greenhouse gas reduction targets. These companies accounted for approximately 20% of the total annual bulk cargo transportation by sea.

After being included in emissions trading systems, shipping companies are required to bear the economic costs associated with emissions. In addition to acquiring carbon allowances through auctions or trading, they also need to cover monitoring costs under the MRV system and ship management expenses. According to estimates, after the inclusion of maritime shipping in the EU ETS, the annual compliance costs for large international shipping companies could increase by millions of euros. Being included in the emissions trading system means that regulated ships must adhere to stringent MRV mechanisms. Ships are required to install fuel consumption data collection systems, which increases the costs for technological upgrades as data transparency is emphasized.

4.3 Transformation and Upgrading of the Upstream and Downstream Supply Chains of Shipping

Due to the IMO's requirements for energy efficiency indices such as Energy Efficiency Existing Ship Index (EEXI), on one hand, large-scale low-carbon retrofitting of ships is underway, leading to a significant increase in demand for components like dual-fuel engines and scrubbers. On the other hand, the ETS accelerates the compliance process for EEXI speeding up the retirement of older ships. As a result, global orders for LNG-powered vessels continue to rise, and LNG bunkering volume is steadily increasing.

4.4 Global Green Shipping Corridors

In November 2021, during the 26th Conference of the Parties to the *United Nations Framework Convention on Climate Change* (COP26), over 20 countries signed the Clydebank Declaration on Green Shipping Corridors. The declaration set the goal of establishing more than six green shipping corridors between two or more ports globally by 2025, with plans to expand the number of green corridors by 2030. This initiative aims to support the global shipping industry in achieving full decarbonization by 2050, marking the formal introduction of the *Green Shipping Corridor* concept.

The declaration specifies that stakeholders across the shipping supply chain, including ports, shipping companies, and fuel suppliers, will collaborate to implement greenhouse gas reductions and even achieve zero emissions on specific routes. These routes will be recognized as green shipping corridors.

By 2023, 44 international green shipping corridor initiatives had been established worldwide. Of these, 22 corridors have specified fuel pathways, with more than half choosing methanol and ammonia as zero-emission fuel options. These fuels are considered the primary scalable choices for medium and large vessels.

COMPETING INTERESTS

The authors have no relevant financial or non-financial interests to disclose.

REFERENCES

- [1] A Christodoulou et al. Inclusion of shipping in the EU-ETS: Assessing the direct costs for the maritime sector using the MRV data. *Energies*, 2021, 14: 3915.
- [2] Asian Development Bank. The Korea emissions trading scheme: Challenges and emerging opportunities. Asian Development Bank, 2018.
- [3] T R S de Aguiar, J Bebbington. Disclosure on climate change: Analysing the UK ETS effects. *Accounting Forum*, 2014, 38: 227.
- [4] R Li, S Perdana, M Vielle. Potential integration of Chinese and European emissions trading market: Welfare distribution analysis. *Mitigation and Adaptation Strategies for Global Change*, 2021, 26: 1.
- [5] M Kotzampasakis. Expanding European climate policy to international shipping. In: *EU External Relations Law and Sustainability*. The Hague: T.M.C. Asser Press, 2024.
- [6] M Tao et al. Enhancing New Zealand's emissions trading scheme: A comprehensive sector-level assessment for a stronger regulatory framework. *Journal of Environmental Management*, 2024, 352: 120106.
- [7] S Nguyen. A multi-aspect framework to support the decision-making process of low carbon emission solutions. *WMU Journal of Maritime Affairs*, 2019, 18: 165.
- [8] S Koesler, M Achtnicht, J Köhler. Course set for a cap? A case study among ship operators on a maritime ETS. *Transport Policy*, 2015, 37: 20.

ASSESSING LANDSCAPE SUSTAINABILITY BY COUPLING ECOSYSTEM SERVICE SUPPLY-DEMAND AND ES-SDG LINKAGES: A CASE STUDY OF YIXING CITY IN THE TAIHU LAKE BASIN

HengHui Xi^{1,2}

¹College of Public Administration, Nanjing Agricultural University, Nanjing 210095, Jiangsu, China.

²China Resources, Environment and Development Academy, Nanjing 210095, Jiangsu, China.

Corresponding Email: 450832939@qq.com

Abstract: Understanding the coupling relationship between ecosystem service (ES) supply-demand matching and Sustainable Development Goals (SDGs) is crucial for achieving landscape sustainability in rapidly urbanizing regions. This study focuses on Yixing City, a typical urbanizing area within the Taihu Lake Basin, and constructs a "Landscape Sustainability Assessment Framework Coupling ES Supply-Demand and ES-SDG Linkages". Using the InVEST model and socioeconomic data, we quantified the supply-demand levels of five key ESs, evaluated SDG attainment across Yixing's townships based on ES-SDG linkages, and comprehensively characterized their landscape sustainability (LS). Key findings include: (1) Significant spatial variability in ES supply-demand balances across townships, with carbon sequestration showing the most pronounced imbalance; (2) SDG 8 (Economic Growth) consistently outperformed other SDGs, while SDG 7 (Clean Energy), SDG 9 (Industry, Innovation, and Infrastructure), and SDG 11 (Sustainable Cities) exhibited lower attainment levels; (3) Among the 18 townships, 12 displayed improving trends in landscape sustainability. Xinzhuang achieved the highest sustainability, whereas Yicheng and Qiting ranked lowest; (4) Targeted strategies—such as ecological restoration tailored to local ES deficits, enhancing critical ES supplies, and prioritizing key SDGs—are needed to improve regional landscape sustainability.

Keywords: Ecosystem service supply and demand; ES-SDG linkages; Landscape sustainability; Taihu lake basin

1 INTRODUCTION

Landscape sustainability science emphasizes harmonizing human well-being and ecological conservation by optimizing the supply-demand relationships of ecosystem services (ES) [1]. Rapid urbanization worldwide has caused severe mismatches between ES supply and demand, posing significant challenges to achieving the United Nations Sustainable Development Goals (SDGs) [2]. The Taihu Lake Basin, a highly urbanized region in eastern China, faces challenges such as water scarcity, water pollution, and shrinking ecological space [3]. Yixing City, located in the upper reaches of Taihu Lake, serves dual roles as an ecological barrier and an economically developed area, experiencing conflicting pressures. Its ES supply-demand dynamics critically influence the basin's ecological security [4].

Matching ES supply and demand is central to sustainable landscape management [5]. For instance, carbon sequestration services are directly linked to SDG 13 (Climate Action), while water purification services support SDG 6 (Clean Water and Sanitation). However, ES supply is typically determined by natural systems, whereas demand is driven by socioeconomic factors, and their spatial mismatches may trigger ecological risks [6]. Although many studies have quantified ES supply [7], few have systematically integrated demand-side analysis, resulting in an incomplete understanding of landscape sustainability. Moreover, existing research often focuses on single-ES assessments, lacking comprehensive analyses that couple supply-demand dynamics with SDG linkages [8]. Additionally, current ES-SDG studies predominantly adopt static linkage frameworks, failing to account for regional heterogeneity [9]. There is an urgent need for spatially explicit methods that can identify priority areas for landscape interventions based on ES mismatches and their impacts on SDGs.

To address these gaps, this study proposes a "Landscape Sustainability Assessment Framework Coupling ES Supply-Demand and ES-SDG Linkages", using Yixing City as a case study. The objectives are: (1) to quantify the spatiotemporal patterns of supply and demand for five key ES (e.g., carbon sequestration, water yield) using the InVEST model and socioeconomic data; (2) to assess regional SDG attainment and integrated landscape sustainability using a modified version of the ES-SDG linkage framework proposed by Wood et al.; (3) to propose landscape optimization strategies for enhancing sustainability. Our study contributes to the field in three ways: (1) We develop a novel assessment framework that captures the dynamic interplay between ecological capacity and human development needs. (2) The study provides spatially explicit guidance for landscape planning while addressing multiple sustainability goals. (3) It offers a replicable methodology for rapidly urbanizing regions facing ecosystem degradation challenges. Furthermore, this research supports decision-making for ecological management in the Taihu Lake Basin and advances the regional application of ES-SDG linkage studies.

2 MATERIALS AND METHODS

2.1 A landscape Sustainability Assessment Framework based on the ES-SDG Linkages

After reviewing the linkages between ecosystem services and SDGs, this study selected five key ecosystem services for the study area: Carbon sequestration (SC), Food production (FP), Nature-based recreation (NbR), Water provision (WP), and Water purification (Wpu). The supply-demand levels and supply-demand ratios of these five services were calculated separately. Based on the ES-SDG linkages, the attainment levels of 15 Sustainable Development Goals were then quantified. Finally, the integrated level of these 15 SDGs was used to characterize the regional landscape sustainability (LS) (Figure 1).

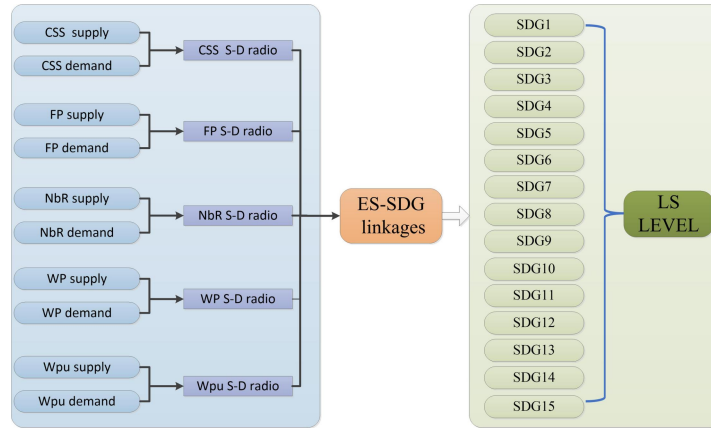


Figure 1 A Landscape Sustainability Assessment Framework based on the ES-SDG Linkages

2.2 Study Area and Data Source

This study selected Yixing City, a typical area in the Taihu Lake Basin, as the research region (Figure 2). Located on the western shore of Taihu Lake, Yixing serves as an important ecological barrier and water conservation area for the basin, with its water system directly influencing the environmental safety of Taihu Lake [10]. In recent years, rapid economic development in the Taihu Lake Basin has intensified land use changes and exacerbated ecological pressures, presenting new challenges to regional ecosystem service supply-demand relationships and landscape sustainability. Considering Yixing's socio-ecological conditions and ecological functional importance, this study selected five key ecosystem services to analyze regional landscape sustainability: carbon sequestration, food production, recreation, water yield, and water purification.

The data used in this study primarily include five categories: (1) Land use and population distribution data were obtained from the Resource and Environment Science and Data Center, Chinese Academy of Sciences (<http://www.resdc.cn>); (2) DEM and soil data were acquired from the Geospatial Data Cloud (www.gscloud.cn) and Harmonized World Soil Database (HWSD), respectively; (3) Precipitation and evapotranspiration data came from the China Meteorological Data Service Center's "Annual Dataset of Chinese Surface Climate Data" (<http://data.cma.cn/>); (4) Per capita carbon emission data were sourced from the China Emission Accounts and Datasets; (5) Per capita water consumption, per capita food consumption, and population data were obtained from the Jiangsu Statistical Yearbook.

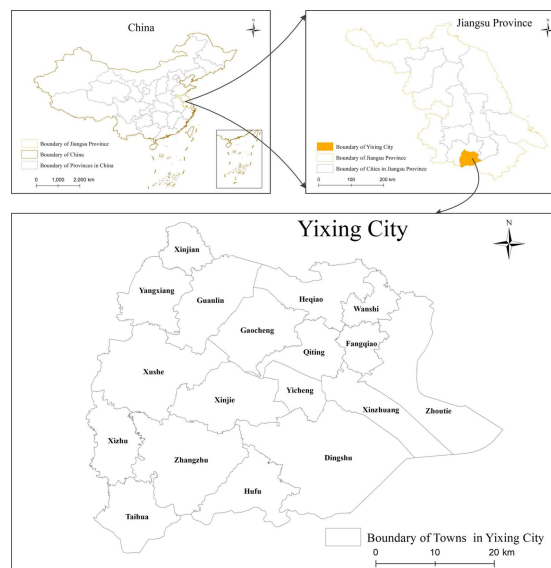


Figure 2 Study Area

2.3 Landscape Sustainability Assessment

2.3.1 Carbon sequestration service

(1) supply

$$S_{CS} = 1.63 \times NPP \quad (1)$$

S_{CS} represents the carbon sequestration service supply per grid, and NPP represents the net primary productivity of vegetation per grid. The carbon sequestration service supply at grid scale was summarized to obtain the carbon sequestration service supply in each study area.

(2) demand

$$D_{CS} = C_{PER} \times POP \quad (2)$$

Demand for carbon sequestration services is represented by actual carbon emissions. According to the product of the per capita carbon Emission of each city and the population of the assessment unit, the per capita carbon emission data of districts and counties were obtained from the China Emission Accounts and Datasets. C_{PER} represents per capita carbon emissions, POP represents the current resident population of the assessed area.

2.3.2 Food provision

(1) supply

Per unit area method and GAEZ (Global Agro-Ecological Zones) model were used to spatial assign the grain yields grain production statistical data [11, 12].

(2) demand

$$D_{FP} = D_{average} \times POP \quad (3)$$

The demand for food production services is calculated based on the per capita grain consumption in Jiangsu Province (2000,2010,2020).

2.3.3 Nature-based recreation

(1) supply

$$A_i = \frac{S_i}{P_i} \quad (4)$$

$$NR_{S_i} = (\sum_{k=1}^k A_i) \times POP_i \quad (5)$$

Nature-based recreation service refers to the total area of ecological land such as forestland, grassland, water body and wetland that can provide leisure and recreation services. 5 km is set as the accessible radius of ecological land for people to enjoy. It is assumed that the ecological land within a grid can provide leisure and recreation services for all people within the accessible radius, and the residents within the grid can enjoy all the ecological land within the accessible radius [13, 14]. S_i is the ecological land area in grid I, is the total population within the reachable radius corresponding to grid i, A_i is the per capita usable area of ecological land in grid i, represents the supply of leisure and recreation services in grid i, j represents all grids within the corresponding buffer radius of grid i, POP_i indicates the total number of people in the i grid.

(2) demand

$$D_{NR} = B_{per} \times POP \quad (6)$$

The demand for Nature-based recreation service can be calculated by the product of per capita green space demand and population. D_{GR} represents the total demand for green space entertainment and leisure services of residents in the evaluation area, B_{per} represents the per capita green space demand area of residents, POP represents the number of populations in the area. According to [14], B_{per} was set to 60m².

2.3.4 Water provision

(1) supply

$$WY_{xj} = \left(1 - \frac{AET_{xj}}{P_{xj}}\right) \times P_x \quad (7)$$

Based on the water production module of the InVEST model, the water production of a grid cell is the difference between rainfall and actual evaporation based on the principle of water balance. The water yield of each study area is obtained by summarizing the calculation results of grid scale water yield.

(2) demand

$$WY_D = D_{per} \times POP \quad (8)$$

The demand for water supply services is determined based on the product of per capita comprehensive water consumption (including agricultural water, industrial water and domestic water) and the current resident population of the assessed area. The data of per capita comprehensive water consumption is derived from the Water Resources Bulletin of Jiangsu Province. WY_D represents the regional water supply service demand, D_{per} represents the comprehensive water consumption per capita of the assessment area in the current year, POP represents the permanent population of the assessment area in the current year.

2.3.5 Water purification

(1) supply

$$S_{WP} = efficiency_n \tag{9}$$

The potential supply of water purification services refers to the maximum retention efficiency of each LULC class in the landscape.

(2) demand

$$D_{PW} = \begin{cases} 0, & \text{if } AVL_{load} \leq Exp_{allow} \\ \frac{AVL_{load} - Exp_{allow}}{AVL_{load}} \times 100\%, & \text{if } AVL_{load} > Exp_{allow} \end{cases} \tag{10}$$

$$Exp_{allow} = \sum Y_x \times \rho \tag{11}$$

Water purification service demand (WPD) is the amount of nitrogen that should be retained and intercepted before entering the water body in order to maintain surface water quality standards. Referring to the water quality standard. This is measured by comparing the total nitrogen load (AVL_{load}) with its allowable nitrogen output. $\sum Y_x$ represents the total regional water production, ρ value is set to 1 g/m^3 , in line with China's national water quality standards.

2.3.6 Level of ecosystem service supply and demand

To account for significant variations in supply-demand ratios across different ecosystem services and ensure equitable consideration of their supply-demand levels, we classified the ecosystem service supply-demand ratio results into six categories (Table 1). Levels 1-4 were divided using equal intervals, while Level 5 (80%-120%) indicates a relatively balanced supply-demand state for the specific ecosystem service. Level 6 (>120%) represents cases where the ecosystem service supply substantially exceeds local demand.

Table 1 Classification of the Ratio between Supply and Demand of Various Ecosystem Services

LEVEL	1	2	3	4	5	6
S-D ratio	<20%	20%-40%	40%-60%	60%-80%	80%-120%	>120%

2.3.7 Landscape sustainability assessment based on ES-SDG linkages

① First, based on the assessed supply-demand values of various ecosystem services and the ES-SDG linkages, we calculated the attainment levels of individual SDG targets (Figure 3). Different ecosystem services contribute to distinct SDG targets with varying degrees of relevance. Drawing upon studies [8, 15, 16] and considering the five selected ecosystem services in this research, we established the strength of connections between ecosystem services and SDG targets to quantify each SDG's contribution to landscape sustainability.

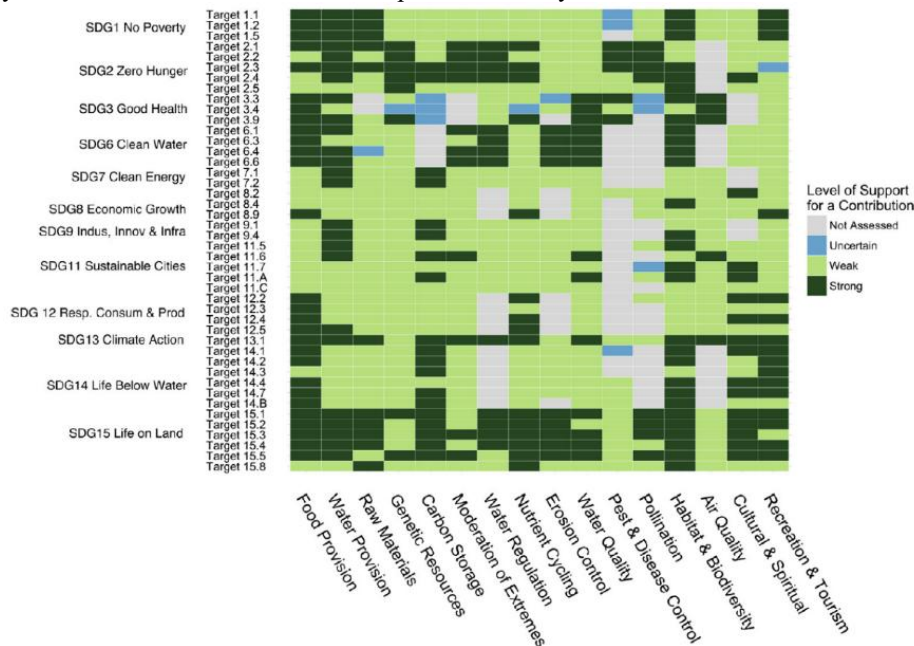


Figure 3 ES-SDG Linkages[8]

② Subsequently, the regional landscape sustainability level was characterized by averaging the attainment levels of all SDG targets. The formula is as follows:

$$LS_{average} = \sum_{i=1}^n Level_{SDG_i} / n \tag{12}$$

$LS_{average}$ represents the composite landscape sustainability level, $Level_{SDG_i}$ denotes the attainment level of SDG_i , n indicates the number of SDGs assessed (here, 15).

3 RESEARCH RESULTS

3.1 Temporal and Spatial Dynamics of Ecosystem Service Supply and Demand

3.1.1 Spatio-temporal dynamics of carbon sequestration service supply and demand

Temporally (Table 2), from 2000 to 2020, the overall carbon sequestration service supply in Yixing City fell far short of local demand, showing a significant decline in the supply-demand ratio from 27.24% to 9.13%. Specifically, carbon storage supply initially decreased slightly before rebounding, while demand for carbon sequestration surged dramatically, leading to a marked deterioration in the supply-demand balance.

Spatially (Figure 4), townships in northeastern Yixing generally exhibited lower carbon sequestration supply-demand levels compared to those in the southwest. All townships experienced substantial declines in carbon sequestration service balance: western and northwestern townships dropped from Level 2 to Level 1, three eastern townships declined from Level 3 to Level 1, while Taihua and Hufu decreased from Level 4 to Level 2. Notably, Qiting, Yicheng, and Dingshu maintained persistently low Level 1 balances throughout the study period.

3.1.2 Spatio-temporal dynamics of Food provision supply and demand

Temporal analysis (Table 2) reveals that from 2000 to 2020, Yixing City's overall food production service supply generally met local demand, with an improving supply-demand ratio that increased from 134% to 246.38% in 2010 before declining to 215.90% in 2020. The food production supply initially showed significant growth followed by a slight decrease, while demand notably dropped in 2010 - primarily due to changes in residents' dietary structure leading to reduced staple food consumption. By 2020, food production demand had increased compared to 2010 levels.

Spatially (Figure 4), central and southern townships exhibited relatively lower but improving food production supply-demand levels. For instance, Yicheng improved from Level 2 to Level 3, while Xinjie and Dingshu advanced from Levels 5 and 4 respectively to Level 6. Most other townships maintained high food production balances, consistently remaining at Levels 5 or 6 throughout the study period.

3.1.3 Spatio-temporal dynamics of Nature-based recreation supply and demand

Temporally (Table 2), during 2000-2020, the supply of recreational services in Yixing City generally well exceeded local demand, showing a slight decline in supply-demand balance while remaining at relatively high levels. The supply of recreational services initially increased before decreasing, while demand continued to grow steadily.

Spatially (Figure 4), except for some townships in the northeastern and central areas, Yixing's recreational service supply-demand balance consistently maintained the highest classification level. Qiting showed a continuous decline from Level 4 to Level 2, Yicheng fluctuated between Levels 5 and 6, while Wanshi persistently remained at the relatively low Level 2 throughout the study period.

3.1.4 Spatio-temporal dynamics of Water provision supply and demand

Temporally (Table 2), from 2000 to 2020, the water yield service supply in Yixing City generally met local demand, with an overall improvement in the supply-demand balance over the two decades. The water yield supply showed a steady increase throughout the period, while demand initially rose before declining, resulting in lower demand in 2020 compared to 2000.

Spatially (Figure 4), most townships in Yixing exhibited improved water yield service supply-demand levels. The central townships of Yicheng and Qiting rose from Level 2 and Level 3 to Level 5 respectively, while all other townships achieved the highest classification level for water yield service balance.

3.1.5 Spatio-temporal dynamics of Water purification supply and demand

Temporally (Table 2), from 2000 to 2020, the supply-demand balance of water purification services in Yixing City showed gradual improvement, though supply still fell short of local demand. The supply-demand ratio increased from 68.24% in 2000 to 85.19% in 2020, with water purification supply steadily increasing while demand gradually decreased.

Spatially (Figure 4), townships in southwestern Yixing generally exhibited higher and improved water purification service supply-demand levels compared to central and northeastern areas, reaching Level 5 or Level 6. However, many central and northern townships remained at Level 4. Some southeastern townships showed improvement, such as Xinzhuang rising from Level 3 to Level 4, while Dingshu and Zhoutie advanced from Level 4 to Level 5, essentially achieving supply-demand balance.

Table 2 Supply and Demand Ratio of Various Ecosystem Services in Yixing City from 2000 to 2020

Year	CSS S-D ratio	FP S-D ratio	NbR S-D ratio	WP S-D ratio	Wpu S-D ratio
2000	27.24%	134.00%	813.69%	121.74%	68.24%
2010	8.56%	246.38%	823.99%	128.13%	73.78%
2020	9.13%	215.90%	719.29%	226.81%	85.19%

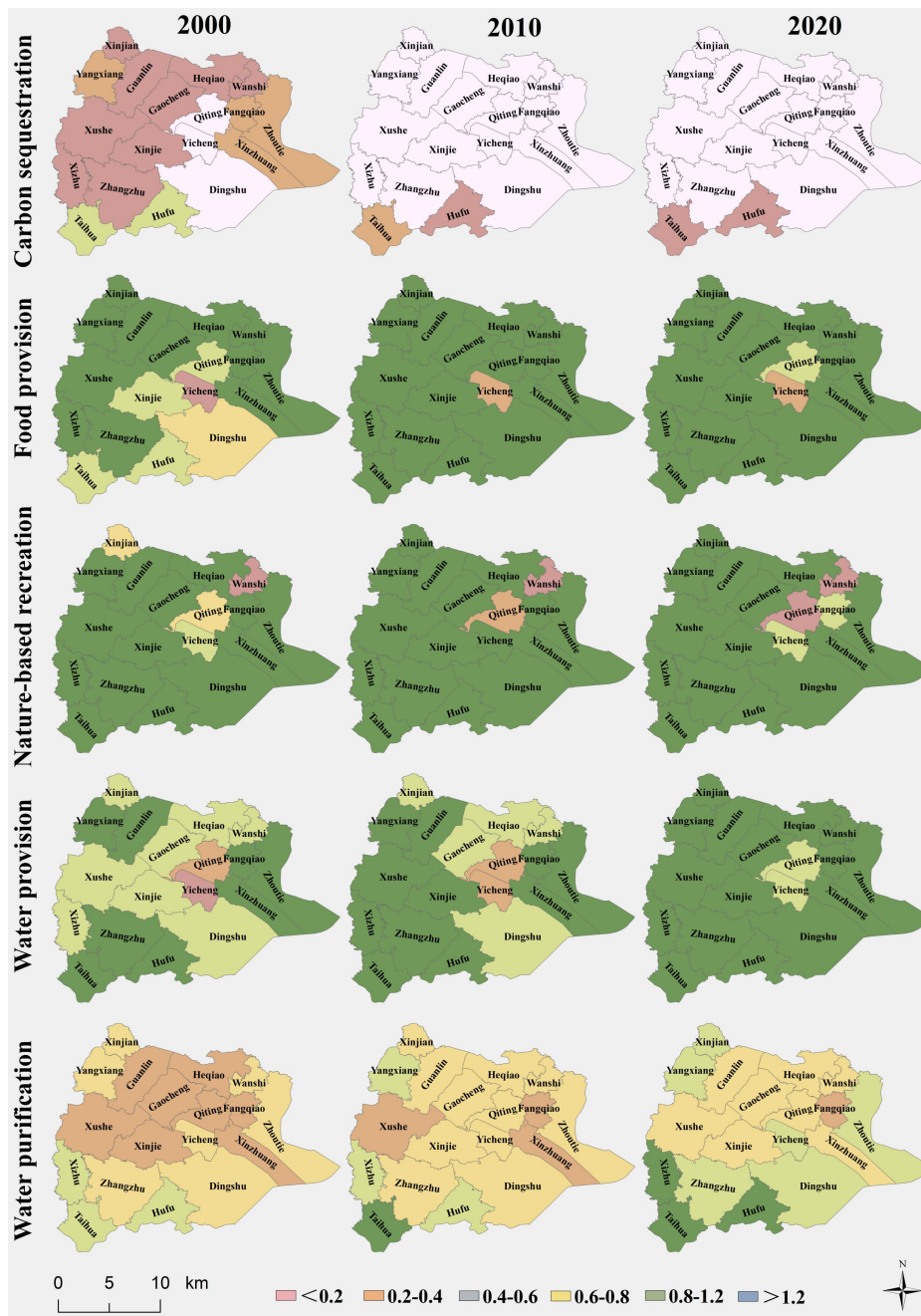


Figure 4 Spatial-Temporal Dynamics of Supply and Demand of 5 Types of Key Ecosystem Services in Yixing City from 2000 to 2020

3.2 Spatial and temporal dynamics of landscape sustainability

In 2000, Xinzhuang exhibited the highest overall SDG attainment level, followed by Zhoutie and Taihua, while Yicheng and Qiting showed the lowest overall SDG performance. Among all SDG targets, SDG 8 (Economic Growth) consistently ranked highest, with SDG 1 (No Poverty) and SDG 14 (Life Below Water) also appearing in the top three. Conversely, SDG 11 (Sustainable Cities) and SDG 9 (Industry, Innovation and Infrastructure) demonstrated relatively lower attainment levels (Figure 5).

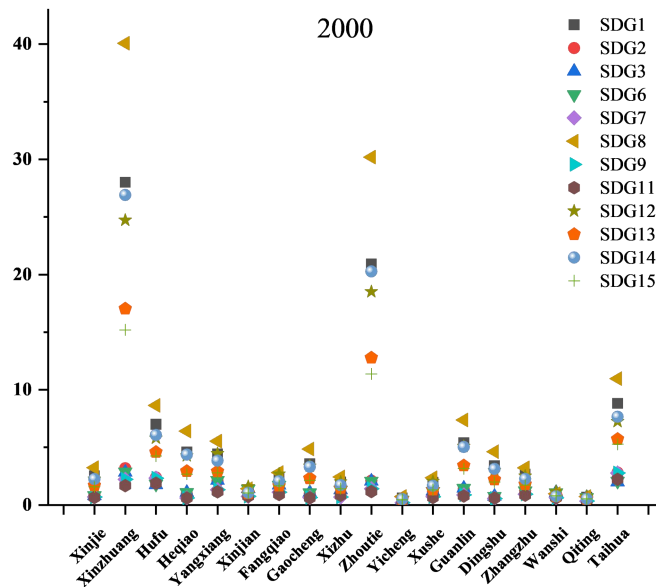


Figure 5 Level of Each SDG in Each Township of Yixing City in 2000

By 2010, Xinzhuang maintained its leading position in SDG performance, with Zhoutie and Taihua remaining second and third respectively, while Yicheng and Qiting continued to rank lowest. SDG 8 still outperformed all other goals, followed by SDG 1, SDG 12 (Responsible Consumption and Production), and SDG 14. The lowest-performing SDGs were SDG 11, SDG 9, and SDG 7 (Affordable and Clean Energy) (Figure 6).

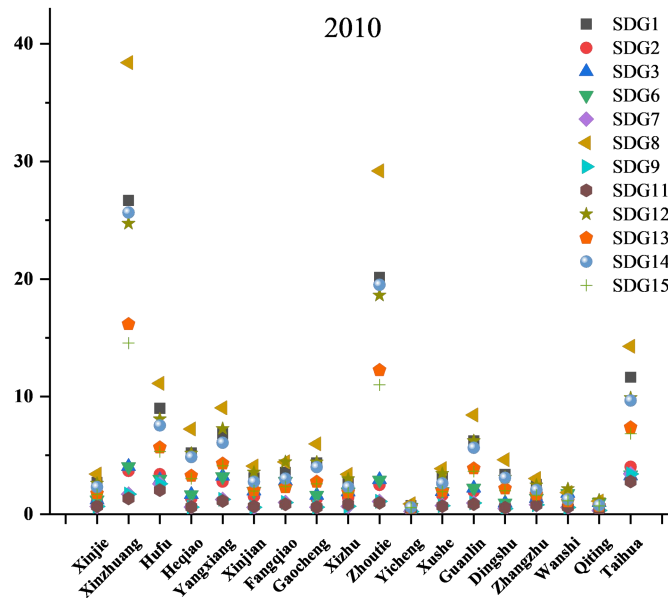


Figure 6 Level of each SDG in Each Township of Yixing City in 2010

In 2020, the top three townships for SDG attainment remained unchanged (Xinzhuang, Zhoutie, and Taihua), with Yicheng and Qiting persistently ranking last. SDG 8 maintained its dominant position, succeeded by SDG 1 and SDG 12, while SDG 11, SDG 9 and SDG 7 consistently showed the poorest performance throughout the study period (Figure 7).

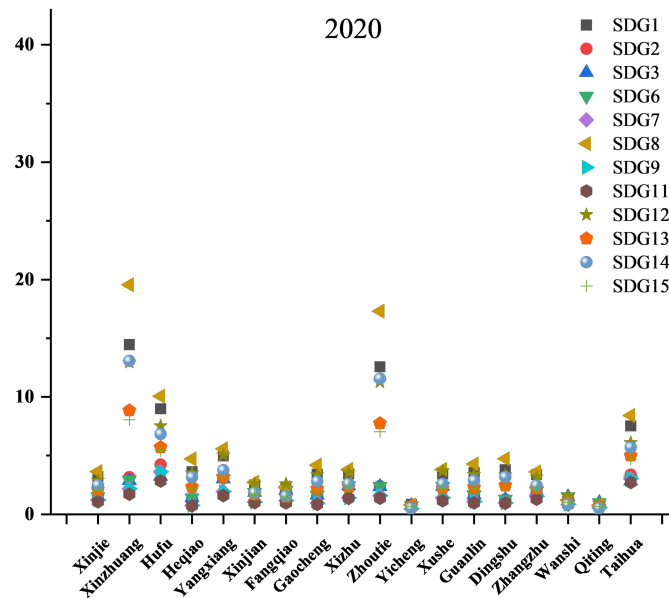


Figure 7 Level of each SDG in Each Township of Yixing City in 2020

Comprehensive assessment of regional landscape sustainability across SDG targets reveals: As shown in Figure 8, Xinzhuang exhibited the highest landscape sustainability level among all townships, followed by Zhoutie and Taihua, though Hufu surpassed Taihua by 2020. The lowest sustainability levels were consistently observed in Yicheng and Qiting.

Among the 18 townships, 12 demonstrated improving trends in landscape sustainability. Notably, Xushe and Xizhu showed remarkable increases of 78.74% and 73.97%, respectively, while Xinjian improved by over 50%. Conversely, 6 townships experienced declines, with Xinzhuang registering the largest reduction (-44.92%), followed by Zhoutie and Guanlin (both exceeding -20%).

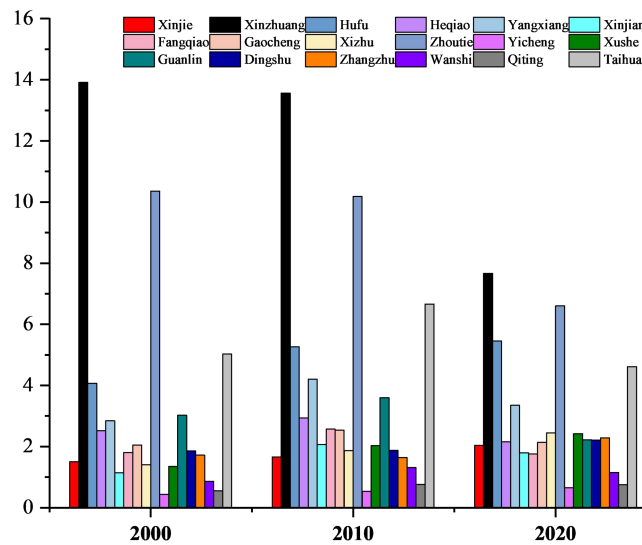


Figure 8 Landscape Sustainability Level of Each Township in Yixing City from 2000 to 2020

4 DISCUSSION AND CONCLUSIONS

4.1 Contributions and Limitations

This study is the first to integrate ecosystem service supply-demand with SDG targets to assess regional landscape sustainability, highlighting the critical role of ecosystem services in supporting sustainable development goals and enhancing regional landscape sustainability. Many sustainable development goals are fundamentally based on the benefits that ecosystem services provide to humans [17, 18]. However, some limitations remain for future research. For example, the ES-SDG linkages were derived from previous studies, but these relationships may vary across regions, necessitating localized ES-SDG assessments in future work. Additionally, using the average of SDG targets to represent regional landscape sustainability overlooks differences in the importance of individual SDGs [15, 19]. Future studies should incorporate varying SDG priorities to better characterize landscape sustainability.

4.2 Conclusions and Policy Recommendations

- (1) Regarding ecosystem service supply-demand, food production, recreation, and water yield services in Yixing generally met local demand, while water purification still fell short of balance, and carbon sequestration supply lagged far behind demand. Supply-demand performance varied significantly across townships and over time.
- (2) Among SDG targets, SDG 8 (Economic Growth) consistently ranked highest, followed by SDG 1 (No Poverty), SDG 12 (Responsible Consumption and Production), and SDG 14 (Life Below Water). SDG 7 (Affordable and Clean Energy) remained the lowest, while SDG 11 (Sustainable Cities) and SDG 9 (Industry, Innovation and Infrastructure) also performed poorly.
- (3) Xinzhuang exhibited the highest landscape sustainability, followed by Zhoutie, Taihua, and Hufu. Yicheng and Qiting ranked lowest. Twelve of the 18 townships showed improving trends, with Xushe and Xizhu demonstrating the greatest gains, while Xinzhuang experienced the largest decline.
- (4) To enhance regional landscape sustainability, targeted ecological conservation and restoration measures should address areas with low ecosystem service supply-demand balances. Simultaneously, differentiated SDG priorities must be addressed—particularly improving underperforming SDGs (e.g., SDG 7, 9, 11) and focusing on lagging regions—to achieve comprehensive sustainable development.

COMPETING INTERESTS

The authors have no relevant financial or non-financial interests to disclose.

FUNDING

This study was supported by the Postgraduate Research & Practice Innovation Program of Jiangsu Province (KYCX24_1011).

REFERENCES

- [1] Wu J. Landscape sustainability science (II): core questions and key approaches. *Landscape Ecology*, 2021, 36(8): 2453–2485.
- [2] Li T, Liu Y, Ouyang X, et al. Sustainable development of urban agglomerations around lakes in China: Achieving SDGs by regulating Ecosystem Service Supply and Demand through New-type Urbanization. *Habitat International*, 2024, 153: 103206.
- [3] Tao Y, Li Z, Sun X, et al. Supply and demand dynamics of hydrologic ecosystem services in the rapidly urbanizing Taihu Lake Basin of China. *Applied Geography*, 2023, 151: 102853.
- [4] Xi H, Huang C, Ou W, et al. An assessment framework for landscape sustainability based on ecosystem service supply-flow-demand. *Landscape Ecology*, 2024, 39(3): 57.
- [5] Burkhard B, Kroll F, Nedkov S, et al. Mapping ecosystem service supply, demand and budgets. *Ecological Indicators*, 2012, 21: 17–29.
- [6] Gao M, Hu Y, Liu X, et al. Revealing multi-scale characteristics of ecosystem services supply and demand imbalance to enhance refined ecosystem management in China. *Ecological Indicators*, 2025, 170: 112971.
- [7] Zhang X, Wang Y, Yuan X, et al. Identifying ecosystem service supply-demand imbalance for sustainable land management in China's Loess Plateau. *Land Use Policy*, 2022, 123: 106423.
- [8] Wood SLR, Jones SK, Johnson JA, et al. Distilling the role of ecosystem services in the Sustainable Development Goals. *Ecosystem Services*, 2018, 29: 70–82.
- [9] Yang Z, Zhan J, Wang C, et al. Coupling coordination analysis and spatiotemporal heterogeneity between sustainable development and ecosystem services in Shanxi Province, China. *Science of The Total Environment*, 2022, 836: 155625.
- [10] Yang L, Zhang L, Li Y, et al. Water-related ecosystem services provided by urban green space: A case study in Yixing City (China). *Landscape and Urban Planning*, 2015, 136: 40–51.
- [11] Liu L, Xu X, Chen X. Assessing the impact of urban expansion on potential crop yield in China during 1990–2010. *Food Security*, 2015, 7(1): 33–43.
- [12] Sun X, Yang P, Tao Y, et al. Improving ecosystem services supply provides insights for sustainable landscape planning: A case study in Beijing, China. *Science of The Total Environment*, 2022, 802: 149849.
- [13] Liu H, Remme RP, Hamel P, et al. Supply and demand assessment of urban recreation service and its implication for greenspace planning—A case study on Guangzhou. *Landscape and Urban Planning*, 2020, 203: 103898.
- [14] Tao Y, Tao Q, Sun X, et al. Mapping ecosystem service supply and demand dynamics under rapid urban expansion: A case study in the Yangtze River Delta of China. *Ecosystem Services*, 2022, 56: 101448.
- [15] Yang S, Zhao W, Liu Y, et al. Prioritizing sustainable development goals and linking them to ecosystem services: A global expert's knowledge evaluation. *Geography and Sustainability*, 2020, 1(4): 321–330.
- [16] Hu S, Yang Y, Li A, et al. Integrating Ecosystem Services Into Assessments of Sustainable Development Goals: A Case Study of the Beijing-Tianjin-Hebei Region, China. *Frontiers in Environmental Science*, 2022, 10.

- [17] Zhao Y, Zhou R, Yu Q, et al. Revealing the contribution of mountain ecosystem services research to sustainable development goals: A systematic and grounded theory driven review. *Journal of Environmental Management*, 2025, 373: 123452.
- [18] Zuo L, Liu G, Zhao J, et al. Spatiotemporal heterogeneity management: Optimizing the critical role of ecosystem services in achieving Sustainable Development Goals. *Geography and Sustainability*, 2025, 6(1): 100211.
- [19] Chen D, Zhao Q, Jiang P, et al. Incorporating ecosystem services to assess progress towards sustainable development goals: A case study of the Yangtze River Economic Belt, China. *Science of The Total Environment*, 2022, 806: 151277.

SUITABILITY EVALUATION OF WATER INDEX UNDER EXTRACTION OF COMPLEX ENVIRONMENTAL WATER BODIES

ZhiHua Liu

JiangXi University of Science and Technology, Ganzhou 341000, Jiangxi, China.

Corresponding Email: 6120220125@mail.jxust.edu.cn

Abstract: With the development of remote sensing technology, remote sensing images are more and more widely used in water monitoring. This paper uses Landsat 8 remote sensing images as the data source, selects Poyang Lake, Taihu Lake and Dingnan County as the study area, and combines NDWI, MNDWI, EWI, SWI, TCW, MBWI, WI2015, AWEInsh and AWEIsh to extract water bodies and evaluate the accuracy of the study area. The results are as follows: 1. The overall extraction accuracy of TCW and MBWI is the highest. 2. For mountain shadow areas, AWEInsh and TCW have the best extraction effect. For shallow water area, TCW and MBWI have the best extraction effect, and the spectral distinction between water and non water is greatly increased. For the eutrophication area of water body, the ten methods have high accuracy, and can distinguish the spectral characteristics of chlorophyll and non water body.

Keywords: Remote sensing image; Research area; water extraction; Water index method; Accuracy evaluation

1 INTRODUCTION

After decades of development, the water extraction of remote sensing images has made great progress. The process includes: artificial visual interpretation, spectral feature extraction, radar image extraction, automation, and the combination of various methods[1].The initial visual interpretation of water extraction can clearly distinguish water bodies but the efficiency is low, and then the semi-automatic water extraction method based on spectral feature extraction of water bodies has greatly improved the work efficiency. Water extraction has also been guaranteed, but in some complex environments, water bodies will be misclassified or missed. Up to now, the fully automated extraction of water bodies [2], scholars are studying deep learning, artificial intelligence and other directions to accurately and efficiently extract water bodies. In the future, more and more extraction methods will emerge in an endless stream.

Based on the automation method ; li Dan and other in-depth summary of the development of these years is very rapid response very popular water extraction based on radar image data, which has a profound significance for water extraction, remote sensing technology to improve rapidly [3]. In general, for water body extraction, we use more optical image information to extract water body, and radar image information to assist water body extraction. In recent years, the rapidly developing radar image has been applied to water resources extraction and water resources protection. Based on optical image data and radar image data, the extraction method and application field can be refined and clarified. The method is as follows. The threshold method can be divided into single-band method and multi-band method. The multi-band method can be divided into inter-spectral relationship method and vegetation index method. Classification can be divided into decision tree, SVM and object-oriented method. Other methods can be divided into deep learning, mixed element decomposition, GIS, spectral matching, BP network, MRF. Radar images are divided into threshold method, filtering method, DEM and GLCM. The method produced by the combination of the two classifications is the model method.

2 WATER EXTRACTION PROCESS

2.1 Pretreatment

The Landsat 8 and Sentinel-2 image data used in this paper need to perform atmospheric correction and radiometric calibration on the landsat 8 remote sensing image. Sentinel-2 remote sensing data can't be opened directly in envi, so it needs to be processed in snap to get data that can be opened in envi. The 2A level data does not require radiometric calibration and atmospheric correction.

2.2 surface Water Extraction Method

The research areas of this paper are Poyang Lake area, Taihu Lake area and Dingnan County area. The main difficulty of water body extraction research is to eliminate the influence of shallow water area, water eutrophication, mountain shadow area and other factors on water body and improve the accuracy of water body. In this paper, ten water body index models are used, including NDWI, MNDWI, EWI, SWI, TCW, MBWI, RNDWI WI2015, AWEInsh, AWEIsh..Ten water index models are shown in Table 1.

Table 1 Ten water index methods and their index models

Index	Source	Equation
TCW[4]	Crist (1985)	$0.0315\rho_{b1}+0.202\rho_{b2}+0.3102\rho_{b3}+0.1594\rho_{b4}-0.6806\rho_{b5}-0.6109\rho_{b7}$
NDWI[5]	Mcfeters(1996)	$\rho_{b2}-\rho_{b4}/\rho_{b2}+\rho_{b4}$
MDNWI[6]	Xu(2006)	$\rho_{b2}-\rho_{b5}/\rho_{b2}+\rho_{b6}$
MBWI[7]	Gao(2004)	$2\rho_{b2}-\rho_{b3}-\rho_{b4}-\rho_{b5}-\rho_{b7}$
AWEInsh[8]	Feyisa(2014)	$4(\rho_{b2}-\rho_{b5})-(0.25\rho_{b4}+2.75\rho_{b6})$
AWEIsh[8]	Feyisa(2014)	$\rho_{b1}-2.5\rho_{b2}-1.5(\rho_{b4}+\rho_{b5})-0.25\rho_{b7}$
WI2015[9]	Fisher(2014)	$1.7204+171\rho_{b2}+3\rho_{b3}-70\rho_{b4}-45\rho_{b5}-71\rho_{b7}$
RNDWI[10]	Cao(2008)	$\rho_{b3}-\rho_{b5}/\rho_{b3}+\rho_{b6}$
EWI[11]	Yan(2007)	$\rho_{b2}-\rho_{b4}-\rho_{b5}/\rho_{b2}+\rho_{b4}+\rho_{b5}$
SWI[12]	Chen(2013)	$\rho_{b1}+\rho_{b2}-\rho_{b4}$

The extraction of Poyang Lake water bodyThe extraction effect of the water body is relatively poor, and the water body is affected by sediment, chlorophyll and some mountain shadows. The size is 3146 * 5155 pixels, including mountains, buildings, lakes, rivers, ponds and other parts. Three kinds of result maps with better extraction effect were selected. Figure 1

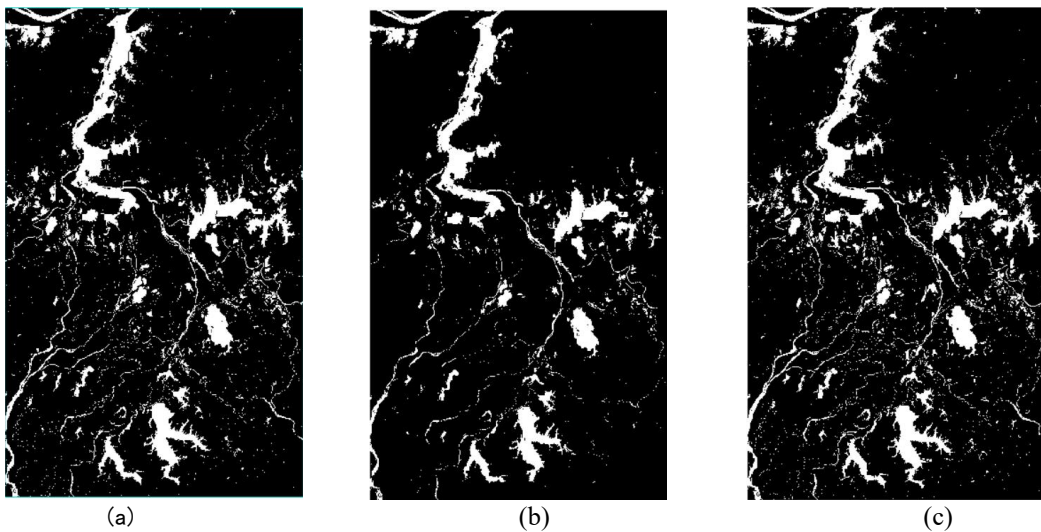


Figure 1 Extraction results of Poyang Lake water body;(a)MBWI;(b)TCW;(c) AWEInsh

Due to the increasing eutrophication of water bodies in Taihu Lake area, some water bodies in the lake are green, which makes it difficult to extract some water bodies well. The image used in this paper is 2480 * 2415 pixels, including surrounding towns and small rivers. Due to image reasons, the blank in the lower left corner is not the research area and does not enter the calculation. Select three kinds of results with better results which can be seen in Figure 2.

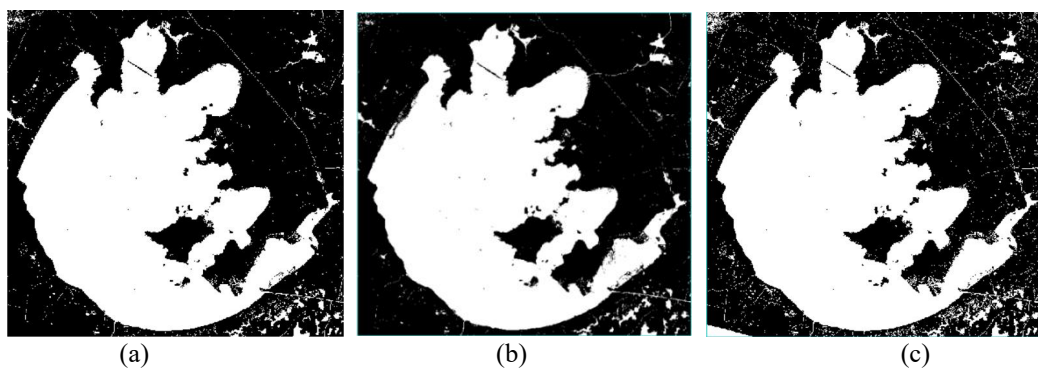


Figure 2 Extraction Results of Taihu Lake Water Body; (a) TCW;(b) MBWI;(c) WI2015

The water body is extracted from mountainous areas such as Dingnan County, with a size of 11428 * 8515 pixels. Because the selected area is relatively large and there are many image factors, the extraction effect is relatively poor. Including high reflectivity cities, mountain shadows, clouds and other factors. Select three better results Figure 3

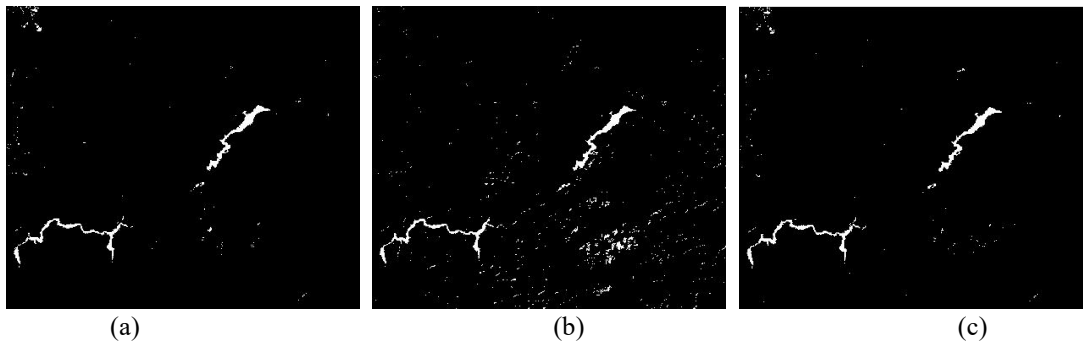


Figure 3 Water Extraction Results of Dingnan County; (a)MBWI;(b) AWEInsh;(c)TCW

3 ACCURACY EVALUATION

In this paper, the method of accuracy evaluation is the confusion matrix method. Its calculation formula is:

$$C_M = \begin{pmatrix} x_{11} & x_{12} & \dots & x_{1n} \\ x_{21} & x_{22} & \dots & x_{2n} \\ \vdots & \vdots & \ddots & \vdots \\ x_{n1} & x_{n2} & \dots & x_{nn} \end{pmatrix} \tag{1}$$

In the formula, x_{ab} ($a, b = 1, 2, 3, n$) elements, this paper only divided into two categories: water and non-water. a is set to 2, which represents the probability that the training samples are divided into non-water bodies, and b represents the probability that the water samples in the training samples are divided into non-water bodies, where the sum of these probabilities is 1. In this paper, the effect map obtained by the water index of ten methods is used to evaluate the accuracy.

Table 2 NDWI Water Extraction Confusion Matrix Results

classification	Water bodies	Non-water bodies	Total
water body	1473300	1026738	2500038
Non-water bodies	119852	13717592	13837444
Total	1593152	14744330	16337482

Table 2 shows the number of pixels in water and non-water bodies. Under this method, the total accuracy is (1473300 + 13717592) / 16337482 = 92.98 %. The total number of pixels in the planned water body is 2500038, of which 1026738 pixels are misclassified into non-water body pixels. The error of misclassification is called misclassification rate, 1026738 / 2500038 = 41.06 %, of which there are 1593152 pixels in the real water body. There are 1373300 pixels in the water body that are correctly distinguished in this area, and there are 119852 pixels in the water body that are not distinguished. The leakage error is 119852 / 1593152 = 7.52 %. The accuracy of these errors provides a basis for the accuracy and evaluation of the method extraction.

3.1 Accuracy Evaluation Results

Table 3 Evaluation of Water Extraction Accuracy of Poyang Lake

Water extraction method	Error/%	Lost/%	accuracy /%
MDNWI	0.391	0.139	0.931
AWEInsh	0.297	0.116	0.951
AWEIsh	0.368	0.110	0.938
EWI	0.462	0.100	0.914
WI2015	0.261	0.100	0.958
MBWI	0.010	0.164	0.982
NDWI	0.455	0.146	0.915
SWI	0.228	0.105	0.963
TCW	0.006	0.081	0.991
RNDWI	0.353	0.096	0.942

From Table 3, the total accuracy of different water extraction methods in Poyang Lake area from high to low is TCW, MBWI, SWI, WI2015, AWEInsh, RNDWI, AWEIsh, MNDWI, NDWI, EWI. The water body error rate extracted by EWI water index is the highest. MBWI water index extraction water omission extraction is the most.

Table 4 Evaluation of Water Extraction Accuracy of Taihu Lake

Water extraction method	Error/%	Lost/%	accuracy/%
AWEInsh	0.005	0.002	0.996
AWEIsh	0.041	0.003	0.978
EWI	0.009	0.009	0.959
MBWI	0.001	0.029	0.985
MNDWI	0.039	0.016	0.973

NDWI	0.103	0.021	0.937
RNDWI	0.040	0.021	0.971
SWI	0.057	0.016	0.964
TCW	0.005	0.010	0.992
WI2015	0.004	0.007	0.973

From Table 4, the total accuracy of different water extraction methods in the Taihu Lake area from high to low is AWEInsh, TCW, MBWI, AWEIsh, WI2015, MNDWI, RNDWI, SWI, EWI, NDWI. The water body error rate extracted by NDWI water index is the highest. MBWI water index extraction water omission extraction is the most.

Table 5 Evaluation of Water Extraction Accuracy in Mountain Shadow Area

Water extraction method	Error/%	Lost/%	accuracy/%
WI2015	0.447	0.050	0.989
TCW	0.009	0.262	0.996
SWI	0.783	0.067	0.953
RNDWI	0.528	0.285	0.985
NDWI	0.852	0.273	0.939
MNDWI	0.130	0.130	0.980
MBWI	0.273	0.273	0.989
EWI	0.281	0.281	0.978
AWEIsh	0.607	0.015	0.979
AWEInsh	0.069	0.287	0.995

From Table 5, the total accuracy of different water extraction methods in Dingnan County from high to low is AWEInsh, TCW, MBWI, AWEIsh, WI2015, MNDWI, RNDWI, SWI, EWI, NDWI. The water body error rate extracted by NDWI water index is the highest. MBWI water index extraction water omission extraction is the most.

4 CONCLUSION

In this paper, starting from different environments (shallow water area, water eutrophication area, mountain shadow area), taking Poyang Lake, Taihu Lake and Dingnan County mountain area as the research area, 10 water body index methods were found to compare the suitability evaluation of water body index in complex environmental water extraction. The conclusions are as follows:

The water index of NDWI and EWI is high in missing extraction rate, high in wrong extraction rate, and low in total accuracy compared with other methods. The error rate of MBWI water index is low, but the missing rate is high and the total accuracy is high. The missing rate and error rate of TCW and AWEInsh water index are relatively low and the total accuracy is very high. Other index methods are similar, and some methods are a special environment. For example, the WI2015 water index is very suitable for water extraction with mountain shadows[13].

2.Shallow water area: The middle of Poyang Lake is on the right side of the water body. The extraction effect of TCW and MBWI is good among the ten methods. The MBWI model greatly improves the spectral distinction between water body and non-water body, so that water body and non-water body can be well distinguished.

Eutrophication area: most of the Taihu Lake, these ten methods for eutrophication area water extraction effect is good, are relatively clear extraction, TCW, MBWI, AWEInsh for Taihu Lake overall

COMPETING INTERESTS

The authors have no relevant financial or non-financial interests to disclose.

REFERENCES

- [1] Du Yunyan, Zhou Chenghu. Automatic extraction method of water bodies from remote sensing information. *Journal of Remote Sensing*, 1998(4): 264-269.
- [2] Wang Hang, Qin Fen. A review of water extraction from remote sensing images. *Science of Surveying and Mapping*, 2018, 43(5): 23-32.
- [3] Li Dan, Wu Baosheng, Chen Bowei, et al. Advances and prospects in water information extraction based on satellite remote sensing. *Journal of Tsinghua University*, 2020, 60(2): 147-161.
- [4] Crist E P. A TM Tasseled Cap equivalent transformation for reflectance factor data. *Remote Sensing of Environment*, 1985, 17(3): 301-306.
- [5] McFeeters S K. The use of the Normalized Difference Water Index (NDWI) in the delineation of open water features. *International Journal of Remote Sensing*, 1996, 17(7): 1425-1432.
- [6] Xu H Q. Modification of normalized difference water index (NDWI) to enhance open water features in remotely sensed imagery. *International Journal of Remote Sensing*, 2006, 27(14): 3025-3033.
- [7] Wang Xiaobiao, Xie Shunping, Du Jinkang. Water index construction and its effectiveness research in complex environments. *Journal of Remote Sensing*, 2018, 22(2): 360-372.

- [8] Feyisa G L, Meilby H, Fensholt R, et al. Automated Water Extraction Index: A new technique for surface water mapping using Landsat imagery. *Remote Sensing of Environment*, 2014, 140: 23-35.
- [9] Fisher A, Flood N, Danaher T. Comparing Landsat water index methods for automated water classification in eastern Australia. *Remote Sensing of Environment*, 2016, 175: 167-182.
- [10] Cao R L, Li C J, Liu L Y, et al. Extracting Miyun Reservoir's water area and monitoring its change based on a revised normalized difference water index. *Science of Surveying and Mapping*, 2008, 33(2): 158-160.
- [11] Yan Pei, Zhang Youjing, Zhang Yuan. Study on extracting water system information in semi-arid regions using Enhanced Water Index (EWI) and GIS noise removal technology. *Remote Sensing Information*, 2007(6): 62-67.
- [12] Wang Jinjie, Ding Jianli, Zhang Cheng, et al. Improved SWI water extraction method based on GF-1 satellite imagery. *Remote Sensing for Land and Resources*, 2017, 29(1): 29-35.
- [13] Wang Y. Efficient Adverse Event Forecasting in Clinical Trials via Transformer-Augmented Survival Analysis. *Preprints*, 2025. DOI:10.20944/preprints202504.2001.v1.

